



**Michigan
Technological
University**

Michigan Technological University
Digital Commons @ Michigan Tech

Dissertations, Master's Theses and Master's Reports

2020

Virus Purification Framework And Enhancement In Aqueous Two-Phase System

Pratik Umesh Joshi


Michigan Technological University, pjoshi1@mtu.edu

Copyright 2020 Pratik Umesh Joshi

Recommended Citation

Joshi, Pratik Umesh, "Virus Purification Framework And Enhancement In Aqueous Two-Phase System", Open Access Dissertation, Michigan Technological University, 2020.
<https://doi.org/10.37099/mtu.dc.etr/1030>

Follow this and additional works at: <https://digitalcommons.mtu.edu/etr>

 Part of the [Biochemical and Biomolecular Engineering Commons](#), [Biochemistry Commons](#), [Polymer and Organic Materials Commons](#), and the [Transport Phenomena Commons](#)

VIRUS PURIFICATION FRAMEWORK AND ENHANCEMENT IN AQUEOUS
TWO-PHASE SYSTEM

By

Pratik Umesh Joshi

A DISSERTATION

Submitted in partial fulfillment of the requirements for the degree of

DOCTOR OF PHILOSOPHY

In Chemical Engineering

MICHIGAN TECHNOLOGICAL UNIVERSITY

2020

© 2020 Pratik U. Joshi

This dissertation has been approved in partial fulfillment of the requirements for the Degree of DOCTOR OF PHILOSOPHY in Chemical Engineering.

Department of Chemical Engineering

Dissertation Advisor: *Dr. Caryn L. Heldt*

Committee Member: *Dr. David Shonnard*

Committee Member: *Dr. Loredana Valenzano-Slough*

Committee Member: *Dr. Silviya Petrova Zustiak*

Department Chair: *Dr. Pradeep Agrawal*

Table of Contents

List of figures.....	vii
List of tables.....	xii
Preface.....	xiv
Acknowledgements.....	xvi
Abstract.....	xviii
1 Introduction.....	1
1.1 Viruses, infectious disease, and immunity.....	2
1.2 Overview.....	5
1.3 Reference.....	8
2 Literature Review.....	9
2.1 Vaccines and biotherapeutics.....	10
2.2 Viral-based Biotherapeutic Manufacturing.....	11
2.2.1 Upstream Processing.....	16
2.2.2 Unit Operation Mechanisms in Downstream Processing.....	17
2.2.2.1 Conventional Methods and their upgrades.....	18
2.2.2.1.1 Size-based separation.....	18
2.2.2.1.2 Charge-based separation.....	23
2.2.2.1.3 Hydrophobicity-based separation.....	26
2.2.2.1.4 Affinity-based separation.....	28
2.2.2.2 The conventional downstream processing train.....	30
2.2.2.3 Continuous Integrated Processing: Vision for Biotherapeutic Manufacturing.....	32
2.2.3 Liquid-Liquid Phase Separation.....	34
2.2.4 ATPS phase diagrams.....	40
2.3 Biomolecule Partitioning Theories in ATPS.....	43
2.3.1 Excluded volume and intermolecular interactions.....	43
2.4 Parameters and their effect on driving forces in ATPS.....	46
2.4.1 Phase forming component parameters.....	46
2.4.1.1 Polymer molecular weight and concentration.....	46
2.4.1.2 Salt type and concentration.....	48
2.4.1.3 pH.....	50
2.4.1.4 Summary of phase parameters and effects.....	51
2.4.2 Biomolecule characteristics and the effect on partitioning behavior.....	51
2.4.2.1 Surface hydrophobicity.....	51

	2.4.2.2	Surface charge.....	53
2.5		Osmolytes.....	54
	2.5.1	Osmoregulators under environmental stress.....	54
	2.5.2	Osmolytes in biomanufacturing.....	54
2.6		References.....	56
3		Tie line framework to optimize non-enveloped virus recovery in aqueous two-phase systems ^{1,2}	75
3.1		Introduction.....	76
3.2		Materials & Methods.....	81
	3.2.1	Materials.....	81
	3.2.2	Methods.....	81
	3.2.2.1	Cell maintenance and virus titration.....	81
	3.2.2.2	Construction of binodal curves and tie lines.....	82
	3.2.2.3	Physical Properties of Systems.....	83
	3.2.2.4	SDS-PAGE.....	84
	3.2.2.5	DNA quantification.....	84
	3.2.2.6	Dynamic Light Scattering (DLS).....	85
3.3		Results.....	85
	3.3.1	Model Virus.....	85
	3.3.2	Binodal curves & tie lines.....	86
	3.3.3	Effect of tie lines & tie line ratios.....	89
	3.3.4	Effect of increased PPV load.....	93
3.4		Discussion.....	95
3.5		Conclusion.....	98
3.6		References.....	99
4		Osmolyte enhanced Aqueous two-phase systems for virus purification ^{3,4}	107
4.1		Introduction.....	108
4.2		Materials and Methods.....	110
	4.2.1	Materials.....	110
	4.2.2	Methods.....	111
	4.2.2.1	Cell maintenance, virus propagation and virus titration 111	
	4.2.2.2	Generation of binodal curve and tie lines.....	111
	4.2.2.3	Osmolyte detection and quantification.....	112
	4.2.2.4	Virus and virus-like particle partitioning.....	112
	4.2.2.5	SDS-PAGE for protein detection.....	113
	4.2.2.6	DNA Quantification.....	113
4.3		Results.....	114

4.3.1	Effect of osmolytes on two-phase behavior.....	114
4.3.2	Model viruses.....	117
4.3.3	Influence of osmolyte class on virus partitioning.....	118
4.3.4	Influence of osmolyte class on protein and HC-DNA partitioning	121
4.3.5	Effect of tie-line framework on virus partitioning.....	123
4.3.6	Effect of pH on virus partitioning.....	125
4.4	Discussion	126
4.5	Conclusion.....	128
4.6	References	128
5	Affinity aqueous two-phase system using multimodal peptide ligand for virus partitioning ⁵	133
5.1	Introduction	134
5.2	Materials & Methods.....	137
5.2.1	Materials	137
5.2.2	Methods.....	138
5.2.2.1	Cell culture, virus propagation, and titration	138
5.2.2.2	Functionalized PEG conjugation and purification.....	138
5.2.2.3	Steady-state fluorescence quenching	139
5.2.2.4	Virus Partitioning and Recovery.....	140
5.3	Results	140
5.3.1	Virus partitioning in the presence of affinity ligand.....	140
5.3.2	Efficiency and characterization of PEG-peptide conjugation.....	146
5.4	Discussion	147
5.5	Conclusions	150
5.6	References	151
6	Conclusions and future work	158
6.1	Conclusions	159
6.2	Future work	162
6.2.1	Viral behavior at interface and mathematical model validation	162
6.2.2	Expanding the viral database	162
6.2.3	Back-extraction of viral product	163
6.2.4	Scale-up and sustainability analysis of ATPS	164
6.3	Dissertation Summary	164
6.4	References	165
A	Supplementary information	167
A.1	Tie-line framework for virus optimization.....	167

A.2	Osmolyte-containing aqueous two-phase systems	171
A.3	Multimodal affinity ligand based aqueous two-phase system for virus purification.....	185
B	Enveloped virus partitioning in ATPS.....	186
C	Copyright documentation.....	190
C.1	Reuse license for Figure 2-5.....	190
C.2	Reuse license for Figure 2-7.....	191
C.3	Reuse license for Figure 2-9.....	191
C.4	Reuse license for Figure 2-10.....	193

List of figures

Figure 1-1. The structural basis of viruses: non-enveloped virus and enveloped virus. Virus images were created in BioRender.....	2
Figure 2-1. General Viral vaccine and biotherapeutic manufacturing scheme.....	12
Figure 2-2. Operating modes of filtration – A) Depth filtration and B) Tangential flow filtration. This image was created in BioRender.	20
Figure 2-3. Principle of virus purification in density gradient centrifugation. This image was created in BioRender.	22
Figure 2-4. Principle of size exclusion chromatography for virus purification. A) Column pores allow diffusion of small contaminant proteins and exclude viruses. B) A typical chromatogram showing increased residence time of proteins, which elute later than viruses.	23
Figure 2-5. Frequency of isoelectric points of viruses reported in literature. Reprinted with permission from [71].	24
Figure 2-6. Unit operations in the DSP train and their purpose. Reused with permission from [59].....	32
Figure 2-7. Different types of two-phase systems used for biomolecule partitioning. The image was created in BioRender.....	35
Figure 2-8. Phase diagram demonstrating binodal curve and tie lines for ATPS.....	41
Figure 2-9. The binodal curve shift with an increasing PEG molecular weight. W_p and W_s represents the PEG and salt concentrations. Reprinted with permission from [186]. Copyright (2018) Elsevier.....	47
Figure 2-10. Comparison of surface hydrophobicity of protein and viruses determined by the elution salt concentration in hydrophobic interaction chromatography. Reprinted with permission from [207].....	52
Figure 3-1. Binodal curve and tie lines. (A) Schematic illustration of ATPS showing binodal curve separating one-phase region from the two-phase region and set of systems characterized by tie lines and TL ratios. (B) Experimentally determined binodal curve and tie lines for PEG 12kDa-citrate ATPS at pH 7.....	87
Figure 3-2. PPV recovery in the PEG-rich phase (A, D, and G) and the citrate-rich phase (B, E, and H) at different TLL. SDS-PAGE of marker (M), starting PPV (S) and the PEG-rich phase (P) and the citrate-rich phase (C) at different TLL and TL	

ratios. The starting titer was \log_{10} 6.5 MTT ₅₀ /ml. Experiments were done in triplicates and the error bars represent the standard deviation.....	91
Figure 3-3. HRV recovery in the PEG-rich phase (A) and the citrate-rich phase (B) at different TLL. SDS-PAGE of marker (M), starting HRV (S), PEG-rich phase (P) and the citrate-rich phase (C) at TLL 15, 25, and 36w/w%. The starting titer was \log_{10} 6.5 MTT ₅₀ /ml. Experiments were done in triplicates, and the error bars represent the standard deviation.....	92
Figure 3-4. Comparison of PPV partitioning at two different loads along (A) TLL 15 w/w%, (B) TLL 25 w/w%, and (C) TLL 36 w/w%. Experiments were repeated in triplicates and error bars represent standard deviation.	94
Figure 3-5. Schematic PPV recovery map in the two-phase region for (A) PEG-rich phase and (B) citrate-rich phase.....	96
Figure 4-1. (A) Binodal curves and (B, C, D) tie lines for PEG 12kDa – citrate systems in presence of various 0.5 M osmolytes. Denaturing osmolyte – (B) urea and protecting osmolytes – (C) mannitol, TMAO, (D) betaine, and glycine.	115
Figure 4-2. Partitioning of the osmolytes at common compositions of ATPS with increasing TLL represented as (A) ln (K) and (B) % recovery in the corresponding citrate-rich phases.	117
Figure 4-3. Effect of different osmolytes on (A) PPV and (B) HIV-gag VLP partitioning. Biomolecule partitioning upon addition of 0.5 M protecting (glycine, betaine, and TMAO) and non-protecting (urea) osmolytes are compared to osmolyte-free (control) system. Experiments were performed in triplicates and the error bars represent standard deviation.	119
Figure 4-4. Contaminant protein (A & B) and HC-DNA (C & D) partitioning at varying TLL in presence of 0.5 M glycine or betaine. Contaminant protein partitioning were visualized on Coomassie stained SDS-PAGE and HC-DNA were quantified using Quant-iT™ PicoGreen® dsDNA assay. The error bars in the DNA partitioning figures represent standard deviations from the experiments done in triplicates.....	122
Figure 4-5. Partition coefficient of PPV in the systems (A) without osmolyte and systems enhanced with 0.5 M protecting osmolytes (B) glycine (C) betaine (D) TMAO (E) mannitol. Experiments were done in triplicates and the error bars represent the standard deviation.	124
Figure 4-6. PPV partitioning at varying TLL in presence of (A) 0.5 M glycine, (B) 0.5 M betaine, and (C) 0.5 M TMAO maintained at pH 5 and 7. The error bars represents standard deviation of experiments done in triplicates.	126

Figure 5-1. Synthesis flow diagram of functionalized PEG-peptide conjugates. A linear PEG-vinyl sulfone is covalently functionalized with a cysteine terminated peptide.139

Figure 5-2. Effect of TLL and TL ratios on PPV partitioning with an inclusion of affinity ligand mPEGVS-WRW. (A) Six systems were selected on three different tie-lines and two TLR. The partitioning coefficients in the presence of 30% PEG-peptide doping are demonstrated at (B) TLR:1 and (C) TLR:2.3 on all the three TLL along with systems without the affinity ligand doping. Experiments were conducted in triplicates and the error bar represents standard deviation. *p-value < 0.05 using Student's t-test as compared to the ligand-free system.143

Figure 5-3. PPV recovery comparison at (A&B) the three TLL and two TLRs in the (C&D) PEG-rich phase and (E&F) citrate-rich phase. Three separate ligands (AAA, GGG, and WRW) were added individually in each system at a 7:3 ratio of PEG 12 kDa to PEG-peptide conjugate and compared with the ligand-free control systems. The error bars represent the standard deviations from three individual experiments.145

Figure 5-4. Conjugation confirmation of mPEGVS and peptides represented as ¹H NMR spectra of (A) mPEGVS, (B) mPEGVS-AAA, (C) mPEGVS-GGG, and (D) mPEGVS-WRW. The orange box at 6, 6.5, and 7 ppm indicates the vinyl sulfone peaks, whose disappearance shows that the reaction between the mPEGVS and the peptides had occurred.146

Figure 5-5. Acrylamide quenching of free WRW peptide and mPEGVS-WRW fluorescence. Fitting of data points to the Stern-Volmer equation yields KSV values of 5.1 ± 0.8 and 13.5 ± 1.1 M⁻¹ for free WRW and mPEGVS-WRW, respectively. Experiments were conducted in triplicates and the error bars represent standard deviations.147

Figure A.1-1. Aggregate ratio of 8 log₁₀ MTT50/ml PPV at varying citrate concentration. Aggregation ratio compares the intensity of the PPV peak to the intensity of the aggregate peak in DLS and can be found in Eq. 3-7. The open bars represent the lack of a PPV peak. Experiments were conducted in triplicate and the error bars represent the standard deviation.170

Figure A.2-1. LC-MS profile of glycine. (A) The area under the elution curve of showing(A) was used in relation to the elution area of glycine-C13 internal standard (Figure A.2-2) to form a standard curve and (B) MS peak used to detect glycine, operated with conditions shown in table A.2-1.172

Figure A.2-2. LC-MS profile of glycine-C13, used as the internal standard for glycine. (A) The area under the elution curve of glycine-C13 was used in relation to the elution area of glycine (Figure A.2-1) to form a standard curve and (B) MS peak used to detect glycine C-13, operated with conditions shown in table A.2-1.173

- Figure A.2-3.** LC-MS profile of betaine. (A) The area under the elution curve of betaine was used in relation to the elution area of betaine-D11 (Figure A.2-4) to form a standard curve and (B) MS peak used to detect betaine, operated with conditions shown in table A.2-1.174
- Figure A.2-4.** LC-MS profile of betaine-D11 used as the internal standard for betaine. (A) The area under the elution curve of betaine-D11 was used in relation to the elution area of betaine (Figure A.2-3) to form a standard curve and (B) MS peak used to detect betaine-D11, operated with conditions shown in table A.2-1.....175
- Figure A.2-5.** LC-MS profile of TMAO. (A) Area under the elution curve of TMAO was used in relation to the elution area of TMAO-D9 (Figure A.2-6) to form a standard curve and (B) MS peak used to detect TMAO, operated with conditions shown in table A.2-1.176
- Figure A.2-6.** LC-MS profile of TMAO-D9 used as internal standard for TMAO. (A) Area under the elution curve of TMAO -D9 was used in relation to the elution area of TMAO (Figure A.2-5) to form a standard curve and (B) MS peak used to detect TMAO-D9, operated with conditions shown in table A.2-1.....177
- Figure A.2-7.** LC-MS profile of mannitol. (A) Area under the elution curve of mannitol was used in relation to the elution area of mannitol-U-13C6 (Figure A.2-8) to form a standard curve and (B) MS peak used to detect mannitol, operated with conditions shown in table A.2-1.178
- Figure A.2-8.** LC-MS profile of mannitol-U-13C6, used as the internal standard for mannitol. (A) Area under the elution curve of mannitol-U-13C6 was used in relation to the elution area of mannitol (Figure A.2-7) to form a standard curve and (B) MS peak used to detect mannitol-U-13C6, operated with conditions shown in table A.2-1.179
- Figure A.2-9.** LC-MS profile of urea. (A) Area under the elution curve of urea was used in relation to the elution area of Urea-C13-2N15 (Figure A.2-9) to form a standard curve and (B) MS peak used to detect urea, operated with conditions shown in table A.2-1.....180
- Figure A.2-10.** LC-MS profile of urea-C13-2N15, used as the internal standard for urea. (A) Area under the elution curve of urea-C13-2N15 was used in relation to the elution area of urea (Figure A.2-9) to form a standard curve and (B) MS peak used to detect urea-C13-2N15, operated with conditions shown in table A.2-1.....181
- Figure A.2-11.** PPV and HIV-gag VLP recoveries in (A & C) PEG-rich and (B & D) citrate-rich phases, at three common global compositions in presence of different osmolytes. The open columns indicate 100% recovery in the represented phase. The error bars represent standard deviation of experiments done in triplicates. The

high error bars are because of the sensitivity of the MTT assay measured in log and converted to percentages.183

Figure A.3-1. Conjugation confirmation of mPEG-VS and GRCD-WRW by (A) relative fluorescence spectra comparison of free WRW peptide and PEGVS-WRW and (B) absorbance spectra comparison of free mPEGVS and mPEGVS-WRW in 1x PBS, pH 7.4. The presence of fluorescence at 310 nm and a high relatively absorbance between 210-280 nm confirms the successful attachment of PEGVS to the peptide with the target sequence of WRW.....185

Figure B-1. HSV-1 partitioning behavior studied with the tie-line framework. (A) Partitioning coefficient of HSV at increasing TLL and TLR. Recovery of HSV-1 in (B) PEG-rich phase and (C) citrate-rich phase. The experiments were performed in triplicates, and the error bars represent standard deviation.....187

Figure B-2. Effect of osmolytes on the partitioning coefficient of HSV in PEG 12kDa-citrate pH 7 systems. The experiments were performed in triplicates. The error bars represent the standard deviation.....188

Figure B-3. Effect of osmolytes on HSV recovery in (A) PEG-rich phase and (B) citrate-rich phase. The experiments were performed in triplicates. The error bars represent the standard deviation.....189

List of tables

Table 1-1. Human virus species and disease [3]	3
Table 2-1. Established cell lines currently used in vaccine production and the virus susceptibility [22].....	14
Table 2-2. Commonly used cell platforms for producing virus-like particles	15
Table 2-3. Advantages and disadvantages of cell platforms for VLP production [35].....	15
Table 2-4. Virus and VLP purification in Capto Core 700 multimodal resin.....	28
Table 2-5. Affinity ligands binding mechanisms and processing attributes [110].....	29
Table 2-6. Phase forming components for ATPS [130].....	37
Table 2-7. Examples of ATPS for purification of different biomolecules.....	39
Table 2-8. Virus and VLP recovery in PEG-rich phases of ATPS	40
Table 3-1. Overview of virus and virus-like particles in PEG/salt ATPS.....	80
Table 3-2. A brief description and comparison of the model viruses (PPV and HRV).....	86
Table 3-3. Comparison of TL ratio (Eq. 3-2) and volume ratio (Eq. 3-3)	88
Table 4-1. Osmolytes and their characteristics	114
Table 4-2. Changes in the TLL and TL slope with addition of osmolytes	116
Table 4-3. Biophysical and biochemical characteristics of model virus/VLP	118
Table 5-1. Hydrophobic and charge characteristics of peptides	150
Table A.1-1. Physical Properties (density and refractive index) of the systems at TLL 15, 25, and 36 w/w%.....	167
Table A.1-2. PEG concentration in the PEG-rich phase at different TLL using refractive index.....	168
Table A.1-3. Standard Refractive Index of increasing concentration of PEG	168
Table A.1-4. HRV titer in the PEG-rich phase and citrate-rich phase as a function of TLL and TL ratio.....	169

Table A.1-5. PPV titer in the PEG-rich phase and citrate-rich phase as a function of TLL and TL ratio.....	170
Table A.2-1. Description of the LC-MS method development parameters for osmolyte detection and quantification. Corresponding stable isotopes of each osmolyte was used as the internal standard.	171
Table A.2-2. Average of PPV titers across TL ratio and TLL in osmolyte-containing ATPS.....	182
Table A.2-3. Viscosities of the PEG-rich phase with and without addition of osmolytes of systems at different TLL.....	184
Table A.3-1. Correlation of tie-line ratio and volume ratios of the selected systems on different tie-line lengths.....	185

Preface

The work described in this dissertation was collaborative research conducted in Dr. Caryn Heldt's Lab in the department of Chemical Engineering at Michigan Technological University (MTU, MI) with assistance from the Chemical Advanced Resolution Methods (ChARM) lab at MTU's Great Lakes Research Center (GLRC) and the department of Biomedical Engineering at Saint Louis University (MO). The hypotheses, experimental design, measurements, and analysis mentioned in the dissertation were developed and written by me with inputs from the collaborators as mentioned below. Dr. Caryn Heldt did the grant writing and funding acquisition that supported this work with some help from me on hypothesis formulation and experimental design.

Chapter 3 discusses the development of the framework by using a phase diagram to understand virus purification in the aqueous two-phase system (ATPS). The experiments were designed by me with guidance from my advisor Dr. Caryn Heldt. Matthew Weiss (undergraduate student) helped me generate the phase diagrams, Michael Schroeder (undergraduate student) helped me repeat the ATPS formation for porcine parvovirus (PPV), and Glendy Escalante-Corbin (MiCUP student) helped me with the ATPS generation for human rhinovirus-14 (HRV). Dylan Turpeinen (Ph.D. Candidate) helped me perform the dynamic light scattering experiment for the determination of PPV aggregation in the presence of citrate. I collected and analyzed the infectivity data and created the figures, under my advisor's supervision. The chapter was written by me, reviewed and edited by Dr. Heldt and reviewed by Dylan. The chapter is published in the *Journal of Chromatography B* (2019).

Chapter 4 demonstrates the virus purification enhancement by osmolyte addition in ATPS. I developed the hypothesis and experimental design with insights and guidance from Dr. Heldt. Undergraduate students Michael Schroeder, Bianca Jones, Audrey Lyons, and Seth Kriz helped with the generation of phase diagrams, system generation for the purification of PPV, and enveloped human immunodeficiency virus-group

specific antigen virus-like particle (HIV-gag-VLP), and physical properties of phases. The method development and quantification assay for osmolyte detection in the citrate-rich phases by LC-MS was performed by Dr. Maryam Khaksari (GLRC). All the figure designs and data analysis were done by me and reviewed by Dr. Heldt. The manuscript is in preparation for submission in a peer-reviewed journal.

Chapter 5 demonstrates the development of a novel ATPS with inclusion of affinity peptide ligand for improved specificity and driving forces. The working hypothesis was generated by me, Dr. Heldt, and Dr. Silviya Zustiak (Saint Louis University, MO). Half of the work was conducted at Saint Louis University in Dr. Zustiak's lab, and the other half was carried out at Michigan Tech in Dr. Heldt's lab. Stephanie Kroger from Dr. Zustiak's lab synthesized and purified the PEG-peptide conjugate and characterized the polymer to confirm the conjugation and ligand accessibility. The virus purification, infectivity assay, contaminant partitioning experiments, and data analysis were performed by me under the guidance of Dr. Heldt. The majority of the chapter was written by me and reviewed by Dr. Heldt and Dr. Zustiak. Dr. Zustiak wrote a part of the method section on synthesis chemistry, NMR, and acrylamide quenching. The manuscript is in preparation for submission to a peer-reviewed journal.

Chapter 6 summarizes the main conclusions from chapters 3, 4, and 5. The findings of each chapter were interpreted and concluded by me with the guidance of Dr. Heldt. Dr. Zustiak helped in interpreting the findings of PEG-peptide conjugate functional analysis from chapter 5. The majority of future works proposed are my thoughts and initiatives discussed with Dr. Heldt. Some of the hypotheses and directions mentioned in the future work are currently being designed and evaluated by current graduate students in Dr. Heldt's lab and at Clemson University in Dr. Sapna Sarupria's lab.

Acknowledgements

I am incredibly thankful to Dr. Caryn Heldt for mentoring and guiding throughout my grad school. Her helpful insights on developing research skills like asking the right and visionary questions, the significance of innumerable controls in biological research, idea formulation, and writing techniques have helped me design experiments and collaborative projects. Her work ethics and dedication have helped improve my professional development skills. I am most grateful for her giving me the opportunity to work in her lab and making me intrigued about the minute yet fascinating species, viruses.

The work conducted in this dissertation was funded by NSF (CBET 1451959, 1510006, and 1818906) and the James and Lorna Mack Chair in Bioengineering, to which I express my deepest gratitude. I am very grateful to the graduate school (MTU) for providing the doctoral finishing fellowship for Summer 2020. I would also like to thank the department of Chemical Engineering (MTU) for providing multiple teaching assistantships. I am thankful to MilliporeSigma (Burlington, MA) for their generous supply of chemicals used in some studies and Esperovax (Plymouth, MI) for providing the HIV-gag-VLP crude stock.

To Dr. David Shonnard and Dr. Faith Morrison, I am thankful for supportive insights and feedbacks during the teaching assistantship. I express my gratitude to my Ph.D. committee members, Dr. David Shonnard, Dr. Loredana Valenzano-Slough, and Dr. Silviya Zustiak, for their continuous support and feedback during grad school. I am very thankful to Dr. Heldt's Bioseparations Lab group members for their constant support. I express utmost gratitude to Dylan Turpeinen, Xue Mi, and Christa Meingast for their insightful discussions and pushing my understanding limits through critiques and questions. To all the undergraduate students who worked on the ATPS projects with dedication and waited patiently for results from the weeklong analytical methods. I am extremely appreciative of Alexis Snell, Taana Blom, and Susan Niemi for their unconditional administrative support and Jerry Norkol, Stefan Wisniewski, and Scott

Wendt for their technical support with the instruments and chemical safety measures in the lab. I also thank Dr. Jeana Collins for reviewing chapter 2.

The academic journey through graduate school would not have been possible without the support of my parents, to whom I dedicate this life's milestone. My sincere appreciation goes to my cousins, whose questions made me gain more insights on biotherapeutics. Finally, I would like to thank all my friends, and mentors from across the countries, for their constant moral support and encouragement.

Abstract

Viral infections regularly pose detrimental health risks to humans. Preventing viral infections through global immunization requires the production of large doses of vaccines. The increasing demand for vaccines, especially during pandemics such as COVID-19, has challenged current manufacturing strategy to develop advanced unit operations with high throughput capability. Over the decade, the upstream processing responsible for synthesizing viral products in cell cultures has shown significant success in yielding high titers of viruses and virus-like particles. The progress in the upstream stage has now shifted the bottleneck to the downstream processing (DSP). Overlooked for decades, the DSP responsible for viral product purification from the cell culture contaminants requires a makeover with the development of new purification strategies and an upgrade in the traditional unit operations. The current DSP train employing chromatography and filtration methods have been suboptimal in efficiently processing comparatively complex and fragile viral particles. Thus, the lack of platform technology for viral vaccine and biotherapeutic DSP has led to a search for alternative and innovative methods that have not only high-throughput capabilities but also have potential for continuous operation.

In the pool of potential technologies, aqueous two-phase system (ATPS) has shown to be a promising candidate with the numerous advantages over conventional methods. However, an unambiguous and complex biomolecule partitioning mechanism has required a large experimental setup for optimizing virus purification. This work focused on a framework utilizing a phase diagram of a rationalized polyethylene glycol-citrate system to optimize virus purification. The partitioning behavior of two non-enveloped viruses, porcine parvovirus (PPV) and human rhinovirus-14 (HRV), were studied in various system compositions. A tie-line length framework was utilized to define the systems and relate the partitioning behavior of viruses with different surface physicochemical characteristics.

1 Introduction

1.1 Viruses, infectious disease, and immunity

Pathogens have been disrupting the functioning of living beings for ages. Viruses are among the five classes of pathogens responsible for causing mild to severe infectious diseases in animals and humans. These pathogens are essentially small parasites made of protein cage housing nucleic acids (**Figure 1-1**) [1]. In some types of viruses, the protein cage is enclosed in an external lipid bilayer (**Figure 1-1**) [1]. Viruses are designed by nature to obligatorily invade a cell utilizing the host cell's metabolic machinery for their replication [2]. The shedding of progeny viruses leads to an infection of adjacent cells that spreads throughout the tissue or organ. During the replication process, viruses seize

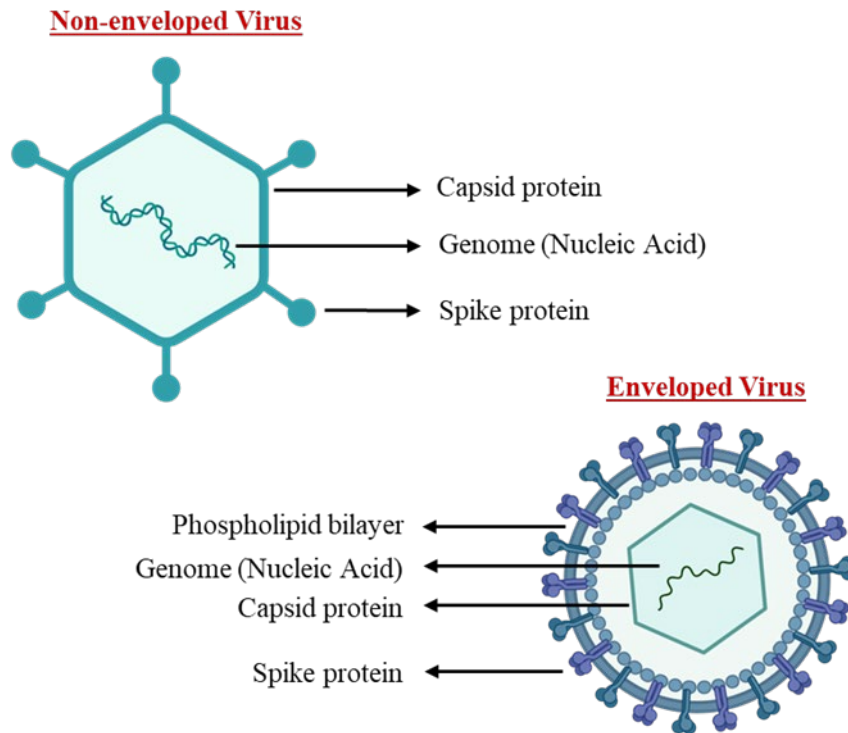


Figure 1-1. The structural basis of viruses: non-enveloped virus and enveloped virus. Virus images were created in BioRender.

the functioning of the host cells, thereby inhibiting the vital operation of a tissue or an organ. A human body encounters numerous types of viruses via different routes of transmission, such as air, water, food, or bodily fluids.

Table 1-1. Human virus species and disease [3]

Virus Species	Structure	Host cell	Disease
Influenza A	Enveloped	Respiratory cells	Flu
Human Immunodeficiency virus		Lymphocytes	AIDS
Hepatitis B		Liver cells	Hepatitis
Herpes simplex virus			Cold sores and genital herpes
Measles		Lung cells	Fever, rash
Polio virus	Non-enveloped	Intestinal cells	poliomyelitis
Hepatitis A		Liver cells	hepatitis
Human papilloma virus		Skin and mucosal cells	Genital/skin warts, cervical cancer
Human rhinovirus		Respiratory cells	Flu
Rotavirus		Gastrointestinal cells	Gastroenteritis

Viruses are one of the integral parts of every ecosystem and have played an essential role in the human evolutionary scheme [4, 5]. However, wild-type viruses are prominently known for causing diseases (common examples of viruses in **Table 1-1**). Woolhouse and coworkers (2012) have listed over 200 viral species known to infect humans, as of 2005 [6], and the list is expected to expand at a rate of 2 viral species/year [7]. With the identification of yellow fever virus in 1901 to severe acute respiratory syndrome virus-coronavirus-2 (SARS-COV-2) in 2019, numerous viruses have been and are causing life-threatening infections in humans. Some viruses such as influenza or rotavirus cause acute diseases, which are sudden and severe infections. Other viruses, such as human immunodeficiency virus (HIV) or human papillomavirus (HPV), tend to persist in causing long-term or chronic diseases. Viral infections of different virus species are linked with a characteristic behavior in terms of etiology, pathology, and epidemiology. Although these areas are a wide field of focus, it is crucial to understand

the viral infections. Each virus species is addressed to infect a specific type of host cells which are present in different parts of the body. It is also established in the previous studies that viral infection vulnerability varies with season [8]. Commonly known seasonal viruses include influenza and common coronavirus, while some of the viruses that spread through direct contact such herpes virus, HIV, hepatitis A virus do not have any seasonal constraints to cause infections.

One of the vital lines of defense is an immune system that is equipped to protect a body against any foreign antigens. If a virus enters a body, the immune system detects the structural composition of the virus or the virus-infected cell and responds to inhibit the viral activity [9]. The immune system operates with two types of responses, i.e., A) innate immune response and B) adaptive (or acquired) immune response [10, 11]. Initially, the innate immune response is triggered when a foreign body or non-self molecules are identified by a family of proteins called pattern recognition receptors (PRR). PRR recognizes a pathogen-associated molecular pattern, such as lipopolysaccharides of gram-negative bacteria, ds-RNA of viruses, or mannan of yeast, which are commonly displayed by a group of germlines [9]. The action by the innate immunity is fast (hours to days). However, the response is generic towards a group of germlines. Simultaneously, the adaptive immune response is triggered that recognizes each pathogen family and species, precisely and in detail. The response action to seize the antigen's activity and proliferation is highly specific. The virus-infected cells and a particular type of professional cells display the antigenic information in the form of epitopes, a small antigenic peptide, on the cell surface. T-cells, a type of immune cell, detect the antigenic peptide through a complex interaction and undergo functional transformation known as maturation to eliminate the virus-infected cells.

In addition to the cell-mediated immune response by T-cells, another group of cells called B-cells, are equipped to synthesize antigen-specific small proteins known as antibodies [12]. The antibodies are designed to attach to a specific region on the virus surface to either neutralize the pathogen or disrupt the virus replication cycle [13]. Both the cell-mediated response by T-cells and antibody-mediated response by B-cells develop

a prolonged memory to detect and neutralize the re-exposure of the same virus. The adaptive immune response is highly efficient and robust as compared to the innate immunity to defend against most viral infections. The response kinetics of the adapted immunity is as fast as the innate response, reaching the peak within hours to days only if the acquired immunity is developed prior to the viral infection. The primary response time is much slower (days to weeks) for the first exposure [10]. The spread of disease due to the exposure of viruses could be averted or mitigated by inducing a stimulated immune response through the safe medical intervention of vaccination.

1.2 Overview

Public health can be protected by designing safe and highly immunogenic vaccines and ensuring a global outreach of the vaccines. A literature review is presented in chapter 2 on the traditional vaccine designs and the current development in designing modular vaccines to improve the immunogenicity and safety for strong long-term protection. Further, the outreach of vaccines depends on the capacity and portfolio flexibility of a production plant. The chapter reviews the vaccine manufacturing stages with a focus on the conventional upstream and downstream processing strategies along with the progress made in each stage to identify and resolve the bottlenecks. As the focus of the dissertation is the downstream purification of the viruses and virus-like particles, mechanisms used in the unit operations of the downstream processing stage have been thoroughly discussed, and the bottlenecks of the conventional unit operations have been identified. Moreover, a potential and unconventional method, aqueous two-phase system (ATPS), a liquid-liquid extraction operation, has been reviewed. In the end, gaps in the understand driving forces of ATPS and optimization framework for preferential biomolecule recovery in ATPS have been identified.

In chapter 3, a framework is proposed to optimize virus recovery and purity in aqueous PEG-citrate system. The system is based on a rational selection of processing parameters and using the phase diagrams consisting of binodal curves and tie lines of aqueous two-phase systems. The recent evidence of unique virus surface characteristics

such as hydrophobicity and charge, combined with the phase forming component characteristics such as polymer amphiphilicity and salting-out ability of ions, were considered in the system selection. Two non-enveloped virus models – porcine parvovirus (PPV) and human rhinovirus-14 (HRV) were included in the study. Further, viral partitioning behavior was studied in the PEG 12kDa-citrate system using a tie line framework to develop an optimization method. A high PPV recovery (~80%) and purity were achieved in the PEG-rich phase at the highest tie-line length studied, owing to a relatively high surface hydrophobicity and net negative surface charge of the virus. The proposed setup significantly reduced the experimental space required for optimizing the virus purification, which is one of the hindrances in commercial implementation. Low recovery of uncharged HRV (~35%), due to the system operated at the isoelectric point of the virus, indicated the necessity of charge in partitioning. The virus models used demonstrated not only the dominance of viral surface hydrophobicity but also indicated the importance of viral surface charge in driving the viral particles to the contaminant-poor phase.

In chapter 4, additives were included in the PEG 12kDa-citrate system to enhance the driving forces for viral partitioning. Water structure modulator molecules, known as osmolytes, were used as additives to achieve high virus recoveries and alleviate the processing conditions such as high system composition and viscosity. Osmolytes glycine, betaine, TMAO, mannitol, and urea were used in the study. Initially, the influence of osmolytes on the phase diagrams was studied to elucidate amendments in the phase characteristics. Further, the efficiency of the osmolyte class on viral partitioning was screened to identify the influential osmolyte. Two virus models, a non-enveloped PPV and an enveloped human immunodeficiency virus-group specific antigen virus-like particles (HIV-gag-VLP), were used to demonstrate the enhanced recovery. The osmolyte efficiency for improving virus recoveries followed the order glycine > betaine > TMAO > urea > osmolyte-free control. Overall, >90% virus recoveries could be achieved in glycine or betaine-containing systems. However, none of the osmolytes affected the contaminant protein partitioning yielding a pure PEG-rich phase with viruses. Further,

the tie line framework was employed for each osmolyte-containing system to demonstrate that high partitioning can be achieved irrespective of the volume ratios of the PEG-rich phase to the citrate-rich phase. Overall, the study demonstrated a strategy to enhance virus purification in ATPS and alleviate high concentration processing conditions that pose challenges in manufacturing.

In chapter 5, the use of a novel affinity ATPS was postulated to improve virus partitioning by enhancing the affinity of the PEG-rich. The specific binding affinity of a trimeric peptide WRW towards PPV was harnessed to enhance the virus recovery in the PEG-rich phase at lower volume ratios, where there are lower PEG-rich phase volumes. 90-100% PPV recovery was obtained in the PEG-rich phase of the systems complemented with the affinity-peptide ligand, without affecting the contaminant partitioning. Further, the affinity peptide-PEG conjugate was characterized by acrylamide quenching that demonstrated the accessibility of the peptide. The accessibility of the peptide was a significant success as PEG chains have shown to shield smaller affinity tags in past experiments. Overall, the use of multimodal affinity peptides achieved high virus recovery in the systems where the PEG-rich phases are the dispersed phase, thereby alleviating the processing challenges of ATPS.

In the concluding chapter (chapter 6), the impact of the current research on the biomanufacturing is expressed by discussing the novel findings. In the end, a course of future work is proposed to gain additional insights into the mechanism of viral partitioning in ATPS and scale-up implementations.

1.3 Reference

1. Carter, J., V. Saunders, and V.A. Saunders, *Virology: principles and applications*. 2007: John Wiley & Sons.
2. Modrow, S., et al., *Molecular virology*. 2013: Springer Berlin Heidelberg.
3. *Human viruses and associated pathologies*. [cited 2020 June 13]; Available from: <https://viralzone.expasy.org/678>.
4. Van Blerkom, L.M., *Role of viruses in human evolution*. Am J Phys Anthropol, 2003. **Suppl 37**: p. 14-46.
5. Löwer, R., J. Löwer, and R. Kurth, *The viruses in all of us: characteristics and biological significance of human endogenous retrovirus sequences*. Proceedings of the National Academy of Sciences, 1996. **93**(11): p. 5177-5184.
6. Woolhouse, M., et al., *Human viruses: discovery and emergence*. Philos Trans R Soc Lond B Biol Sci, 2012. **367**(1604): p. 2864-71.
7. Woolhouse, M.E., et al., *Temporal trends in the discovery of human viruses*. Proc Biol Sci, 2008. **275**(1647): p. 2111-5.
8. Fisman, D., *Seasonality of viral infections: mechanisms and unknowns*. Clinical Microbiology and Infection, 2012. **18**(10): p. 946-954.
9. Clem, A.S., *Fundamentals of Vaccine Immunology*. Journal of Global Infectious Diseases, 2011. **3**(1): p. 73-78.
10. Leo, O., A. Cunningham, and P.L. Stern, *Vaccine immunology*. Perspectives in Vaccinology, 2011. **1**(1): p. 25-59.
11. Medzhitov, R. and C.A. Janeway, *Innate immunity: impact on the adaptive immune response*. Current Opinion in Immunology, 1997. **9**(1): p. 4-9.
12. Chaplin, D.D., *Overview of the immune response*. J Allergy Clin Immunol, 2010. **125**(2 Suppl 2): p. S3-23.
13. Burton, D.R., *Antibodies, viruses and vaccines*. Nature Reviews Immunology, 2002. **2**(9): p. 706-713.

2 Literature Review

2.1 Vaccines and biotherapeutics

One of the ways to protect an individual or public health is to develop an individual or herd immunity against viral infection through vaccination. As stated earlier, the immune system generates a robust defense mechanism if it recognizes a generic or specific component of a virus. This is what the vaccines are intended to do. The main constituent of a vaccine is a virus component immunogen presented to the body to induce an immune response against the injected agent. The injected immunogen stimulates an immune response in the same way as the virus exposure. The adaptive immune system generates a memorized pathway to inactivate the virus which is undertaken by the innate immune system in the event of reoccurrence of a similar antigen [1]. The memory of the immune system results in a short or long-term immunity against the virus exposure.

There are numerous ways to present an immunogen to the immune system. Conventional vaccines are composed of live attenuated viruses (LAV) and inactivated viruses. The two types of vaccines are prepared using a whole wild-type virus. The attenuation of virus is done by passing the wild-type virus in a novel growth condition or reassorting the genotypes of virus species [2, 3]. The unfamiliar growth condition involves a repeated propagation of a wild-type virus in a non-human cell line or an abnormal growth media and temperature, which renders the virus less virulent or non-pathogenic to the original host [3-5]. The later found reassortment method could be accomplished by coinfecting multiple viruses of similar family but different serotypes or subspecies [6-8]. The coinfection results in a mismatch of the interspecies virus genes producing viruses with structural components of the co-infected viruses. A specific virus isolate with immunologically relevant segment and attenuating segment is chosen as a vaccine strain [5]. The second type of whole-virus immunogen is an inactivated vaccine. The inactivated vaccine type comprises of viruses that have been treated chemically by formaldehyde, formalin, and β -propiolactone, or physically by gamma irradiation to disable the infection process [9]. The other types of vaccine designs include presenting a virus structural fragment such as spike protein and nucleic acid, which are called as subunit vaccines. The subunit vaccines are the safest of all the types of vaccines,

however, they provide lowest immunogenicity [10]. Monovalent hepatitis B is one of the well-established viral subunit vaccines available in the market and approved by the WHO [11]. A lower immune response by the subunit vaccines require higher amounts of immune-adjuvants or carriers to optimize the antigen presentation and enhance immunogenicity [12, 13]. Recent developments in the antigen presentation have used VLP as a modular vaccine. VLPs are either viruses void of genomes or antigenic proteins self-assembled to mimic the authenticity of virus structure [14]. Hepatitis B and HPV vaccines are some of the widely accepted and commercially available vaccines [15, 16]. As the VLP-based vaccines have recently gained attention, there are fewer approved vaccines than the whole virus vaccines. However, a substantial progress is being done with more than 20 vaccines approved or in clinical trials [17].

2.2 Viral-based Biotherapeutic Manufacturing

Extensive progress has been made to identify various virus forms as biotherapeutic modalities to induce immunity and treat pre-existing diseases. However, the outreach of biotherapeutics across the world is possible only if they can be produced in sufficient quantities to meet the demand of the ever-growing population and strict regulatory norms. Manufacturing effective biotherapeutics in large quantities has been a challenging question for decades due to their complex nature and behavior. Production of biotherapeutics is majorly divided into three stages (**Figure 2-2**). The upstream stage that deals with the synthesis of active biological ingredients through high-level expressing cell lines, followed by the downstream processing (DSP) to recover and purify the active ingredient from a complex biological broth, containing contaminants such as host cell proteins (HCP), nucleic acids, and growth media components. The final stage of formulation ensures the targeted biologic is suspended in a specifically composed solution to provide prolonged biotherapeutic stabilization during transportation and storage. Although the manufacturing stages remain broadly the same, the process design of the individual stage differs for different viral products due to a high diversity in the

tropism and physicochemical properties. The current focus of the discussion will be the upstream and downstream processing of viral- and viral-like particle-based biotherapeutics and vaccines. The challenges and advances of each stage are explored in the following sub-sections.

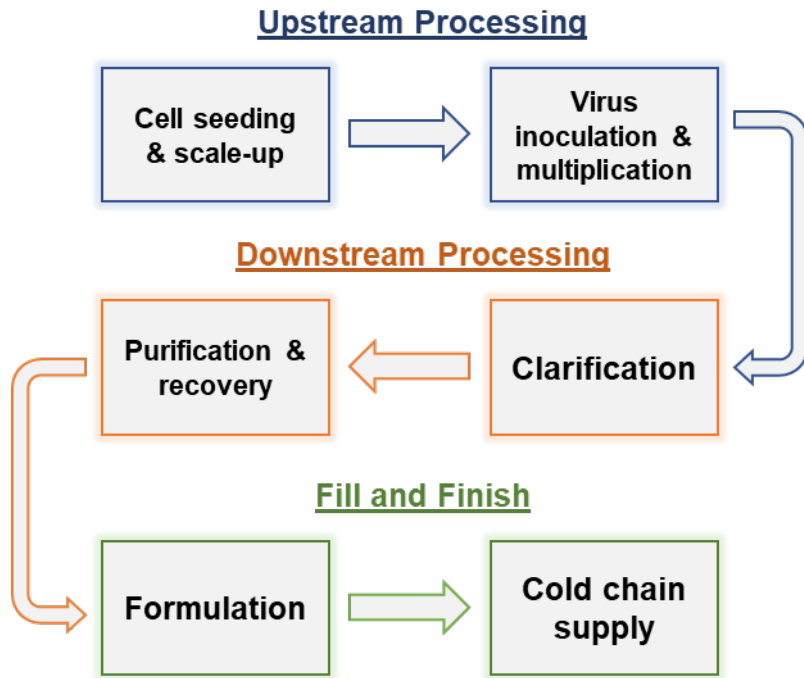


Figure 2-1. General Viral vaccine and biotherapeutic manufacturing scheme

Before understanding the manufacturing strategies of the viral biotherapeutics, it is essential to grasp the research efforts made in the pre-upstream stage to determine the feasibility of an appropriate cell platform for viral vaccine production. Various cell lines are susceptible and permissive for a virus infection. The production of whole virus vaccines has been mainly focused on mammalian, insect, and chicken embryonic (eggs) cell lines (**Table 2-1**). The traditional methods to produce vaccines have utilized chicken embryonic fibroblast (eggs) cell line [2]. However, the vaccines produced in egg-based cell line had shortcomings due to lack of egg supply, possible virus strain mutations,

difficulty in quick adaptation to produce circulating virus strains, possibility of allergies and anaphylactic reactions [18-20]. Thus, the newer generation of vaccines are majorly produced in the primary or diploid cell lines [21]. However, not every cell line has the potential to produce high titers of virus. Different virus species have different sites of replication, mechanisms of virus-host interaction, and growth kinetics [22]. Some viruses require cell nucleus for replication such as influenza virus, herpes simplex virus-1, and adenovirus [23, 24]. Other viruses replicate in the cytoplasm, such as poliovirus, severe acute respiratory syndrome coronavirus (SARS-CoV) [24, 25]. Moreover, most viruses replicate in mitotically functional cells with a few exceptions that can replicate in non-dividing cells such as human immunodeficiency virus (HIV) [26, 27]. Progeny viruses utilize different modes of cell-to-cell transmission, such as extracellular space or cell-cell direct contact sites [28, 29]. Overall, the factors associated with the host cell susceptibility and viral life cycle are considered while choosing an appropriate cell substrate, and even the susceptible cell lines are genetically modified to yield a clone that increases the viral titer [22].

The current motivation is to design a platform cell substrate for a wide range of viral vaccines. However, a potential cell line is screened for multiple characteristics such as the ability to produce high titers of potent viruses, maintain the cell culture stability for longer passages, and meet the safety guidelines of identity, stability, and purity of master cell banks [30, 31]. Most manufacturers are currently inclined towards the approved host cells for a faster commercialization of vaccines due to the strict safety regulations by the FDA and WHO [32]. In this interest, Vero cell line has been widely accepted in the industries for the production of vaccines [30, 32-34].

Table 2-1. Established cell lines currently used in vaccine production and the virus susceptibility [22].

Cell line	Origin	Virus susceptibility
Vero	Green monkey kidney	Poliovirus, influenza A virus, respiratory syncytial virus,
Madin-Darby canine kidney (MDCK)	Dog Kidney	Influenza A, influenza B
MRC5	Human embryonic lung	Varicella zoster virus, rabies, hepatitis A
WI-38	Human embryonic lung	Rubella, adenovirus

A VLP may be a type of subunit vaccines self-assembled to resemble a virus structure or an empty capsid of wild-type virus void of genetic material, making it a non-infectious antigen. VLP expressions have been successfully demonstrated in a wide range of cell platforms such as bacteria, yeast, insect cells, mammalian cells, and plant cells (**Table 2-2**). However, each of the cell platforms has advantages and disadvantages, which are mentioned in **Table 2-3**. The main factors that differentiate between the cell platforms are feasibility of expression by gene recombination or delivery, expression levels for higher antigen concentrations, and post-translational modifications for a close resemblance of a wild-type antigen [17, 35, 36]. Recently licensed VLP vaccines for HepB virus [37] and Gardasil for HPV [38] have utilized yeast-based cell substrates for the VLP expressions.

Table 2-2. Commonly used cell platforms for producing virus-like particles
Commonly used cell platforms for producing virus-like particles

Virus-like particle	Expression system	Cell line	References
HBsAg*	Yeast	Saccharomyces cerevisiae	[37]
HPV 6, 11, 16, and 18	Yeast	Saccharomyces cerevisiae	[39]
HPV 16 and 18	Baculovirus - Insect	Trichoplusia ni Rix4446	[39]
Ebola	Mammalian	HEK-293T	[40]
Zika	Mammalian	Expi293F	[41]

*HBsAg: Hepatitis B surface antigen

Table 2-3. Advantages and disadvantages of cell platforms for VLP production [35]

Cell platform	Advantages	Disadvantages
Yeast	<ul style="list-style-type: none"> • Ease expression • Scale-up potential • Low production cost 	<ul style="list-style-type: none"> • Improper protein glycosylation • Inconsistent folding & assembly
Bacteria (<i>E. coli</i>)	<ul style="list-style-type: none"> • Easy expression • Scale-up potential • Low production cost 	<ul style="list-style-type: none"> • Forbid glycosylation • Presence of endotoxins
Mammalian Cell	<ul style="list-style-type: none"> • Closely related to natural host • Appropriate post translational modifications 	<ul style="list-style-type: none"> • High production cost • Lower titers
Insect Cell	<ul style="list-style-type: none"> • Scale-up potential • High titers of correctly folded VLP • Minimum risk of other pathogens as compared to mammalian cell lines 	<ul style="list-style-type: none"> • Limited post translational modification • Difficult baculovirus contaminant removal

Some of the schemes for viruses and VLP manufacturing are similar in the upstream and downstream stages if a similar cell platform is used to produce VLP as

traditional virus vaccine. The current discussion will focus on the infectious virus production from the mammalian cell platform.

2.2.1 Upstream Processing

The advancements in the host cell screening, and media composition have contributed significantly towards increasing the throughput of the biotherapeutics and vaccines at a lab-scale. However, scale-up of biotherapeutic manufacturing is very challenging as the dynamics of the culture environment changes significantly at larger scales. The following focus to improve the production capacity of viral vaccines was shifted to optimize the bioreactor designing and operation to yield highly potent antigens. Currently, the adherent cell lines, that proliferate when attached to a surface, are predominantly used in the biotherapeutic manufacturing [42]. Moreover, cells maintain their productivity in the exponential growth phase and incur a productivity loss when the growth kinetics reaches equilibrium with the death kinetics due to apoptosis and autophagy [43, 44]. However, some viruses are produced with a single harvest with higher cell densities of metabolically active cells with a low multiplicity of infection (MOI) [45, 46]. The common strategy to scale-up the cultivation is a stepwise increment in the bioreactor size, which is performed in different formats of bioreactor systems [47].

There are two major types of cultivation methods used for cell proliferation and virus propagation- static and dynamic systems [48]. The static bioreactors such as T-flasks, cell stacks, and roller bottles are vessels with unagitated culture media. The dynamic systems such as stirred tank, and wave bioreactors have mechanical agitators to induce mixing for uniform distribution of the media components. Roller bottles are preferably employed for small scale cell culturing, seed cells and inoculate viruses. For a large-scale production, the dynamic systems are used. The systems that achieve higher cell densities ($\sim 10^6$ cell/mL) are of great interest [49]. In this interest, stirred tank bioreactor is preferentially used in the industries for its expertise in operation and hydrodynamic modelling [42]. Most cells are adherent cell lines that is they require a

surface to proliferate except some newly adapted suspension cell lines such as Vero [50, 51] and MDCK [52]. Current operation of stirred tank bioreactors utilizes microcarriers made of polymers as a substrate for the cells to grow [43, 46]. Trabelsi et. Al. (2012) were able to achieve 4×10^6 cells/mL of MRC5 cell lines and produce $10^{6.5}$ infectious measles virus/day using a non-porous cytodex 1 microcarrier in 7 L stirred tank bioreactor. Fixed bed bioreactor is another option being explored for to achieve a high cell density and higher titer of viruses. A study demonstrated that the iCeLLis Nano, a packed bed bioreactor with medical grade polyester microfibers by Pall Corporation, achieved a high cell density of 4×10^6 cells/mL of Vero cells [53]. Moreover, there was a significant increase in the hepatitis A and chikungunya viral vaccine doses as compared to the roller bottle and other undisclosed commercial packed bed bioreactors.

The efforts made to increase the virus production capacity in the upstream sector are impressive. However, the increased virus titer and higher cell densities increases the complexity of the culture broth that has pushed downstream sector to purify and recover high amounts of viruses from a complex HCP profile. Thus, the current bottleneck in the vaccine manufacturing has been recognized to be the downstream processing and efforts are being geared towards the recovering viruses from crude stock [54].

2.2.2 Unit Operation Mechanisms in Downstream Processing

A high vaccine production throughput relies on the yield of unit operations employed to recover viral agents from the contaminants. The purification of viral particles is crucial as the contaminants from the culture broth are unwanted agents in the vaccines and biotherapeutics. The regulatory bodies such as the FDA, CDC, and WHO have imposed stringent guidelines for the industries to evaluate and demonstrate that the final product has minimal traces of the contaminants. For example, the limitations suggested on the residual HC-DNA originating from non-tumorigenic continuous cell lines, e.g, Vero, is less than 10 ng/dose for parental inoculation and 100 μ g/dose for oral vaccines [55]. A robust process design must be implemented to ensure the final products

are nearly free of contaminants. The purification process exploits the differences in the surface characteristics of the viral particles and contaminants (proteins and nuclei acids) to gently separate them without disturbing the structural and functional integrity of the antigens. However, the virus surface and behavior are very complex, and they share some physicochemical properties with the contaminants. This makes the purification process very complicated and thus utilizes a train of unit operations each harnessing a unique intermolecular interaction to differentially interact with the biomolecules. The methodology, advantages, and disadvantages of these separation technologies are discussed below.

2.2.2.1 *Conventional Methods and their upgrades*

2.2.2.1.1 Size-based separation

One of the characteristic differences between a virus and contaminants is the size. A typical hydrodynamic diameter of viruses (20-300 nm) is much larger than the contaminants' size (< 20 nm). Obviously, the separation of these biomolecules based on the size differences was the first choice in developing the unit operation. Three types of methods – filtration, ultracentrifugation, and size exclusion chromatography, have been developed which use size as the driving parameter. The membrane-based filtration is used at multiple stages of the downstream processing. The filtration at the clarification step is used to remove larger contaminant particles such as cell debris and microcarriers, if used, from the culture broth [56]. Commonly used filtration-based technique utilize a microfiltration mode with pore sizes ranging from 0.45 μm to 10 μm [57]. This pore size range retains the larger contaminants on the filter and allows the smaller particles, viruses, proteins, and nucleic acids, to flow through the filter. This method is widely used in most of the biotherapeutic manufacturing strategy. The other filtration technique - diafiltration is used post-purification step as a buffer exchanger to resuspend the viruses in the desired solution for the formulation of the vaccines and biotherapeutics. Diafiltration is a type of ultrafiltration which exchanges the pre-suspended buffer with a new buffer by mixing the retentate with the desired buffer and repeating the filtration

again until the pre-suspended buffer dilutes down to an acceptable concentration [58]. The ultrafiltration membranes are rated as the molecular weight cutoff (MWCO), which retain any particulate with a larger molecular weight than the rated MWCO. A typical filter used in this step has a MWCO range of 100 kDa (~10 nm) to 1000 kDa (~100 nm). Appropriately selected membranes yield a high step recovery and high flowrate, however, are prone to viral losses due to virus-filter non-specific interactions and high shear rates [57, 59].

The membrane chemistry is an important aspect while selecting a filter, as the polymers used to prepare the filters affect the separation efficiency. Polypropylene, regenerated cellulose, cellulose acetate, and polyether sulfone are some of the prevalent membrane filters used in the biomanufacturing. Viruses adsorb on the filter due to specific and non-specific interactions with the filter material. Most viruses are negatively charged at the physiological pH (~7), as the pI of the viruses are generally between pH 3.5-7 [60]. Negatively charged viruses have been shown to adsorb on the positively charged membranes [61]. Therefore, such membranes might be useful in the antibody manufacturing where antibodies are the target product and viruses are contaminants. Moreover, the hydrophobic membranes, such as polyether sulfone, cause biofouling due to the virus adsorption by hydrophobic interaction [62]. If the viruses are the target biomolecules, more hydrophilic membranes with low zeta potentials might be used to avoid any electrostatic and hydrophobic interactions [63]. Such intermolecular interactions are easily mitigated by selecting the appropriate buffer compositions and surface modifications to membrane or inert materials such as polypropylene [64]. However, these interactions are not significant as compared to the fouling and shearing phenomena that hinders the yield of viruses [65].

Filtration is operated in two modes – dead-end/depth mode and tangential/cross flow (TFF) mode. The feed flow is parallel to the permeate stream in the depth filtration mode and tangential in the crossflow filtration (See **Figure 2-2**). The depth filtration generally achieves a high purity in the retentate with a decreasing permeate flux. A higher feed volume leads to membrane fouling due to particulate accumulation at the

membrane interface causing a high degree of concentration polarization. The plugged pores cause a high transmembrane pressure that affects the potency of the viral products due to structural damage, especially enveloped viruses, and aggregation [54, 66]. A TFF mode is used to alleviate the flux issues and structural damage to viruses. This mode of operation reduces the concentration polarization along a membrane by sweeping the viral particles off from the membrane [63]. The flux reduces until an equilibrium concentration polarization is reached and attains a saturation. However, shear sensitive viruses are still susceptible for structural damage. Moreover, TFF are more suitable for low cell density cultures, as TFF is operated at much lower pressures (~0.7 bar) [54, 67]. Among the two modes of filtration, the tangential flow filtration is commonly used to optimize the processing capacity and time. Overall, the microfiltration and ultrafiltration techniques are still highly preferred method for clarification and post-polishing steps due to its ease of operation, scale-up ability, and versatility.

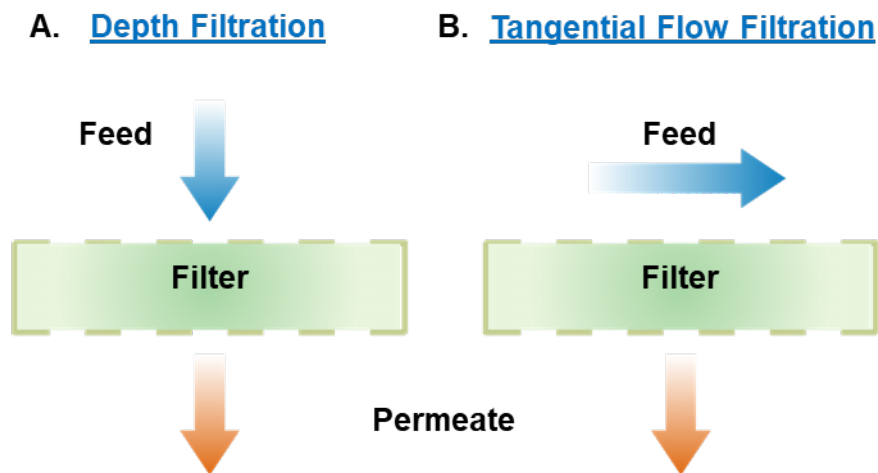


Figure 2-2. Operating modes of filtration – A) Depth filtration and B) Tangential flow filtration. This image was created in BioRender.

Another method using size-based separation of biomolecules is the ultracentrifugation. This centrifugation technique utilizes density gradient mechanism to

separate viruses from the contaminants (see **Figure 2-3**). The solutions such as sucrose, caesium chloride (CsCl) [68], and iodixanol [69] are prepared in graduated concentrations and layered in a tube with the decreasing concentration from the bottom. A crude stock applied at the top comprising of the minimum density layer and centrifuged at high speeds in the range of 30000-300000 x g [68, 69]. Viruses being denser than contaminant proteins and DNA settle in the heavier layer as compared to the contaminants (see **Figure 2-3**). Two types of approaches used to develop a density gradient are - rate-zonal centrifugation and isopycnic centrifugation. The rate-zonal separation is a method in which the crude is added to the top layer of the density gradient and centrifuged for an optimized time. In this method, the density of the media should be lower than the density of target biomolecule [70]. The biomolecules settle at a different density layer depending on the characteristic sedimentation rate which is a function of the size, density, centrifugal force, and the physicochemical profile (density and viscosity) of the gradient [71]. Segura et. Al. (2006) demonstrated a 36.5% retroviral recovery in 10-30% continuous iodixanol gradient [72]. Such a low recovery of the virus in a single step is not feasible to produce a high throughput of the viral biotherapeutics. On the other hand, isopycnic centrifugation operated by pre-formed gradients in a tube separate the biomolecules solely based on the density difference [71]. Gias et. Al. (2008) demonstrated a 71% recovery of human respiratory syncytial virus in an iodixanol gradient centrifugation [73]. This recovery is acceptable for a large-scale manufacturing. The density gradient centrifugation has the capacity to both purify and concentrate the viral particles in a single step [54]. This is one of the oldest techniques used at a laboratory scale. However, this method is not feasible to be used at industrial scale because of the disadvantages of labor-intensive and non-scalable [65].

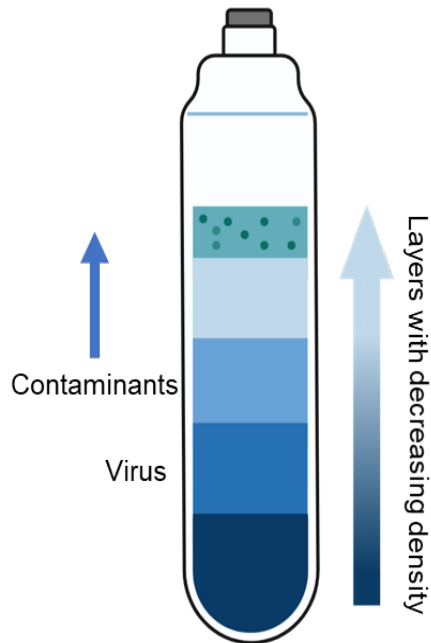


Figure 2-3. Principle of virus purification in density gradient centrifugation.
This image was created in BioRender.

The third method of purification that uses differences in the size of biomolecules is a size exclusion chromatography (SEC). This column chromatographic method is one of the four modes of chromatography-based separation. A column is packed with beads having crevices or pores with some rated MWCO as the filters. The separation of biomolecules depends on the residence time in the column before eluting out of the column (See **Figure 2-4**). Viruses are larger than the pore size of the bead crevices and are thus excluded from the pores. Viruses follow a path of inter-bead void volume to elute from the column. On the other hand, smaller contaminants diffuse in the pores which increases their residence time in the column. The viral particles with the lower residence time elute earlier than the contaminants thereby separating from the contaminants. However, it has been shown that viruses and other biomolecules might interact with the packing materials [74, 75], generally composed of agarose gel-based complexes or synthetic polymers like methacrylate-based copolymers [75]. The

interaction between the virus and the packing material increases the residence thereby decreasing the resolution of separation. However, the main disadvantages of SEC are dilution of the product, low processing capability, and poor distribution of media flow at larger scales [54]. For the larger scale operations, SEC is possibly replaced by the ultrafiltration method [54].

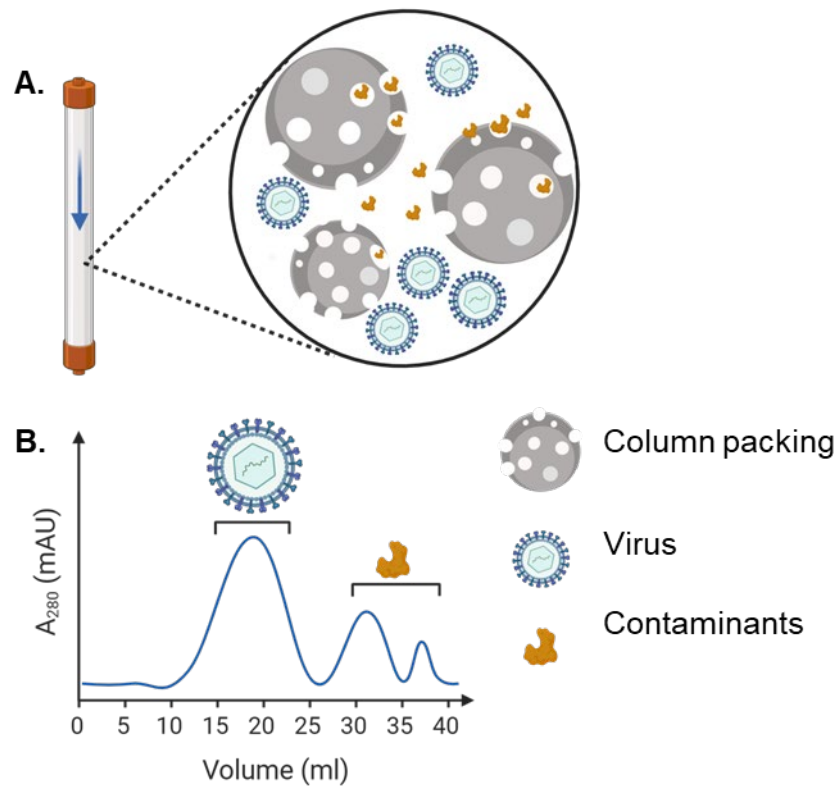


Figure 2-4. Principle of size exclusion chromatography for virus purification. A) Column pores allow diffusion of small contaminant proteins and exclude viruses. B) A typical chromatogram showing increased residence time of proteins, which elute later than viruses.

2.2.2.1.2 Charge-based separation

The charge on amino acids determines the net charge of a protein. An amino acid is negatively charged in a solution with pH higher than the pKa and positively charged if

the pH is lower than the pKa. However, if the solution pH is identical to the isoelectric point (pI) of a protein, the net surface charge is zero. Most viruses have a

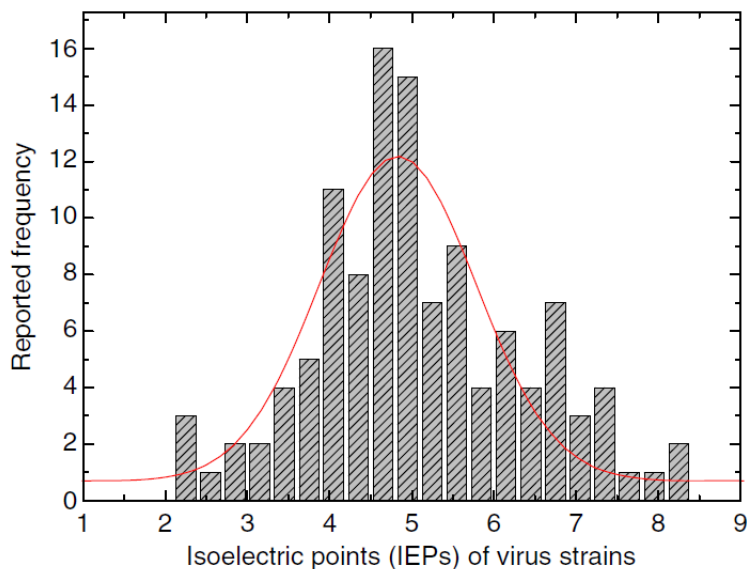


Figure 2-5. Frequency of isoelectric points of viruses reported in literature. Reprinted with permission from [71].

pI in the pH range of 2.1 – 8.3 with a mean of 5.0 (see **Figure 2-5**, [60]), while HCP impurities can range from 2-11 [76]. The change in the pH away from the pI also changes the net and relative surface charge of the biomolecules, which is commonly measured using a bulk characterizing measurements - zeta potential, isoelectric focusing, and electrophoretic titration curves [65]. The charge distribution on the surface is regulated by the complex and long sequences of amino acids with varying pIs and electrostatic interactions with the ions in a solution [77]. The difference in the net charge and the charge densities between viruses and impurities are utilized to purify viruses.

Ion exchange chromatography (IEC), one of the four modes of chromatography, is one of the prominently used methods in biotherapeutic manufacturing during the purification step [78]. The IEX column is packed with resins (stationary phase) carrying ionic charges, either positive (anion exchanger, AEX) or negative (cation exchanger, CEX) charges. The electrostatic interaction between the virus and resin is promoted by

the mobile phase using a pH at which the viruses are oppositely charged. AEX with quaternary amine or primary amine-functionalized resins are commonly used, as most of the viruses with $pI \leq 7.4$ bind to the positively charged resins. The binding conditions may allow the majority of the contaminant proteins to elute in the flow-through without binding to the resin. The differential elution of viruses and some bound protein impurities can be achieved by varying the pH or increasing the salt concentration [79]. However, the stability of monodispersed viruses, especially enveloped viruses, persists in a narrow pH range [65, 80]. Thus, salt gradient, in the range of 100 – 1500 mM, is commonly used in the virus purification, where the contaminant proteins elute at lower concentrations as compared to viruses [81, 82]. A careful selection of salt gradient combined with a pH change can achieve high resolution in the elution profiles, even for closely related physicochemical properties of virus and protein impurity. However, some of the challenges faced in this purification method are pore inaccessibility for viruses, low dynamic binding capacities, mass transfer properties, and limited flow rates [54].

The commercial resins have pore sizes ranging from 30-300 nm, and smaller proteins with higher diffusion rates occupy these pores, excluding the larger sized, low diffusive viral particles [83]. The inaccessibility of the surface area for virus-resin interaction lowers the dynamic binding capacities of the resins [83]. Recent studies suggest the use of membranes to improve the binding capacities and mass transfer properties [84]. Mass transport in these setups is regulated by the convection, thereby overcoming the diffusion limitation in the resin pores [85]. One of the studies explored the impact of increasing DAAE (diethylaminoethyl) ligand densities to enhance the recombinant baculovirus yield [86]. However, a lower ligand density demonstrated a 20% increase in the yield as compared to the commercial membrane [86], suggesting that the optimum ligand density depends on the virus species. One common challenge faced is that the multiple binding sites with different binding strengths hinder a smooth elution through the column and add to the shearing of viruses. Moreover, it has been shown that unwanted interactions, such as hydrophobic interaction of viruses with the resins, also

makes the choice of elution conditions difficult [87]. Thus, more control over the elution media and condition needs to be explored to improve the purification efficiency.

2.2.2.1.3 Hydrophobicity-based separation

One of the surface characteristics that differentiate biomolecules is surface hydrophobicity. A molecular composition with a lower solvent-exposed hydrophilic to hydrophobic ratio increases the hydrophobicity of a biomolecule. In proteins and virus capsids, amino acids with aliphatic and aromatic side chains contribute to the hydrophobicity of the structure. Enveloped viruses have some solvent side glycoproteins that contribute towards the surface hydrophobicity, while the solvent-exposed lipid bilayer is extremely hydrophilic due to the polar head group. The detailed surface characteristics of viruses are not well understood, as this is still a growing area of interest. However, the differential hydrophobic interactions between viruses or proteins with a hydrophobic functional group of a third molecule have been studied.

Hydrophobic interaction chromatography (HIC) is a mode of chromatography that utilizes the differences in the hydrophobic interaction strength of viruses and proteins with the hydrophobic ligands immobilized on resins. The interaction with the ligands is induced by loading the crude at high salt concentration [88]. The kosmotropic ions and biomolecules compete to maintain the hydration shell. The excess ions, beyond the thermodynamic equilibrium, result in the weakening of the hydration shell of biomolecules, thereby exposing hydrophobic patches on the surface. The exposure of hydrophobic components decreases the system entropy and increases the biomolecule free energy, which promotes the interaction between the hydrophobic patch and immobilized ligand to reconfigure the hydration shell of the complex. The biomolecule-ligand complex strength varies depending on the type and number of hydrophobic components involved, which is regulated by the ionic strength of the mobile phase. Lowering the salt concentration of the mobile phase disrupts the hydrophobic interaction, which allows the biomolecule to elute from the column. Larger viruses contain more

hydrophobic patches than proteins, the virus complexes are disrupted at much lower salt concentrations than proteins. Thus, the salt gradient applied in the mobile phase separates the viruses from the protein impurities.

Various hydrophobic ligands are commercially available, displaying alkyl (butyl, octyl, ether, and isopropyl) and aryl (phenyl) functional groups [89]. Longer alkyl chains provide stronger hydrophobic interactions and phenyl groups supplement the hydrophobic interactions with the π - π interaction [90]. One of the studies showed a 92% recovery of inactivated foot-mouth-disease virus (FMDV) using butyl Sepharose resin and 26% recovery with phenyl Sepharose [88]. It demonstrated that the viruses were bound too strongly at 0.8 M $(\text{NH})_2\text{SO}_4$ to enrich the product in the elution step using phenyl Sepharose resin. If the interaction is too strong the recovery and purity both decreases, on the other hand, if the interaction is too weak viral loss might incur in the flow-through [91]. Moreover, this study also demonstrated that the HIC (60%) achieved much higher recovery than IEX (17%) for Mumps and Measles viruses. However, HIC is seldomly used in industry for vaccine manufacturing. The virus elution from the stationary phase require high salt concentrations and the column chromatography induces shear stress, both disrupting the structural integrity of viruses [54].

Recent interest has geared towards the use of ligands utilizing multiple physiochemical properties (charge, hydrophobicity, and hydrogen bonding) of the biomolecules to increase the specificity of binding and elution in the chromatographic methods [92]. The conventional multimodal ligands comprise of small functional molecules such as octyl amine (CaptoTM Core 700, GE Healthcare), N-benzyl methyl ethanolamine (CaptoTM adhere, GE Healthcare), and N-benzoyl-homocysteine (CaptoTM MMC, GE Healthcare). The binding and elution conditions are unique to a given biomolecule that not only improves the recovery but also enriches the purity of the vaccine product. However, the binding mechanisms of each virus has to be studied in detail to understand the optimal processing conditions. The binding studies of phages PR772, PP7, and Φ X-174 with the Capto adhere showed that the comparatively hydrophobic phages PR772 and PP7 bound to the resin via synergistic electrostatic and

hydrophobic interactions as compared, while the less hydrophobic Φ X-174 bound to the resin only through the electrostatic interaction [93]. This suggests that the process development of every virus product with Capto adhere resin would need extensive research. Thus, Capto 700 resin is more frequently being studied as this resin is developed based on the flow-through mode as compared to the bind-and-elute mode of other resins. The flow-through mode is when the target viruses are collected in the flow-through during the loading step, while the impurities bind to the resin [94]. The Capto Core 700 uses a functionalized core and an unfunctionalized shell that allows smaller proteins to diffuse into the pores to strongly interact with the ligands [95]. Viruses, unable to diffuse into the pores due to size exclusion, elute without interacting with any ligands [95]. Some recent studies showing the efficiency of multimodal chromatography are shown in **Table 2-5**.

Table 2-4. Virus and VLP purification in Capto Core 700 multimodal resin

Virus	Recovery (%)	Purity (%)	Reference
Influenza A VLP	89	60	[95]
Influenza A virus	79	66	[96]
Zika VLP	90	112	[97]
Yellow fever VLP	89	98	[97]
Yellow fever virus	65	99	[98]
Respiratory syncytial virus	100	87	[99]
Rabies virus	87	94	[100]

2.2.2.1.4 Affinity-based separation

The multimodal resins, such as Capto Core 700, have shown promise in the polishing step but may need additional chromatography steps beforehand to achieve the desired purity of vaccines [98, 100]. With more steps, higher losses are incurred in the virus yield [101]. A novel approach to mitigate the footprint of the process equipment has been the affinity ligand development to increase the specificity in the bind-and-elute

mode for viral particles. The affinity ligands explored to date include virus-specific antibodies [102, 103], protein-based lectin [104, 105], metal ions [106, 107], and polysaccharide-based heparin and heparan sulfate [108, 109]. The mechanism and advantages of these ligands are described in **Table 2-6**.

Table 2-5. Affinity ligands binding mechanisms and processing attributes [110]

Affinity ligand	Binding mechanism	Advantages	Disadvantages
Antibodies	Antibodies interact with specific antigen domain	<ul style="list-style-type: none"> • High specificity • Yields high purity 	<ul style="list-style-type: none"> • High production cost • Complex molecules with stability issues
Lectin	Carbohydrate recognition domain of lectin binds to specific antigen carbohydrate	<ul style="list-style-type: none"> • Specific binding to virus surface glycoproteins • Used for intact virus purification 	<ul style="list-style-type: none"> • Possible affinity to cell culture-derived glycosylated proteins • Lacks consistency for batch-to-batch variation in glycosylation pattern of contaminants and target
Immobilized metals	Metal ions interact with electro donor groups on target virus surface	<ul style="list-style-type: none"> • High ligand stability • Low cost 	Production issues to achieve purified tags
Heparin and heparan sulfates	Resemble receptor ligands of host substrate	<ul style="list-style-type: none"> • Stable ligand structure • High tolerance for denaturing agents in process stream 	<ul style="list-style-type: none"> • Promotes non-specific binding of contaminant proteins • Requires high ionic strength for dissociation and elution

Among the above-mentioned ligands, an antigen-specific antibody shows the highest binding specificity towards viruses, which can yield a high purity of the viral particles. Due to the antibody production cost and stability issues, the approach has been directed towards developing short peptides with 3-12 amino acid residues that mimic the specific interaction mechanism of antibodies [101, 110]. The high affinity peptides can be

either a closed ring cyclic structure or an open chain linear structure. Ho et al. (2017) identified cyclic peptides C-WSFFSNI-C and C-WPFWGPW-C that bind tightly to HBcAg as the previously screened linear peptide LLGRMK [111]. The binding mechanism of peptides with viruses can vary. The high affinity of cyclic peptide C-WSFFSNI-C towards HBcAg was suggested as the hydrogen bonding mechanism while the other cyclic peptide C-WPFWGPW-C was anticipated to interact with the hydrophobic regions on the surface [111]. An octamer, DWDLRLLY, identified was found to bind to the hydrophobic residues of the major coat protein VP1 of murine polyomavirus like particles [112]. In another study, YKLYYY hexamer binding to the VP2 capsid protein of porcine parvovirus was suggested to be constrained to the secondary structure of the hexamer, docking in the capsomere pocket [113]. The large library of screened affinity peptides has the potential to be included in the purification step. However, more studies are needed to identify optimal conditions for the processing of viral particles. Overall, there is still a gap in the comparison studies between the novel chromatographic modes with traditional methods, and economic feasibility analysis needs to be evaluated [110].

2.2.2.2 The conventional downstream processing train

The yields obtained in a single unit operation, using any separation mechanism, is generally not enough to meet the regulatory criteria of purity. Thus, multiple unit operations functioning with different mechanisms are employed in a series to achieve the desired purity, final buffer solution, and dose concentration (**Figure 2-6**). Unlike antibody production, vaccine manufacturing lacks a platform downstream processing strategy. Every virus has a unique behavior with a wide range of characteristics. The virus surface topologies are complex, and studies have employed different mechanisms to separate viral particles from the different classes of contaminants at each DSP stage (**Figure 2-6**). Bandeira et al. (2012) utilized depth filtration for clarification, DEAE AEX in the purification step, 100 kDa vivaflow ultrafiltration for concentration, and SEC for the polishing step to develop a DSP train for lentivirus production [114]. The chromatographic steps were the least yielding unit operations (80% in AEX, and 68% in

SEC), which achieved a cumulative virus recovery of 36%. In another study of inactivated HAV vaccine (VAQTA®) production, a long series of the traditional methods were utilized in the DSP [115]. The clarification was performed using ultrafiltration, which was followed by Benzonase® treatment. The clarified product was processed through AEX, followed by PEG precipitation and solvent extraction in the purification step. The polishing step included AEX followed by SEC. The viral product was then inactivated using formaldehyde for the vaccine formulation. The use of three chromatography modes, and a time-consuming laborious PEG precipitation yielded a final virus recovery of 20% and 99% purity [115].

The strategy to include novel modes of chromatography for increasing the selectivity and recovery of viral particles has been shown in some studies. One of the steps where this reform was explored is the polishing step by using a multimodal-based Capto Core 700 resin in the negative mode chromatography. For example, the proposed DSP train of inactivated yellow fever virus vaccine included clarification by microfiltration followed by AEX in the purification step with a final polishing step using Capto Core 700 [98]. This two-step purification process (regarded clarification as a midstream stage) yielded an overall 53% virus recovery with ~99% purity. Overall, the progress is being made rapidly to explore and include novel methods in the DSP train.

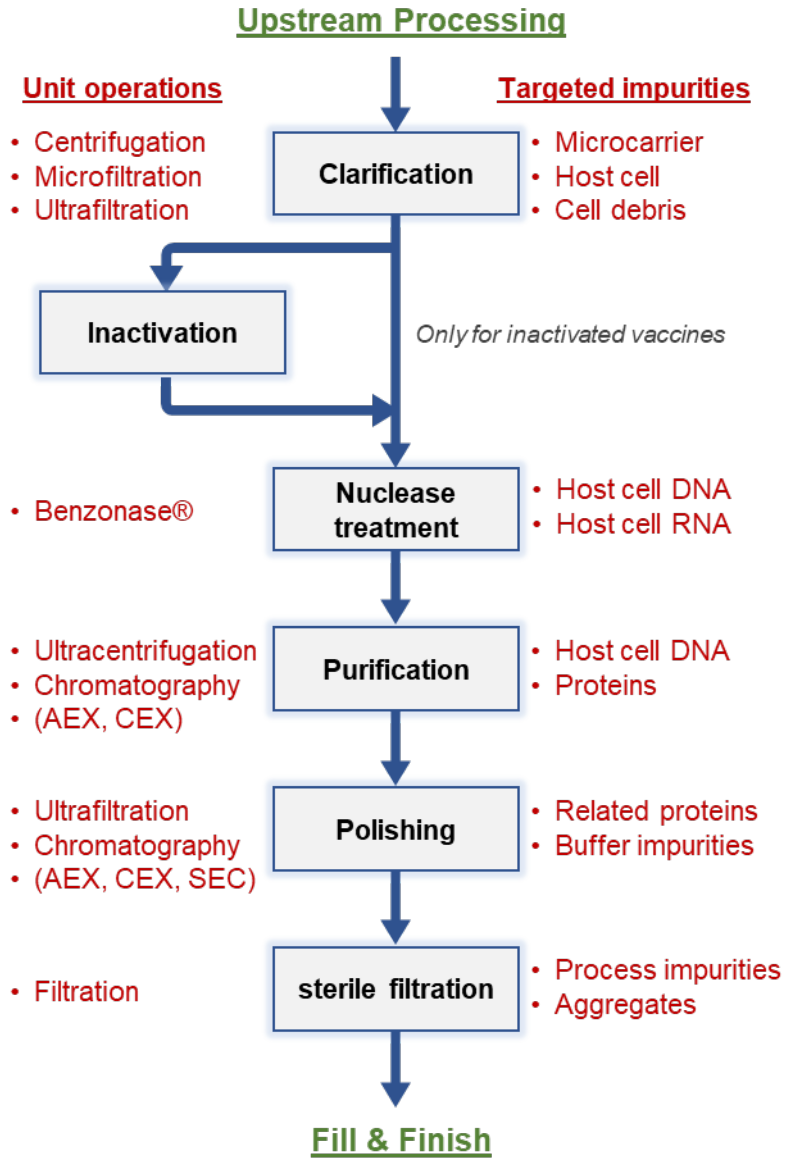


Figure 2-6. Unit operations in the DSP train and their purpose. Reused with permission from [59]

2.2.2.3 Continuous Integrated Processing: Vision for Biotherapeutic Manufacturing

The rapid growth in the demand for the vaccines and biotherapeutics, along with the need to reduce the production cost and increase product quality, has motivated scientists and engineers to explore next-gen strategies [116]. One of the strategies

currently being considered to enhance productivity and economic benefits is the continuous manufacturing capability with integrated processes [117]. Most of the existing biomanufacturing facilities operate in the batch mode, for which the way to enhance the productivity is by improving the yield of individual unit operations combined with scaling up the size of the unit operations. However, an increase in the scale-up not only increases the facility footprint but might also hinder the flexibility of the product portfolio [118]. Some studies have evaluated the economic benefits of shifting to continuous processing and have shown to reduce the costs substantially [119, 120]. The idea of continuous manufacturing is to integrate the upstream processing and downstream processing with minimum or no hold up in between each of the unit operations. One study suggested a hybrid model where some unit operations function in the batch mode and others in the continuous mode [121]. The combination evaluated for a fed-batch culture integrated with a continuous capture step and a batch polishing step for monoclonal antibodies was found to be more economically feasible and flexible for the companies of all sizes with multiple product portfolios [121]. However, such feasibility studies have rarely been performed for viral manufacturing. The general vision with the integrated continuous viral manufacturing is to develop a downsized ballroom like facility which would still produce the required number of high-quality doses [122, 123].

Focusing on downstream processing, one of the major bottlenecks in continuous operation is the chromatographic method of separation [124]. Advances are being made to address this issue. Some strategies recommended to operate a continuous chromatography included the use of multiple columns to keep a constant output flow [124]. The concept of using multiple columns is to keep the process steady by utilizing the columns alternatively in the active and passive state. This is achieved by simulated moving bed (SMB), which indicates a periodical use of columns for loading and eluting the biomolecules [125]. However, the use of multiple chromatography columns might only increase the facility size and is counter-intuitive to the future paradigm of ballroom-sized biomanufacturing. Moreover, it has also been shown that an increase in the chromatography steps increases the process mass index, which is the amount of raw

materials used per unit mass of active pharmaceutical ingredients [126]. The impact of increased process mass index was suggested to harm the sustainable and green biomanufacturing initiative [126, 127]. Some studies have shown that the use of SMB reduces the processing cost, buffer, and water usage but increases the resin cost, which is one of the major expenses of the DSP [128]. Thus, some of the groups have been exploring unconventional methods to potentially substitute for the current challenges of productivity, cost, time and energy consumption, facility architecture, and environmental factors in the biomanufacturing.

There is a motivation to improve the DSP by reducing the number of unit operations and equipment used in the unit operations while increasing the production capacity. One such method being explored is a liquid-liquid extraction (LLE)-based unit operation.

2.2.3 Liquid-Liquid Phase Separation

The conventional use of LLE in the petroleum refineries employ organic-organic or organic-water phases to extract a solute from the mixture into either organic phase or aqueous phase. However, most organic solvents such as benzene, toluene, and acetonitrile, etc. are denaturants for biological materials. The discovery of two-phase systems (ATPS) composing of aqueous solutions, by Beijerinck (1896), opened opportunities for various applications for the bio micro and macromolecules [129]. The formation of two incompatible phases was observed after a certain critical concentration of phase forming components, while the lower compositions yielded a homogeneous solution. In contrast to the completely immiscible organic-water systems, the aqueous two-phase systems (ATPS) are partially miscible systems that generate two incompatible phases. The partially miscible phases signify that a fraction of both the aqueous solutions is distributed between the two incompatible phases. The component distribution in the phases leads to one phase being rich in one of the components, and the other phase rich in the counter component used to form two-phases. The partially miscible aqueous solutions form two incompatible micro (precipitate and complex coacervate) or macro-phases

[129]. Two such microphase separation methods are polyethylene glycol (PEG) precipitation in high ionic strength aqueous solution and colloidal complex coacervation of oppositely charged polymers in low ionic strength aqueous solution (see **Figure 2-7**). The immiscibility of the incompatible aqueous phases is an excellent means to separate biological materials by preferentially partitioning the target biomolecule in one phase (preferentially in the microphase) and the contaminants in the other phase. However, due to their time consuming and labor-intensive operation, they might not be feasible for large-scale bioprocessing. The use of aqueous solutions that form two macro-phases upon separating is notable for the downstream processing of biomolecules (see **Figure 2-7**).

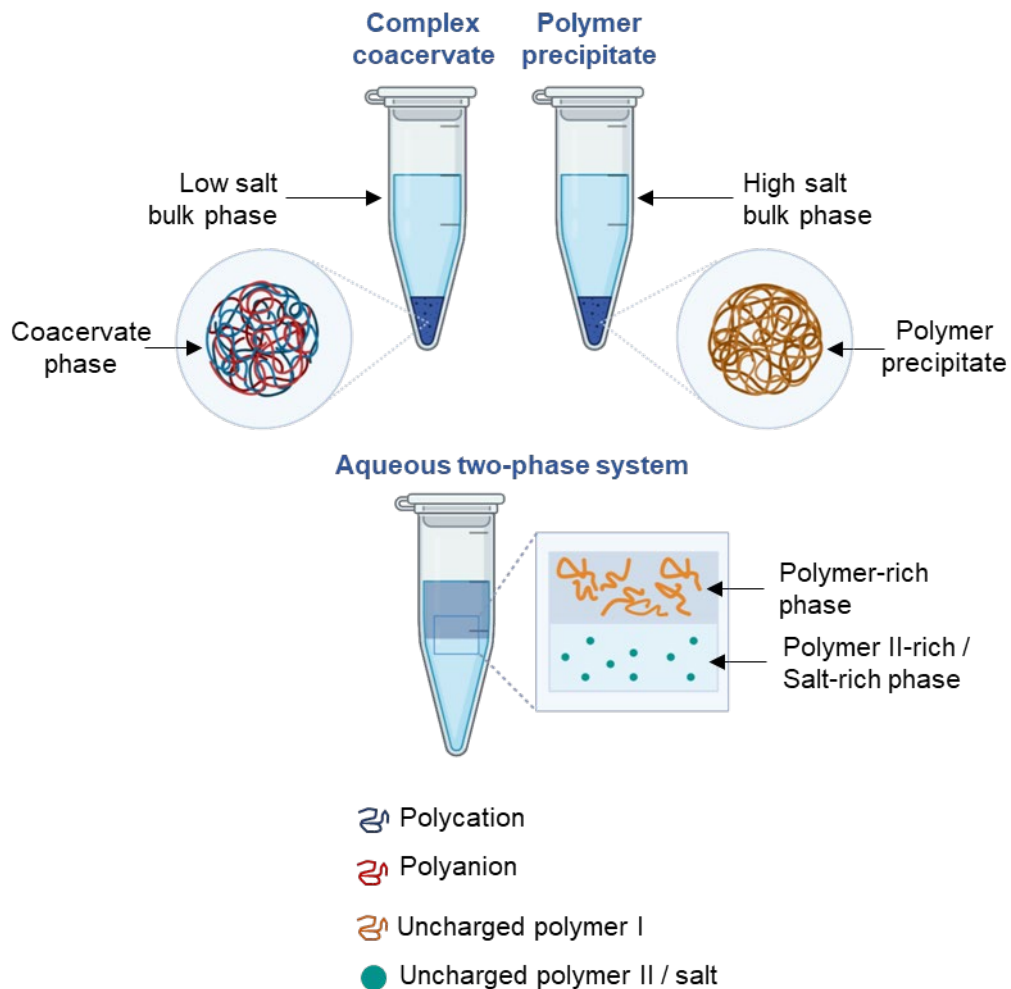


Figure 2-7. Different types of two-phase systems used for biomolecule partitioning. The image was created in BioRender.

The macro aqueous t/wo-phase systems (ATPS) were traditionally generated using aqueous polymer-polymer or polymer-salt pairs (**Table 2-7**). Polyethylene glycol-dextran/dextran sulfate is a commonly used polymer-polymer system. The separation of two phases yields a PEG-rich phase and a dextran-rich phase with a fraction of the complementary component in each of the polymer-rich phases. Similarly, a PEG-salt system yields a PEG-rich phase and a salt-rich phase. The equilibrated two immiscible phases have been suggested to prevail as hydrophobic-hydrophilic pairs [129]. For example, the hydrophobic PEG-rich phase is complemented with a hydrophilic dextran-rich phase or salt-rich phase. A combination of these phase property differences and biomolecule surface properties drive the biomolecules either to the top phase (polymer-rich phase), the bottom phase (polymer/salt-rich phase), or the interface between the top and the bottom phase. The variation in the physicochemical characteristics of different biomolecules decides the target partitioning phase for a given system, which is used to segregate biomolecules between the two-phases. The partitioning of biomolecules between the two phases is given by a partitioning coefficient (K), as shown in equation 2-1 [129]

$$K_C = \frac{C_T}{C_B} \quad (2-1)$$

where, C is the concentration of biomolecule in the top phase (T) or bottom phase (B). The systems are designed to achieve a distinct partition coefficient for the target biomolecule and contaminants to achieve separation. Novel phase forming component pairs such as ionic liquid-salts (**Table 2-6**) are being investigated for their added relative deviation in the physicochemical characteristics to achieve better separation of target and contaminants.

Table 2-6. Phase forming components for ATPS [130]

ATPS type	Phase forming components
Polymer - polymer	PEG - dextran
	UCON - dextran
	PEG - sodium polyacrylate
Polymer - salt	PEG - phosphate
	PEG - sulfate
	PEG - citrate
Ionic liquid - salt	[N _{2,2,2,2}] Br - citrate
	[Bmim] BF ₄ - phosphate
	[C ₄ MIM] Br - sulfate
Micellar	Triton X-100 - citrate
	PEG - Triton X-100

ATPS has been explored as a potential alternative to conventional unit operations, mainly chromatography. ATPS consists of water as a major component (>70%), which is essential for the stability of biological materials. Moreover, the two-phase systems provide processing advantages such as low-cost raw materials, gentle environments for biologics, easy scalability, and continuous operation [131, 132]. The phase forming components such as PEG, dextran, salts are less expensive than the chromatography resins. A direct comparison of IEX and ATPS for penicillin acylase demonstrated a lower operational cost and higher recovery of the enzyme in the PEG-phosphate system [133]. Rosa et al. (2011) assessed the operating cost of ATPS and concluded that ATPS would alleviate the operating cost by 1.5 fold as compared to the protein A chromatography used for antibody purification [134]. However, such process economic analysis has not been performed for the viral vaccine manufacturing scenario. Another benefit of ATPS is easy scalability. The scale-up of ATPS has been shown to yield similar partitioning behavior of proteins with high recovery [132]. Conventional LLE equipment, such as

mixer-settler and counter-current partitioning, which are commonly utilized in chemical industries, can be easily adapted to the bioprocessing [135, 136]. Moreover, ATPS has been demonstrated to easily adapt to continuous operation and integrate into the downstream processing at the laboratory scale [137, 138]. Common process design for continuous operation may include an inline or online static mixer with a tubular separator or a conventional mixer tank with a separator [138, 139]. These advantages have motivated the exploration of the potential of ATPS as a purification method for numerous biological materials.

ATPS has been applied in the purification of numerous biomolecules. However, many studies have focused on antibody and enzyme purification. Purification of biotherapeutics using ATPS has been focused on cells, antibodies, nucleic acids, and viruses. The biotherapeutic applications have targeted the primary clarification and purification steps of the DSP train [132]. Cell-based regenerative therapeutics have gained interest in treating diseases such as osteoarthritis, Parkinson's disease, ALS, and heart failure [140]. Stem cell therapy involves a differentiated form of the pluripotent cell and demands the separation of differentiated and undifferentiated cells in the DSP [141]. The antibody therapy, such as monoclonal IgG, targeted to bind an antigen-presenting cell, are predominantly expressed in mammalian cell lines, such as Chinese hamster ovary (CHO) [142]. The DSP is intended to purify antibodies from cell culture contaminants. The novel DNA vaccines produced in various cell platforms have host cell DNA and RNA contaminants, and studies have explored ATPS as the potential method for the separation of the therapeutic DNA from HC-nucleic acids [143]. Some examples of ATPS used for the purification are listed in **Table 2-7**.

Table 2-7. Examples of ATPS for purification of different biomolecules

System	Target molecule	Recovery (%) ^{\$}	Purity (%)	Reference
Cells				
Ficoll T400 - Dex T70	CD133 ⁺ stem cells	59	60	[144]
PEG 8000 - Dex T500	CD11b ⁺ HL-60 cells	93	99	[145]
Proteins				
PEG 3350 – citrate	IgG	97	76	[146]
PEG 600 – phosphate	Xylose reductase	117	1.2*	[147]
Nucleic acids				
PEG 8000 – polyacrylate T240 - sulfate	Plasmid DNA	55	-	[143]
PEG 8000 – polyacrylate T240 - sulfate	DNA fragments (< 6000 bp)	60	~100	[148]

^{\$}Recovery in the top phase; *purification factor

The inclusion of ATPS for viral-based biotherapeutic and vaccine DSP has recently gained interest. However, the complex viral tropism and fragile structure had challenged the method optimization for infectious virus recovery. Some studies have shown higher recoveries of VLPs (up to 80%) as compared to viruses (**Table 2-8**). The VLPs, void of genetic material and replication deficient, are assessed with the major quality attributes pertaining to the structural integrity and immunogenic glycoprotein conformation retention [149]. On the other hand, whole virus vaccines and biotherapeutics such as LAV and gene therapy vectors have comparatively complex quality attributes. One of the unique critical attributes for LAVs is the potency of the viral product, which is measured by the infectivity assays (cell-based assay to quantify infectious dose) and quantitative PCR (counts the number of gene copies) [3]. The viral infectivity losses incurred during DSP reduces the product yield. This is generally

observed with the lower virus recoveries measured using the infectivity assays. Moreover, traditional ATPSs have been utilizing polymer-polymer systems [129, 150, 151]. Recently, PEG-salt systems have been in demand due to lower interfacial tensions, viscosities, and cost as compared to the polymer-polymer systems [152, 153].

Table 2-8. Virus and VLP recovery in PEG-rich phases of ATPS

System	Virus / VLP	Recovery (%)	Reference
PEG 400 - phosphate	Rotavirus-like particle	60	[154]
PEG 6000 - Dex T500	HIV-1	60	[155]
PEG 1000 - MgSO ₄	B19 VLP	58 - VP2	[156]
PEG 400 - phosphate	B19 VLP	98	[157]
PEG 400 – phosphate	M13 bacteriophage	83	[158]

2.2.4 ATPS phase diagrams

The experimental design for a given pair of phase-forming components is governed by a graphical representation of the concentration of the components. The two-phase systems formed above certain concentrations of the phase forming solutions are represented by a binodal curve. The system compositions above a binodal curve form two-phases upon mixing, and the systems below form homogenous solutions with a single phase (**Figure 2-8**). The position of the binodal curve and system compositions within the two-phase region govern the driving forces for the partitioning of biomolecules (see Section 2.2.5 for details). The area of the two-phase region is dictated by the type and characteristics of the phase-forming components such as polymer and salt type, polymer molecular weight, pH, and temperature [153]. The binodal curves for a given system, pH, and temperature are generated using a turbidity method [153]. High system compositions are chosen that form two phases, which is indicated by turbid mixture, and titrated with water to dilute the systems until the turbidity disappears. The system compositions calculated at which a bare turbidity is present, form a binodal curve.

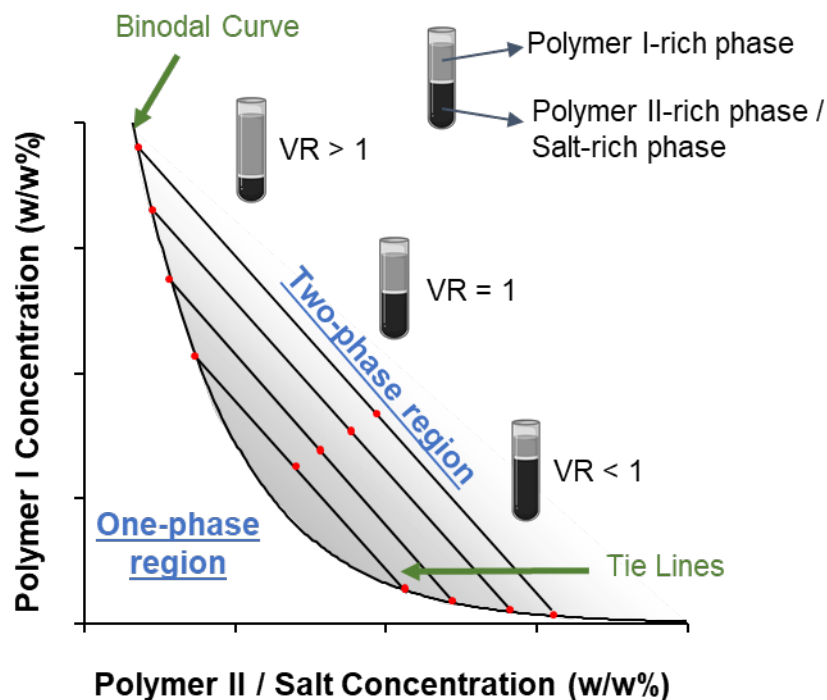


Figure 2-8. Phase diagram demonstrating binodal curve and tie lines for ATPS

The closer the curve is to the origin or axes, the higher the driving forces involved in the phase formation are. This means that the lower system compositions that can form two-phases have better immiscibility. In PEG-salt systems, the immiscibility of the phases is suggested to be the effect of salting-out nonelectrolyte polymer (PEG) from the salt-rich phase [159]. The salting-out effect of PEG was determined to be in the order of the Hoffmeister series for anions as phosphate > citrate > carbonate > sulfate > hydroxide [159, 160]. The salts of anions in the higher order of the Hoffmeister series cause depression in the binodal curve, resulting in the immiscibility at lower compositions [160]. The multivalent cations (Mg^{2+} and Zn^{2+}) have been indicated to favorably interact with the ether oxygens to form a complex causing a higher salting-in of PEG chains as compared to the monovalent cations (Na^+ and $(NH_4)^+$) [159]. However, the depression of binodal curve has been shown in the order of $Na^+ > (NH_4)^+ > Zn^{2+} > Mg^{2+}$ [160]. The

counter-intuitive effect of the multivalent and monovalent cations was supported with the complexation ability of the multivalent cations. On the other hand, binodal curve has also been shown to be affected by the PEG molecular weight. Longer PEG chains have added hydrophobic character to the polymer due to the increased hydrophobic methyl to hydrophilic oxide groups. The increased hydrophobicity has been shown to aid in the salting-out PEG leading to immiscibility at lower concentrations of salt and depression in the binodal curve [161]. The physicochemical factors affecting the binodal curve changes the experimental workspace to choose an appropriate system for the partitioning of the biomolecules.

The other characteristics of the systems are the phase compositions. A set of systems within the two-phase region separate into two phases with identical equilibrium phase compositions, which are represented by tie lines (**Figure 2-9**). While the equilibrium phase compositions remain the same, the phase volume ratio decreases as the systems compositions approach the bottom node [153]. The volume ratio is defined by the ratio of PEG-rich phase volume to salt-rich-phase volume. A tie line is defined by the length of the tie line (TLL) joining the two nodes on the binodal curve and is expressed as shown in the equation 2-2 [153]

$$TLL = \sqrt{\Delta x_{PEG}^2 + \Delta x_{salt}^2} \quad (2-2)$$

Δx represents the concentration difference of the component (PEG or salt) in the PEG-rich phase and salt-rich phase. An increase in the TLL increases the phase concentrations. The difference in the phase composition is characterized by a tie line slope, which is expressed as equation 2-3 [153]

$$TL \text{ slope} = \frac{\Delta x_{PEG}}{\Delta x_{salt}} \quad (2-3)$$

The TL slope is unique for a given system PEG molecular weight, salt type, and pH. For a given system composition, the TL slope dictates the final composition of the PEG-rich phase and salt-rich phase. Further, the phase compositions aid in the separation of

biomolecules (see Section 2.6.6 for details). The phase diagrams are the blueprint of a given pair of the phase forming components to study the partitioning behavior of biomolecules. However, the phase diagrams being unique to each pair, the optimization of the biomolecule purification using ATPS generates an extensive experimental space. The previous works have used a lab-specific or wide range of phase forming components varying in PEG molecular weight, salt type, and pH to optimize virus recovery in the PEG-salt system [154, 156-158]. The goal of current biotherapeutic manufacturing is to develop a standard method of purification with a minimum variation in the processing conditions for faster FDA approval. The lack of a standard system or optimization method for optimization of virus recovery is the bottleneck of ATPS for biotherapeutic processing applications.

2.3 Biomolecule Partitioning Theories in ATPS

2.3.1 Excluded volume and intermolecular interactions

The commercial implementation of ATPS is lacking due to an ambiguity in understanding the partitioning mechanism of the biomolecules and lack of expertise in the process development for large-scale production [162, 163]. There have been numerous studies to elucidate the partitioning mechanisms of biomolecules in the ATPS. The two major theories argue the role of excluded-volume effect [154, 158, 164] and intermolecular interactions [129, 164, 165]. The excluded volume theory states that the volume occupied by a polymer chain in the polymer-rich phase is saturated with the polymer chains and hydration molecules [164]. The unavailability of the free volume leads to a steric hindrance for comparatively larger sized globular biomolecules (proteins, cells, and viruses), resulting in the exclusion of the biomolecules from the phase [156, 166]. Benavides et al. (2006) demonstrated that the majority of double layer rotavirus-like particle partitioned in the PEG-rich phase when PEG 400 Da was used, and the partitioning shifted to the interface when the molecular weight was >1000 Da [154]. The partitioning shift from the PEG-rich phase to the interface was suggested due to the reduced free volume of the PEG-rich phase with the increased PEG MW supporting

previous observations of protein partitioning [167, 168]. A similar argument was made by Gonzalez-Mora et al. (2017) when the partitioning of M13 bacteriophage shifted from the PEG-rich phase to the interface when the cation type of phosphate salt was changed from Na^+ to K^+ in the PEG-salt system [158]. It was proposed that Na^+ with more water molecules in the hydration shell, as compared to the larger sized K^+ ion, reduces the availability of free water molecules for bacteriophage hydration in the PEG-rich phase, resulting in the interface partitioning [158]. However, the interpretation of the ion effects on biomolecule partitioning is at the edge of the excluded volume theory and intermolecular interactions.

Another partitioning mechanism proposed was the net effect of intermolecular interactions. The driving forces governing the partitioning was proposed to include hydrophobic interactions, electrostatic interactions, and phase-specific affinity [129, 165]. Over the years, studies have suggested that the hydrophobic interactions of biomolecules with the PEG-rich phase and electrostatic interactions with the salt-rich phase majorly influence the partitioning [169, 170]. It has been shown that the hydrophobic patches of proteins interact with the ethyl groups of PEG [171, 172]. The attractive forces between some proteins and PEG aids in the preferential partitioning of the proteins in the PEG-rich phase. On the other hand, the electrostatic interaction of charged biomolecules with the ions in the salt-rich phase either helps in salting-out or salting-in proteins [146, 165]. In a way, the principle of hydrophobic interaction of combined salting-out effect and induced hydrophobic interaction has been suggested to govern the biomolecule partitioning. The specific affinity of the biomolecules towards the PEG-rich phase in a PEG-salt system can be interpreted as the interaction of biomolecules, especially proteins, with the higher molecular weight of PEG (>10 kDa) [172]. However, this effect may be negligible in the studies that utilized lower molecular weight PEG (< 10 kDa). The specific affinity has also been shown to supplement the driving force if an affinity functionalized PEG or affinity ligands are used in the systems to enhance the specificity of a target biomolecule [173]. Moreover, intermolecular interactions have been shown to be determinant of the biomolecule size and conformation [129, 165]. The overall

partitioning coefficient (K) of a biomolecule is the net effect of these intermolecular interactions, which was proposed as equation 2-4 [129, 174]

$$K = K_O \cdot K_H \cdot K_E \cdot K_A \cdot K_S \cdot K_C \quad (2-4)$$

where the subscripts H , E , A , S , and C are the contributions of hydrophobicity, electrostatics, affinity, size, and conformation to the partitioning coefficients, respectively. The subscript O represents the miscellaneous contributions affecting the partitioning of biomolecules as there are other factors that influence the partitioning [165]. Overall, Grilo et al. (2016) suggested that the influence of excluded-volume effects, hydrophobicity, and electrostatics depends on the chosen system and target biomolecule [163].

The biomolecule transport from one phase to another is also governed by the interfacial characteristics. The characteristics that affect the partitioning are interfacial tension and electrostatic potential difference [163, 175]. The initial step in phase partitioning of a biomolecule is the adsorption at the interface. The interfacial tension governs the free energy profile of biomolecule [176]. If the free energy of a biomolecule reaches equilibrium at the interface, the biomolecule diffusion across the barrier is seized [176, 177]. A previous study demonstrated that the partitioning of skin cancer cells was shifted from the dextran-rich phase to the interface and PEG-rich phase when the interfacial tension was increased beyond a certain limit [176]. However, the embryonic stem cells partitioned majorly at the interface without diffusing to the PEG-rich phase, which was suggested due to the free energy minimization at the interface of stem cells as compared to the cancer cells [176]. On the other hand, the biomolecule partitioning has been shown to increase in the PEG-rich phase as the system compositions increase [178, 179]. An increase in the system composition also elevates the interfacial tension [180, 181]. This indicates that interfacial tension aids in the biomolecule partitioning between the phases until a certain limit, after which it hinders the transport leading to the interfacial partitioning of biomolecules.

The other physicochemical characteristics that drive the partitioning behavior of biomolecules is the electrostatic potential difference between the phases [175]. The differences in the partitioning of cations and anions in the PEG-dextran system have been shown to generate a potential difference across the interface [175, 182]. It has been reported that the PEG-salt systems generate a positive potential difference, typically in the range of -30 to 30 mV for PEG-phosphate or sulfate systems, measured as the difference between the top (PEG-rich) and bottom phase (salt-rich) [183]. Sufficient charge on a biomolecule results in the partitioning behavior that yields a net electroneutrality of the phases [183, 184].

2.4 Parameters and their effect on driving forces in ATPS

The optimization of a target biomolecule's recovery in a PEG-salt system includes designing a system to yield an optimal balance of the driving forces. Previous studies reported a list of characteristics of the phase forming components that have a direct effect on the driving forces. The parameters influencing hydrophobic interaction, electrostatic interaction, and interfacial mass transport properties depend on the PEG and salt characteristics [183]. These phase forming components directly affect the phase diagrams yielding different driving forces. The effects of these parameters on the phase diagrams and driving forces are discussed below.

2.4.1 Phase forming component parameters

2.4.1.1 *Polymer molecular weight and concentration*

PEG is the most common polymer utilized in ATPS of both polymer-polymer and polymer-salt system (**Tables 2-7** and **2-8**). PEG MW significantly affects the phase characteristics by changing the phase diagrams. An increase in MW has been shown to reduce the system compositions that form two phases, resulting in depression of the binodal curve (see **Figure 2-9**) [161]. It has also been shown that the tie line slope decreases with an increase in MW [185]. This signifies that for a given system

composition with a higher PEG MW, the equilibrium salt-rich phase has a lower composition, and the PEG-rich phase has a higher composition (see **Figure 2-10**).

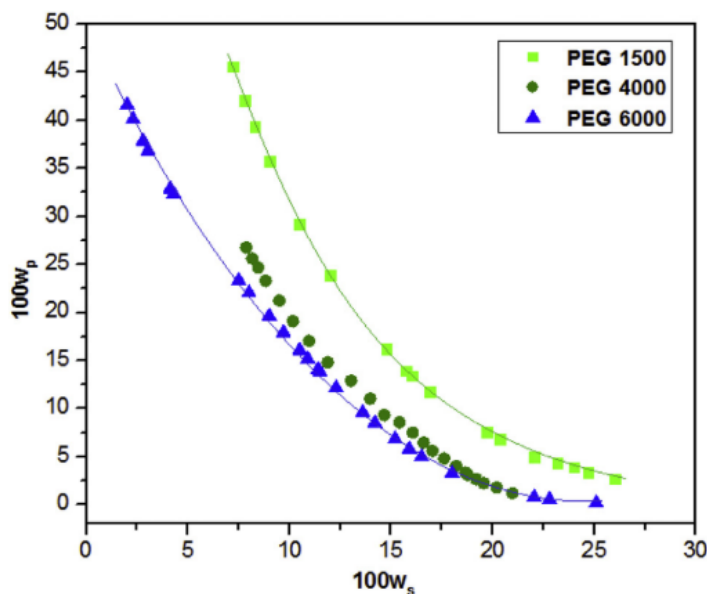


Figure 2-9. The binodal curve shift with an increasing PEG molecular weight. W_p and W_s represents the PEG and salt concentrations. Reprinted with permission from [186]. Copyright (2018) Elsevier.

An increase in the PEG MW has been shown to decrease the partitioning of proteins to the PEG-rich phase [187, 188]. The reduced partitioning has been argued with both steric exclusion [154, 187] and hydrophobicity [163] mechanisms. The steric exclusion was suggested based on the reduced free volume of the PEG-rich phase. An increase in the PEG MW for a constant PEG concentration reduces the number of ethylene oxide in the PEG-rich phase, thereby reducing the hydrophobicity of the PEG-rich phase [163]. On the other hand, Asenjo et al. (2011) states that for a given polymer, an increase in the PEG MW increases the hydrophobicity of the polymer due to an increase in the ethyl to oxygen group ratio [165]. An elevated hydrophobicity of the higher MW PEG has been shown to favorably interact with the hydrophobic patches of

the proteins [172]. Moreover, the PEG-rich phase yields a higher phase composition with a higher PEG MW for a given system composition that has shown to increase the partitioning of relatively hydrophobic proteins [165]. The discrepancy in the arguments of the effect of PEG MW causing steric exclusion and changing hydrophobicity of the PEG-rich phase needs more characterization of the phases to elucidate the exact mechanism.

The proposed theory of hydrophobicity as one of the dominant driving forces has also been studied by increasing the PEG concentration. The increased PEG concentration increases the number of PEG chains in the PEG-rich phase, thereby dehydrating the phase and increasing the phase hydrophobicity [165]. However, a study demonstrated that the PEG concentration does not affect the partitioning of IgG in the PEG-phosphate system, and the antibodies preferentially partitioned to the PEG-rich phase irrespective of the PEG and phosphate concentration [189]. In the other study, the α -Lactalbumin partition coefficient increased up to a certain PEG concentration and then decreased [190]. While others reviewed that increasing the PEG concentration decreases protein partitioning in the PEG-rich phase due to steric hindrance exhibited by the increased PEG chains in the PEG-rich phase [163]. The different partitioning behavior of proteins demonstrates that the biomolecule characteristics play important role that interact with PEG-rich phase uniquely.

2.4.1.2 Salt type and concentration

Salts play a significant role as the drivers of electrostatic interactions for biomolecule partitioning. One of the primary roles of salts is to induce a preferential salting-out for a target biomolecule. The salting-out ability of different ions studied was by Hofmeister postulated a kosmotropic series for ions. The anion kosmotropic series for the salting-out ability was given as $\text{PO}_4^{3-} > \text{citrate}^{3-} > \text{CO}_3^{2-} > \text{SO}_4^{2-} > \text{Cl}^-$ [191]. On the other hand, the kosmotropic series for cations was given as $\text{Na}^+ > \text{K}^+ > \text{NH}_4^+$ [191]. The salt type has been shown to modulate the binodal curve and tie line slope. A higher kosmotropic salt in the series increases the two-phase region by pulling the binodal curve

closer to the axes, similar to binodal curve behavior shown in **Figure 2-9** [192, 193]. However, it was observed that the anion effect on the binodal curve was more influential and shifted the curve more prominently towards the axes as compared to the cations [193]. Moreover, the tie line slopes get steeper for higher kosmotropic anions, indicating that lower salt-rich phase compositions have higher salting-out ability to yield a more concentrated PEG-rich phase [194]. However, one study demonstrated that sulfate ion was better at salting-out HIV-GFP-VLP as compared to the phosphate and citrate ions [195]. There have been some studies indicating that the salting-out effect by anions does follow the Hofmeister series due to other non-specific interactions of salts with biomolecules [196]. On the other hand, it has been shown that Na^+ salts increase the relative hydrophobicity of the PEG-rich phase as compared to Mg^{2+} [197]. Moreover, a salt of highly kosmotropic ion generates a high electrostatic potential difference, which is postulated to highly influence biomolecule partitioning to the PEG-rich phase [183].

The kosmotropic anions, such as citrate and phosphate, have been shown to induce the salting-out effect of biomolecules at much lower concentrations as compared to the other salts [198]. It has been shown that the preferential hydration ability of kosmotropes causes an increase in the surface tension near a biomolecule surface that leads to aggregation and interfacial interactions of biomolecules [146, 199, 200]. In the ATPS, a kosmotropic salt aids in the interfacial interaction of biomolecules with the PEG-rich phase caused by the salting-out effect. A previous study showed that, for a constant PEG molecular weight, porcine parvovirus partition more towards the interface or PEG-rich phase [178]. In another study, M13 bacteriophage recovery in systems containing sodium phosphate decreased when crude stock with contaminants was fed as compared to the pre-purified bacteriophage feedstock [158]. However, the system containing potassium phosphate demonstrated a similar bacteriophage recovery irrespective of the feedstock [158]. The authors proposed that as Na^+ ions are highly hydrated as compared to K^+ ions, the PEG-rich phase where cations partition is easily saturated when Na^+ ions are used. Overall, the literature demonstrates the effect of different ion-biomolecule pair for a given system composition and limited studies have

focused on showing the effect of selecting systems of different salts which yield similar salt-rich phase composition.

The salting-out ability for a given salt type depends on the ionic strength of the solution. An increase in the ionic strength by increasing the salt concentration has been shown to induce the salting-out effect [158]. The salting-out of dlrotavirus-like particles were shown to recover at the interface but not in the PEG-rich phase [154]. It might be due to an insufficient hydrophobic driving force that the VLPs did not partition to the PEG-rich phase at all the PEG MW studied.

2.4.1.3 *pH*

Ion charge on is one of the influential parameters in governing the driving forces for biomolecule partitioning, as discussed above. The ionic charge depends on the pH of the solution, and modulating the pH affects the phase characteristics and biomolecule partitioning. An increase in the pH causes depression in the binodal curve towards the axes for a given PEG-salt system [185]. The slope of tie lines increases with an increase in system pH, indicating lower equilibrium salt-rich phase composition and higher PEG-rich phase composition for a given system composition [201].

The change in the phase characteristics due to pH affects the biomolecule partitioning. An increase in the system pH increases the biomolecule partitioning to the PEG-rich phase [167, 170]. The partitioning behavior of biomolecules has been associated with the free volumes of the phases [183, 202]. Oxygen atoms of PEG interact with metal ions and exclude divalent and trivalent anions, thereby causing the phase formations. A lower pH decreases the free volume of the PEG-rich phase by reducing the metal ion availability causing a lower partitioning of the biomolecules in the PEG-rich phase [167]. Moreover, pH modulates the charge on biomolecules by changing the protonated to deprotonated sites that supplements the change in the partition behavior of biomolecules (see Section 2.4.2).

2.4.1.4 Summary of phase parameters and effects

The driving forces involved in phase formation and biomolecule partitioning have been discussed as a complex synergy of free volume and intermolecular interactions. These driving forces are influenced by multiple characteristics of the phase forming components, and a net effect is provided to allow for biomolecule partitioning in either phase. In summary, the studies have indicated different theories for which the phase forming components affect the driving forces which are maintained. Moreover, most of the studies have been focused on proteins, enzymes. Very few studies were performed to understand viral behavior in the ATPS, and the studies that were completed focused on the polymer-polymer systems [150, 151, 203]. Recently, studies are showing interest for the viral behavior in the PEG-salt systems, but the effects of phase parameters were correlated with the protein partitioning behavior [154, 156, 158, 195]. Most studies have reported an experimental design by changing one parameter at a time, such as PEG MW, PEG concentration, salt type, and concentration by keeping the other factors constant. However, the conventional setup might not be appropriate to study viral partitioning behavior in ATPS as the physical characteristics of the phases such as volume ratio, tie line length, and equilibrium phase compositions, change thereby deviating from the expected partitioning behavior. While the conventional setup is very crucial for an initial understanding of viral behavior in the ATPS, this setup is not optimal to develop a clear picture of the phase parameters as the empirical models have not been validated for complex structures such as viruses. A systematic approach by understanding the differences in viral and protein behavior is needed to achieve similar success as comparatively smaller proteins.

2.4.2 Biomolecule characteristics and the effect on partitioning behavior

2.4.2.1 Surface hydrophobicity

The hydrophobic and electrostatic interactions were shown to be the dominating driving forces for the biomolecule partitioning. The proteins composed of amino acids display some amino groups on the solvent accessible side while the rest being solvent

inaccessible due to secondary and tertiary structures. The solvent accessible amino acids have a mixture of hydrophobic and hydrophilic side chains, and the ratio of these side chains determine a net hydrophobicity of proteins. Studies performed with small peptides with a different number of hydrophobic amino acids have demonstrated, that for a given PEG-salt system, relatively more hydrophobic peptides readily partition to the PEG-rich phase [204, 205]. A similar study performed on an array of proteins characterized by the surface hydrophobicity demonstrated a linear correlation in the partition coefficient with the surface hydrophobicity in a PEG-citrate system [206]. Thus, the partitioning behavior indicates a strong relation to the surface hydrophobicity of biomolecules.

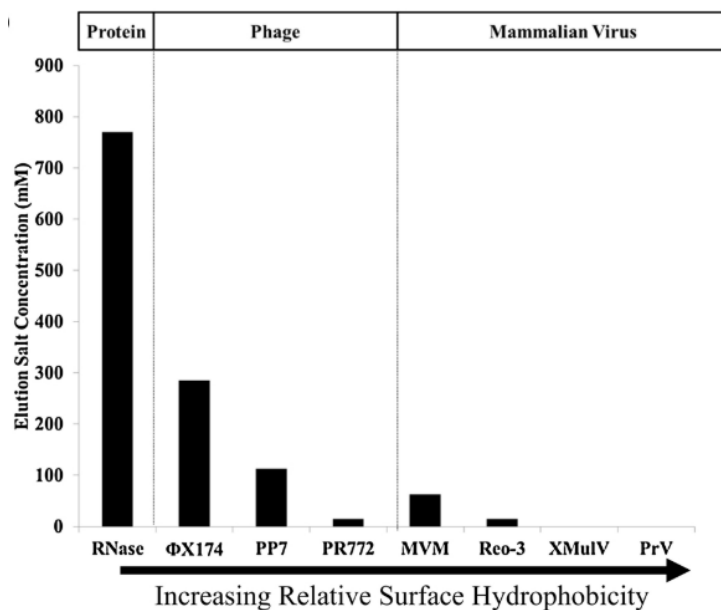


Figure 2-10. Comparison of surface hydrophobicity of protein and viruses determined by the elution salt concentration in hydrophobic interaction chromatography. Reprinted with permission from [207].

There is growing evidence that viruses are relatively more hydrophobic than proteins. A study characterized the hydrophobicity of a range of proteins and viruses by a HIC framework and showed that proteins such as RNase, ovalbumin, and lysozyme

eluted from the hydrophobic resins at higher salt concentrations as compared to the bacteriophages such as Φ X174, PP7, and PR72 [207]. The mammalian viruses, such as minute virus of mice, xenotropic murine leukemia virus, reovirus, and pseudorabies virus, retained on the resin until much lower salt concentrations than bacteriophages, indicating the higher hydrophobic character of mammalian viruses (see **Figure 2-10**) [208]. Most studies have indicated that viral particles are often excluded from the relatively PEG-rich phase due to the steric exclusion when either PEG concentration or PEG MW are increased [154, 158]. However, a recent study demonstrated that high recoveries can be obtained with a higher PEG MW and concentration [178].

2.4.2.2 Surface charge

The other physicochemical characteristic of biomolecules that affect partitioning behavior is the surface charge. The electrostatic interaction induced by the salt-rich phase on a biomolecule depends on the pH of the solution. The presence of amine and carboxyl groups on amino acids have different pKa that are protonated or deprotonated depending on the solution pH. Thus, a change in solution pH changes the surface charge of the biomolecule. The pH at which the net surface charge nears zero is determined as the isoelectric point (pI) of a biomolecule. The surface becomes negatively charged if the solution pH is above the pI of the biomolecule and carries a positive charge if $\text{pH} < \text{pI}$. Negatively charged viruses effectively partition to the interface or PEG-rich and positively charged viruses partition to the salt-rich phase [178, 209].

The virus purification has not been studied systematically by relating the phase characteristics and viral surface characteristics. The viruses are much larger particles as compared to proteins and their behavior cannot be easily predicted in the two-phase systems. Maintaining the infectivity of viruses and surface tropism during processing adds to the challenge and unambiguity in predicting the behavior. Thus, a more studies need to be conducted to understand the viral behavior in ATPS.

2.5 Osmolytes

2.5.1 Osmoregulators under environmental stress

Osmolytes are naturally occurring compounds synthesized in most of the cell types in response to environmental stress [210]. Osmolytes change the water structure in the environment that allow living creatures to regulate the osmotic pressure and water content in the cells to survive [210]. Deep-sea fishes habituated in high salt concentration environment and hydrostatic pressure have known to produce significantly higher amounts of trimethyl amine-N-oxide (TMAO), a type of osmolyte [211]. Osmolyte production has shown to counteract the hydrostatic pressure, counterbalance the osmotic stress, and aid in metabolic functioning [212, 213]. On the other hand, osmolytes are also utilized in the drought conditions by plants [214]. Osmolyte accumulation has shown to regulate cell protein stabilization to maintain the functionality under abiotic stress [214].

Different organisms have shown to produce different types of osmolytes in response to abiotic stress [215]. The osmolytes classes range from amino acids, amino acid derivatives, polyols, and amine-oxides [210]. However, the osmolytes are further characterized depending on the effect on proteins - protecting and denaturing. The osmoprotectants or protecting osmolytes such as proline, glycine, TMAO, and sorbitol, which are found in the organisms that survive under stress, enhance the protein stability [216]. Denaturing osmolytes such as urea and guanidinium hydrochloride destabilize the protein structures by unfolding [216].

2.5.2 Osmolytes in biomanufacturing

The protecting osmolytes are extensively used in the biomanufacturing due to their ability to promote protein stability [217, 218], and assist protein assembly to capsid [219]. The prominent use of protecting osmolytes has been shown in the formulation stage of biomanufacturing. The formulation of biopharmaceutical products involves a mixture of target biomolecule and compounds such as stabilizers for long term storage

and adjuvants [220, 221]. The osmolytes are used as stabilizers as they help protect proteins against unfolding [222]. Commonly used osmolytes as stabilizers are glycine, trehalose, sucrose, mannitol, and arginine [218]. In one study, glycine was shown to protect a recombinant protein-based vaccine against antigen modification upon long-term storage at 37 °C [223]. In the other study, the addition of a combination of the disaccharide, such as sucrose or trehalose, and glycine was shown to thermally stabilize the H1N1 influenza subunit vaccine upon freeze-drying for long-term storage and possibly eliminate the cold-storage [224]. Numerous such osmolytes have been used in the biopharmaceutical formulations and approved by the FDA [218].

The protein structure stabilization mechanism by protecting osmolytes is still unclear. However, more studies are being performed both at macro and micro scale to understand the role of osmolytes in the protein structure fluctuations. A thermodynamic study suggests that the free energy of unfolded proteins increases in the presence of osmoprotectants, thus favoring the folded state [225]. A computational study demonstrated that osmoprotectant, glycine-betaine (commonly known as betaine) has a high affinity towards water molecules, thereby leading to preferential hydration of self-molecules in a matrix of proteins, ions, osmolyte, and solvent [226]. The protein backbone has shown to exclude both osmolyte and water in the case of osmolytes (betaine, TMAO, and proline) or enrich with osmolyte and water (trehalose and sarcosine) [227]. Both the cases of exclusion and enrichment have shown to stabilize the proteins by compaction of the structure.

The effect of osmolytes on viruses has been shown to differ from proteins. Viral surfaces are relatively hydrophobic when compared to proteins [207, 228]. The preferential hydration of mannitol and alanine resulted in the viral particle flocculation [229]. The viral flocculation was suggested to be due to hydrophobic interaction between the hydrophobic viral surface [198]. The promotion of hydrophobic interaction by osmolytes has also been demonstrated for a hydrophobic polymer, elastin [230]. Glycine and betaine partitioned away from the polymer-water interface, thereby promoting the hydrophobic interaction of the non-polar groups of elastin and causing the polymer to

collapse [230]. The difference in protein and virus behavior under the influence of osmolytes can be used in the DSP to upgrade the virus purification methods.

2.6 References

1. Clem, A.S., *Fundamentals of Vaccine Immunology*. Journal of Global Infectious Diseases, 2011. **3**(1): p. 73-78.
2. Bonanni, P., and J.I. Santos, *Vaccine evolution*. Perspectives in Vaccinology, 2011. **1**(1): p. 1-24.
3. Galinski, M.S., et al., *Live Attenuated Viral Vaccines*, in *Vaccine Analysis: Strategies, Principles, and Control*, B. Nunnally, V. Turula, and R. Sitrin, Editors. 2015, Springer: Berlin, Heidelberg. p. 1-44.
4. Badgett, M.R., et al., *Evolutionary Dynamics of Viral Attenuation*. Journal of Virology, 2002. **76**(20): p. 10524-10529.
5. Plotkin, S.A., *Vaccines, vaccination, and vaccinology*. The Journal of infectious diseases, 2003. **187**(9): p. 1349-1359.
6. Lukashevich, I.S., et al., *A live attenuated vaccine for Lassa fever made by reassortment of Lassa and Mopeia viruses*. J Virol, 2005. **79**(22): p. 13934-42.
7. Hause, B.M., et al., *In vitro reassortment between endemic H1N2 and 2009 H1N1 pandemic swine influenza viruses generates attenuated viruses*. PLoS One, 2012. **7**(6): p. e39177.
8. Glass, R.I., J. Gentsch, and J.C. Smith, *Rotavirus Vaccines: Success by Reassortment?* Science, 1994. **265**(5177): p. 1389-1391.
9. Sanders, B., M. Koldijk, and H. Schuitemaker, *Inactivated Viral Vaccines*, in *Vaccine Analysis: Strategies, Principles, and Control*, B.K. Nunnally, V.E. Turula, and R.D. Sitrin, Editors. 2015, Springer. p. 45-80.
10. WHO. *Subunit vaccines*. Vaccine Safety Basics 2020 [cited 2020 06/14]; Available from: <https://vaccine-safety-training.org/subunit-vaccines.html>.
11. WHO, *Hepatitis B vaccines: WHO position paper*. 2009. **84**(40): p. 405-420.
12. Leo, O., A. Cunningham, and P.L. Stern, *Vaccine immunology*. Perspectives in Vaccinology, 2011. **1**(1): p. 25-59.

13. Vartak, A. and S.J. Sucheck, *Recent Advances in Subunit Vaccine Carriers*. Vaccines (Basel), 2016. **4**(2).
14. Noad, R. and P. Roy, *Virus-like particles as immunogens*. Trends in Microbiology, 2003. **11**(9): p. 438-444.
15. Roldao, A., et al., *Virus-like particles in vaccine development*. Expert Rev Vaccines, 2010. **9**(10): p. 1149-76.
16. Mohsen, M.O., et al., *Major findings and recent advances in virus-like particle (VLP)-based vaccines*. Seminars in Immunology, 2017. **34**: p. 123-132.
17. Huang, X., et al., *Escherichia coli-derived virus-like particles in vaccine development*. NPJ Vaccines, 2017. **2**: p. 3.
18. Frey, S., et al., *Clinical efficacy of cell culture-derived and egg-derived inactivated subunit influenza vaccines in healthy adults*. Clin Infect Dis, 2010. **51**(9): p. 997-1004.
19. Baxter, D.N., *Measles immunization in children with a history of egg allergy*. Vaccine, 1996. **14**(2): p. 131-134.
20. Zeiger, R.S., *Current issues with influenza vaccination in egg allergy*. Journal of Allergy and Clinical Immunology, 2002. **110**(6): p. 834-840.
21. Barrett, P.N., et al., *Vero cell platform in vaccine production: moving towards cell culture-based viral vaccines*. Expert Review of Vaccines, 2009. **8**(5): p. 607-618.
22. Genzel, Y., *Designing cell lines for viral vaccine production: Where do we stand?* Biotechnol J, 2015. **10**(5): p. 728-40.
23. Cohen, S., S. Au, and N. Pante, *How viruses access the nucleus*. Biochim Biophys Acta, 2011. **1813**(9): p. 1634-45.
24. Follett, E.A.C., et al., *Virus Replication in Enucleate Cells: Vesicular Stomatitis Virus and Influenza Virus*. Journal of Virology, 1974. **13**(2): p. 394.
25. den Boon, J.A., A. Diaz, and P. Ahlquist, *Cytoplasmic viral replication complexes*. Cell Host Microbe, 2010. **8**(1): p. 77-85.
26. Yamashita, M. and M. Emerman, *Retroviral infection of non-dividing cells: old and new perspectives*. Virology, 2006. **344**(1): p. 88-93.
27. Vodicka, M.A., *Determinants for Lentiviral Infection of Non-Dividing Cells*. Somatic Cell and Molecular Genetics, 2001. **26**(1): p. 35-49.

28. Zhong, P., et al., *Cell-to-cell transmission of viruses*. *Curr Opin Virol*, 2013. **3**(1): p. 44-50.
29. Mothes, W., et al., *Virus cell-to-cell transmission*. *J Virol*, 2010. **84**(17): p. 8360-8.
30. Hess, R.D., et al., *Regulatory, biosafety and safety challenges for novel cells as substrates for human vaccines*. *Vaccine*, 2012. **30**(17): p. 2715-27.
31. *Recommendations for the evaluation of animal cell cultures as substrates for the manufacture of biological medicinal products and for the characterization of cell banks*, in *WHO Technical Reports Series 978, Annex 3*. 2013, World Health Organization.
32. van der Pol, L.A. and W.A.M. Bakker, *How to choose the correct cell line for producing your viral vaccine: what is important?* *Pharmaceutical Bioprocessing*, 2014. **2**(3): p. 207-210.
33. Rodrigues, A.F., et al., *Viral vaccines and their manufacturing cell substrates: New trends and designs in modern vaccinology*. *Biotechnology Journal*, 2015. **10**(9): p. 1329-1344.
34. Knezevic, I., et al., *Evaluation of cell substrates for the production of biologicals: Revision of WHO recommendations. Report of the WHO Study Group on Cell Substrates for the Production of Biologicals, 22-23 April 2009, Bethesda, USA*. *Biologicals*, 2010. **38**(1): p. 162-9.
35. Fuenmayor, J., F. Godia, and L. Cervera, *Production of virus-like particles for vaccines*. *N Biotechnol*, 2017. **39**(Pt B): p. 174-180.
36. Fernandes, F., et al., *Insect cells as a production platform of complex virus-like particles*. *Expert Rev Vaccines*, 2013. **12**(2): p. 225-36.
37. McAleer, W.J., et al., *Human hepatitis B vaccine from recombinant yeast*. *Nature*, 1984. **307**(5947): p. 178-180.
38. Govan, V.A., *A novel vaccine for cervical cancer: quadrivalent human papillomavirus (types 6, 11, 16 and 18) recombinant vaccine (Gardasil)*. *Therapeutics and clinical risk management*, 2008. **4**(1): p. 65-70.
39. Bonanni, P., *Human Papillomavirus Vaccines*, in *Pediatric Vaccines and Vaccinations*. 2017. p. 127-136.
40. Warfield, K.L., et al., *Ebola virus-like particle-based vaccine protects nonhuman primates against lethal Ebola virus challenge*. *J Infect Dis*, 2007. **196** Suppl 2: p. S430-7.

41. Boigard, H., et al., *Zika virus-like particle (VLP) based vaccine*. PLoS Negl Trop Dis, 2017. **11**(5): p. e0005608.
42. Merten, O.-W., et al., *Manufacturing of viral vectors for gene therapy: part I. Upstream processing*. Pharmaceutical Bioprocessing, 2014. **2**(2): p. 183-203.
43. Genzel, Y., et al., *Metabolism of MDCK cells during cell growth and influenza virus production in large-scale microcarrier culture*. Vaccine, 2004. **22**(17-18): p. 2202-8.
44. Krampe, B. and M. Al-Rubeai, *Cell death in mammalian cell culture: molecular mechanisms and cell line engineering strategies*. Cytotechnology, 2010. **62**(3): p. 175-88.
45. Yokomizo, A.Y., et al., *Rabies virus production in high vero cell density cultures on macroporous microcarriers*. Biotechnol Bioeng, 2004. **85**(5): p. 506-15.
46. Aggarwal, K., et al., *Bioprocess optimization for cell culture based influenza vaccine production*. Vaccine, 2011. **29**(17): p. 3320-8.
47. Whitford, W.G. and A. Fairbank, *Considerations in scale-up of viral vaccine production*. BioProcess Int, 2011. **9**(8): p. 16-28.
48. Gallo-Ramirez, L.E., et al., *Bioreactor concepts for cell culture-based viral vaccine production*. Expert Rev Vaccines, 2015. **14**(9): p. 1181-95.
49. Tapia, F., et al., *Bioreactors for high cell density and continuous multi-stage cultivations: options for process intensification in cell culture-based viral vaccine production*. Appl Microbiol Biotechnol, 2016. **100**(5): p. 2121-32.
50. Paillet, C., et al., *Suspension-Vero cell cultures as a platform for viral vaccine production*. Vaccine, 2009. **27**(46): p. 6464-7.
51. Shen, C.F., et al., *Development of suspension adapted Vero cell culture process technology for production of viral vaccines*. Vaccine, 2019. **37**(47): p. 6996-7002.
52. Lohr, V., et al., *A new MDCK suspension line cultivated in a fully defined medium in stirred-tank and wave bioreactor*. Vaccine, 2010. **28**(38): p. 6256-64.
53. Rajendran, R., et al., *Assessment of packed bed bioreactor systems in the production of viral vaccines*. AMB Express, 2014. **4**(1): p. 25.
54. Nestola, P., et al., *Improved virus purification processes for vaccines and gene therapy*. Biotechnol Bioeng, 2015. **112**(5): p. 843-57.

55. CBER, *Characterization and Qualification of Cell Substrates and Other Biological Materials Used in the Production of Viral Vaccines for Infectious Disease Indications* U.D.o.H.a.H. Services, Editor. 2010, Food and Drug Administration.
56. Kalbfuss, B., et al., *Harvesting and concentration of human influenza A virus produced in serum-free mammalian cell culture for the production of vaccines*. Biotechnol Bioeng, 2007. **97**(1): p. 73-85.
57. Besnard, L., et al., *Clarification of vaccines: An overview of filter based technology trends and best practices*. Biotechnol Adv, 2016. **34**(1): p. 1-13.
58. Harrison, R.G., et al., *Bioseparations science and engineering*. 2015: Oxford University Press, USA.
59. Wolf, M.W. and U. Reichl, *Downstream processing of cell culture-derived virus particles*. Expert Rev Vaccines, 2011. **10**(10): p. 1451-75.
60. Michen, B. and T. Graule, *Isoelectric points of viruses*. J Appl Microbiol, 2010. **109**(2): p. 388-97.
61. Venkiteswaran, A., et al., *Mechanistic evaluation of virus clearance by depth filtration*. Biotechnol Prog, 2015. **31**(2): p. 431-7.
62. Alenazi, N.A., et al., *Modified polyether-sulfone membrane: a mini review*. Des Monomers Polym, 2017. **20**(1): p. 532-546.
63. van Reis, R. and A. Zydney, *Bioprocess membrane technology*. Journal of Membrane Science, 2007. **297**(1-2): p. 16-50.
64. Farrah, S.R., *Chemical factors influencing adsorption of bacteriophage MS2 to membrane filters*. Applied and Environmental Microbiology, 1982. **43**(3): p. 659.
65. Morenweiser, R., *Downstream processing of viral vectors and vaccines*. Gene therapy, 2005. **12**: p. S103-S110.
66. Kamen, A. and O. Henry, *Development and optimization of an adenovirus production process*. J Gene Med, 2004. **6 Suppl 1**: p. S184-92.
67. Liu, H.F., et al., *Recovery and purification process development for monoclonal antibody production*. MAbs, 2010. **2**(5): p. 480-99.
68. Nasukawa, T., et al., *Virus purification by CsCl density gradient using general centrifugation*. Archives of virology, 2017. **162**(11): p. 3523-3528.

69. Araldi, R.P., et al., *Bovine papillomavirus isolation by ultracentrifugation*. J Virol Methods, 2014. **208**: p. 119-24.
70. Wang, J., J. Ma, and X. Wen, *Basic Concepts of Density Gradient Ultracentrifugation*, in *Nanoseparation Using Density Gradient Ultracentrifugation: Mechanism, Methods and Applications*, X. Sun, et al., Editors. 2018, Springer Singapore: Singapore. p. 21-36.
71. Killington, R.A., A. Stokes, and J.C. Hierholzer, *Virus purification*, in *Virology Methods Manual*, B.W.J. Mahy and H.O. Kangro, Editors. 1996, Academic Press: London. p. 71-89.
72. Segura, M.M., A. Garnier, and A. Kamen, *Purification and characterization of retrovirus vector particles by rate zonal ultracentrifugation*. J Virol Methods, 2006. **133**(1): p. 82-91.
73. Gias, E., et al., *Purification of human respiratory syncytial virus by ultracentrifugation in iodixanol density gradient*. J Virol Methods, 2008. **147**(2): p. 328-32.
74. Vajda, J., et al., *Size distribution analysis of influenza virus particles using size exclusion chromatography*. J Chromatogr A, 2016. **1465**: p. 117-25.
75. Štulík, K., V. Pacáková, and M. Tichá, *Some potentialities and drawbacks of contemporary size-exclusion chromatography*. Journal of Biochemical and Biophysical Methods, 2003. **56**(1): p. 1-13.
76. Singh, N., et al., *Clarification technologies for monoclonal antibody manufacturing processes: Current state and future perspectives*. Biotechnol Bioeng, 2016. **113**(4): p. 698-716.
77. Nap, R.J., et al., *The role of solution conditions in the bacteriophage PP7 capsid charge regulation*. Biophys J, 2014. **107**(8): p. 1970-1979.
78. Merten, O.-W., et al., *Manufacturing of viral vectors: Part II. Downstream processing and safety aspects*. Pharmaceutical Bioprocessing, 2014. **2**(3): p. 237-251.
79. Jungbauer, A. and R. Hahn, *Ion-exchange chromatography*, in *Methods in enzymology*, R.R. Burgess and M.P. Deutscher, Editors. 2009, Elsevier. p. 349-371.
80. Salo, R.J. and D.O. Cliver, *Effect of acid pH, salts, and temperature on the infectivity and physical integrity of enteroviruses*. Archives of Virology, 1976. **52**(4): p. 269-282.

81. Sviben, D., et al., *Recovery of infective virus particles in ion-exchange and hydrophobic interaction monolith chromatography is influenced by particle charge and total-to-infective particle ratio*. J Chromatogr B Analyt Technol Biomed Life Sci, 2017. **1054**: p. 10-19.
82. Monjezi, R., et al., *Purification of bacteriophage M13 by anion exchange chromatography*. J Chromatogr B Analyt Technol Biomed Life Sci, 2010. **878**(21): p. 1855-9.
83. Trilisky, E.I. and A.M. Lenhoff, *Sorption processes in ion-exchange chromatography of viruses*. J Chromatogr A, 2007. **1142**(1): p. 2-12.
84. Orr, V., et al., *Recent advances in bioprocessing application of membrane chromatography*. Biotechnol Adv, 2013. **31**(4): p. 450-65.
85. Jungbauer, A., *Chromatographic media for bioseparation*. Journal of Chromatography A, 2005. **1065**(1): p. 3-12.
86. Vicente, T., et al., *Impact of ligand density on the optimization of ion-exchange membrane chromatography for viral vector purification*. Biotechnol Bioeng, 2011. **108**(6): p. 1347-59.
87. Strauss, D.M., et al., *Understanding the mechanism of virus removal by Q sepharose fast flow chromatography during the purification of CHO-cell derived biotherapeutics*. Biotechnol Bioeng, 2009. **104**(2): p. 371-80.
88. Li, H., et al., *A hydrophobic interaction chromatography strategy for purification of inactivated foot-and-mouth disease virus*. Protein Expr Purif, 2015. **113**: p. 23-9.
89. GEHealthcare, *Hydrophobic Interaction in Practice*, in *Hydrophobic Interaction and Reversed Phase Chromatography: Principles and Methods*.
90. McCue, J.T., *Theory and Use of Hydrophobic Interaction Chromatography in Protein Purification Applications*, in *Methods in Enzymology*, R.R. Burgess and M.P. Deutscher, Editors. 2009, Academic Press. p. 405-414.
91. Li, Z., et al., *Strong hydrophobicity enables efficient purification of HBc VLPs displaying various antigen epitopes through hydrophobic interaction chromatography*. Biochemical Engineering Journal, 2018. **140**: p. 157-167.
92. Kallberg, K., H.O. Johansson, and L. Bulow, *Multimodal chromatography: an efficient tool in downstream processing of proteins*. Biotechnology journal, 2012. **7**(12): p. 1485-1495.

93. Brown, M.R., et al., *A step-wise approach to define binding mechanisms of surrogate viral particles to multi-modal anion exchange resin in a single solute system*. Biotechnol Bioeng, 2017. **114**(7): p. 1487-1494.
94. Weigel, T., et al., *A flow-through chromatography process for influenza A and B virus purification*. J Virol Methods, 2014. **207**: p. 45-53.
95. Lagoutte, P., et al., *Scalable chromatography-based purification of virus-like particle carrier for epitope based influenza A vaccine produced in Escherichia coli*. J Virol Methods, 2016. **232**: p. 8-11.
96. Tseng, Y.F., et al., *A fast and efficient purification platform for cell-based influenza viruses by flow-through chromatography*. Vaccine, 2018. **36**(22): p. 3146-3152.
97. Lima, T.M., M.O. Souza, and L.R. Castilho, *Purification of flavivirus VLPs by a two-step chromatographic process*. Vaccine, 2019. **37**(47): p. 7061-7069.
98. Pato, T.P., et al., *Purification of yellow fever virus produced in Vero cells for inactivated vaccine manufacture*. Vaccine, 2019. **37**(24): p. 3214-3220.
99. Mundle, S.T., et al., *Core bead chromatography for preparation of highly pure, infectious respiratory syncytial virus in the negative purification mode*. Vaccine, 2016. **34**(32): p. 3690-6.
100. Trabelsi, K., M. Ben Zakour, and H. Kallel, *Purification of rabies virus produced in Vero cells grown in serum free medium*. Vaccine, 2019. **37**(47): p. 7052-7060.
101. Lacki, K.M. and F.J. Riske, *Affinity Chromatography: An Enabling Technology for Large-Scale Bioprocessing*. Biotechnol J, 2020. **15**(1): p. e1800397.
102. Brgles, M., et al., *Nonspecific native elution of proteins and mumps virus in immunoaffinity chromatography*. Journal of Chromatography A, 2016. **1447**: p. 107-114.
103. Elkana, Y., A. Thornton, and A.J. Zuckerman, *Purification of hepatitis A virus by affinity chromatography*. Journal of immunological methods, 1979. **25**(2): p. 185-187.
104. Opitz, L., et al., *Lectin-affinity chromatography for downstream processing of MDCK cell culture derived human influenza A viruses*. Vaccine, 2007. **25**(5): p. 939-47.
105. Olofsson, S., S. Jeansson, and E. Lycke, *Unusual lectin-binding properties of a herpes simplex virus type 1-specific glycoprotein*. Journal of virology, 1981. **38**(2): p. 564-570.

106. Opitz, L., et al., *Purification of cell culture-derived influenza virus A/Puerto Rico/8/34 by membrane-based immobilized metal affinity chromatography*. J Virol Methods, 2009. **161**(2): p. 312-6.
107. Jiang, C., et al., *Immobilized cobalt affinity chromatography provides a novel, efficient method for herpes simplex virus type 1 gene vector purification*. J Virol, 2004. **78**(17): p. 8994-9006.
108. del Cañizo, A.A.N., et al., *Foot and mouth disease virus concentration and purification by affinity chromatography*. Applied biochemistry and biotechnology, 1997. **61**(3): p. 399-409.
109. Du, P., et al., *Purification of foot-and-mouth disease virus by heparin as ligand for certain strains*. J Chromatogr B Analyt Technol Biomed Life Sci, 2017. **1049-1050**: p. 16-23.
110. Zhao, M., et al., *Affinity chromatography for vaccines manufacturing: Finally ready for prime time?* Vaccine, 2019. **37**(36): p. 5491-5503.
111. Ho, K.L., et al., *Selection of high affinity ligands to hepatitis B core antigen from a phage-displayed cyclic peptide library*. J Med Virol, 2003. **69**(1): p. 27-32.
112. Li, Y., et al., *Biomimetic design of affinity peptide ligand for capsomere of virus-like particle*. Langmuir, 2014. **30**(28): p. 8500-8.
113. Heldt, C.L., et al., *Porcine parvovirus removal using trimer and biased hexamer peptides*. Biotechnol J, 2012. **7**(4): p. 558-65.
114. Bandeira, V., et al., *Downstream processing of lentiviral vectors: releasing bottlenecks*. Hum Gene Ther Methods, 2012. **23**(4): p. 255-63.
115. Hagen, A., et al., *Development, preparation, and testing of VAQTA®*, a highly purified hepatitis A vaccine. Bioprocess Engineering, 2000. **23**(5): p. 439-449.
116. Zydney, A.L., *Perspectives on integrated continuous bioprocessing—opportunities and challenges*. Current Opinion in Chemical Engineering, 2015. **10**: p. 8-13.
117. Hernandez, R., *Continuous manufacturing: a changing processing paradigm*. BioPharm International, 2015. **28**(4): p. 20–27.
118. Fisher, A.C., et al., *The Current Scientific and Regulatory Landscape in Advancing Integrated Continuous Biopharmaceutical Manufacturing*. Trends Biotechnol, 2019. **37**(3): p. 253-267.

119. Schaber, S.D., et al., *Economic Analysis of Integrated Continuous and Batch Pharmaceutical Manufacturing: A Case Study*. Industrial & Engineering Chemistry Research, 2011. **50**(17): p. 10083-10092.
120. Walther, J., et al., *The business impact of an integrated continuous biomanufacturing platform for recombinant protein production*. J Biotechnol, 2015. **213**: p. 3-12.
121. Pollock, J., et al., *Integrated continuous bioprocessing: Economic, operational, and environmental feasibility for clinical and commercial antibody manufacture*. Biotechnol Prog, 2017. **33**(4): p. 854-866.
122. Boedeker, B., A. Goldstein, and E. Mahajan, *Fully Disposable Manufacturing Concepts for Clinical and Commercial Manufacturing and Ballroom Concepts*, in *New Bioprocessing Strategies: Development and Manufacturing of Recombinant Antibodies and Proteins*, B. Kiss, U. Gottschalk, and M. Pohlscheidt, Editors. 2018, Springer International Publishing: Cham. p. 179-210.
123. Klutz, S., et al., *Developing the biofacility of the future based on continuous processing and single-use technology*. J Biotechnol, 2015. **213**: p. 120-30.
124. Jungbauer, A., *Continuous downstream processing of biopharmaceuticals*. Trends Biotechnol, 2013. **31**(8): p. 479-92.
125. Bisschops, M. and M. Brower, *The impact of continuous multicolumn chromatography on biomanufacturing efficiency*. Pharmaceutical Bioprocessing, 2013. **1**(4): p. 361-372.
126. Budzinski, K., et al., *Introduction of a process mass intensity metric for biologics*. N Biotechnol, 2019. **49**: p. 37-42.
127. Budzinski, K.L., et al., *A call for industry to embrace green biopharma*. Nat Biotechnol, 2016. **34**(3): p. 234-5.
128. Xenopoulos, A., *A new, integrated, continuous purification process template for monoclonal antibodies: Process modeling and cost of goods studies*. Journal of Biotechnology, 2015. **213**: p. 42-53.
129. Albertsson, P.-A., *Partition of cell particles and macromolecules in polymer two phase systems*. Advances in protein chemistry, 1970. **24**: p. 309-341.
130. Rito-Palomares, M. and J. Benavides, *Aqueous two-phase systems for bioprocess development for the recovery of biological products*. 2017: Springer.

131. Soares, R.R., et al., *Partitioning in aqueous two-phase systems: Analysis of strengths, weaknesses, opportunities and threats*. Biotechnol J, 2015. **10**(8): p. 1158-69.
132. Rosa, P.A., et al., *Aqueous two-phase systems: A viable platform in the manufacturing of biopharmaceuticals*. J Chromatogr A, 2010. **1217**(16): p. 2296-305.
133. Aguilar, O., et al., *Direct comparison between ion-exchange chromatography and aqueous two-phase processes for the partial purification of penicillin acylase produced by E. coli*. J Chromatogr B Analyt Technol Biomed Life Sci, 2006. **835**(1-2): p. 77-83.
134. Rosa, P.A., et al., *Aqueous two-phase extraction as a platform in the biomanufacturing industry: economical and environmental sustainability*. Biotechnol Adv, 2011. **29**(6): p. 559-67.
135. Glyk, A., T. Scheper, and S. Beutel, *PEG-salt aqueous two-phase systems: an attractive and versatile liquid-liquid extraction technology for the downstream processing of proteins and enzymes*. Applied Microbiology and Biotechnology, 2015. **99**(16): p. 6599-6616.
136. Cunha, T. and R. Aires-Barros, *Large-scale extraction of proteins*. Molecular biotechnology, 2002. **20**(1): p. 29-40.
137. Singh, K.K., A.U. Renjith, and K.T. Shenoy, *Liquid-liquid extraction in microchannels and conventional stage-wise extractors: A comparative study*. Chemical Engineering and Processing: Process Intensification, 2015. **98**: p. 95-105.
138. Vázquez-Villegas, P., O. Aguilar, and M. Rito-Palomares, *Study of biomolecules partition coefficients on a novel continuous separator using polymer-salt aqueous two-phase systems*. Separation and Purification Technology, 2011. **78**(1): p. 69-75.
139. Espitia-Saloma, E., et al., *Continuous aqueous two-phase systems devices for the recovery of biological products*. Food and Bioproducts Processing, 2014. **92**(2): p. 101-112.
140. Trounson, A. and C. McDonald, *Stem Cell Therapies in Clinical Trials: Progress and Challenges*. Cell Stem Cell, 2015. **17**(1): p. 11-22.
141. González-González, M. and M. Rito-Palomares, *Cell-based aqueous two-phase systems for therapeutics*. Journal of Chemical Technology & Biotechnology, 2019. **95**(1): p. 8-10.

142. Birch, J.R. and A.J. Racher, *Antibody production*. Advanced drug delivery reviews, 2006. **58**(5-6): p. 671-685.
143. Johansson, H.O., et al., *Plasmid DNA partitioning and separation using poly(ethylene glycol)/poly(acrylate)/salt aqueous two-phase systems*. J Chromatogr A, 2012. **1233**: p. 30-5.
144. Gonzalez-Gonzalez, M., M. Rito-Palomares, and O. Mendez Quintero, *Partition behavior of CD133(+) stem cells from human umbilical cord blood in aqueous two-phase systems: In route to establish novel stem cell primary recovery strategies*. Biotechnol Prog, 2014. **30**(3): p. 700-7.
145. Zimmermann, S., et al., *High-throughput downstream process development for cell-based products using aqueous two-phase systems*. J Chromatogr A, 2016. **1464**: p. 1-11.
146. Azevedo, A.M., et al., *Partitioning of human antibodies in polyethylene glycol–sodium citrate aqueous two-phase systems*. Separation and Purification Technology, 2009. **65**(1): p. 14-21.
147. Mayerhoff, Z.D.V.L., I.C. Roberto, and T.T. Franco, *Purification of xylose reductase from Candida mogii in aqueous two-phase systems*. Biochemical Engineering Journal, 2004. **18**(3): p. 217-223.
148. Matos, T., et al., *Isolation of PCR DNA fragments using aqueous two-phase systems*. Separation and Purification Technology, 2014. **122**: p. 144-148.
149. Zhao, Q., et al., *Virus-like particle-based human vaccines: quality assessment based on structural and functional properties*. Trends in Biotechnology, 2013. **31**(11): p. 654-663.
150. Norrby, E.C.J. and P. Albertsson, *Concentration of poliovirus by an aqueous polymer two-phase system*. Nature, 1960. **188**(4755): p. 1047-1048.
151. Philipson, L., P.Å. Albertsson, and G. Frick, *The purification and concentration of viruses by aqueous polymer phase systems*. Virology, 1960. **11**(3): p. 553-571.
152. Mayolo-Deloisa, K., M. Rito-Palomares, and J. Benavides, *General Concepts and Definitions of Aqueous Two-Phase Systems*, in *Aqueous two-phase systems for bioprocess development for the recovery of biological products*, M. Rito-Palomares and J. Benavides, Editors. 2017, Springer. p. 1-18.
153. Hatti-Kaul, R., *Aqueous Two-Phase Systems_ Methods and Protocols*. Methods in Biotechnology, ed. J.M. Walker. Vol. 11. 2000: Springer Science & Business Media.

154. Benavides, J., et al., *Rotavirus-like particles primary recovery from insect cells in aqueous two-phase systems*. J Chromatogr B Analyt Technol Biomed Life Sci, 2006. **842**(1): p. 48-57.
155. Hammar, L. and G. Gilljam, *Extraction of HIV-1 in Aqueous Two-Phase Systems To Obtain a High Yield of gp120*. AIDS Research and Human Retroviruses, 1990. **6**(12): p. 1379-1388.
156. Luechau, F., T.C. Ling, and A. Lyddiatt, *Recovery of B19 virus-like particles by aqueous two-phase systems*. Food and Bioproducts Processing, 2011. **89**(4): p. 322-327.
157. Ladd Effio, C., et al., *Downstream processing of virus-like particles: single-stage and multi-stage aqueous two-phase extraction*. J Chromatogr A, 2015. **1383**: p. 35-46.
158. González-Mora, A., et al., *Recovery and primary purification of bacteriophage M13 using aqueous two-phase systems*. Journal of Chemical Technology & Biotechnology, 2017. **92**(11): p. 2808-2816.
159. Ananthapadmanabhan, K.P. and E.D. Goddard, *Aqueous biphasic formation in polyethylene oxide-inorganic salt systems*. Langmuir, 1987. **3**(1): p. 25-31.
160. Hey, M.J., D.P. Jackson, and H. Yan, *The salting-out effect and phase separation in aqueous solutions of electrolytes and poly(ethylene glycol)*. Polymer, 2005. **46**(8): p. 2567-2572.
161. Wysoczanska, K. and E.A. Macedo, *Influence of the Molecular Weight of PEG on the Polymer/Salt Phase Diagrams of Aqueous Two-Phase Systems*. Journal of Chemical & Engineering Data, 2016. **61**(12): p. 4229-4235.
162. Azevedo, A.M., et al., *Chromatography-free recovery of biopharmaceuticals through aqueous two-phase processing*. Trends Biotechnol, 2009. **27**(4): p. 240-7.
163. Grilo, A.L., M. Raquel Aires-Barros, and A.M. Azevedo, *Partitioning in Aqueous Two-Phase Systems: Fundamentals, Applications and Trends*. Separation & Purification Reviews, 2014. **45**(1): p. 68-80.
164. Cabezas Jr. , H., *Theory of phase formation in aqueous two phase system*. Journal of Chromatography B, 1996. **680**(1-2): p. 3-30.
165. Asenjo, J.A. and B.A. Andrews, *Aqueous two-phase systems for protein separation: a perspective*. J Chromatogr A, 2011. **1218**(49): p. 8826-35.

166. Guan, Y., T.H. Lilley, and T.E. Treffry, *A new excluded volume theory and its application to the coexistence curves of aqueous polymer two-phase systems*. *Macromolecules*, 1993. **26**(15): p. 3971-3979.
167. Huddleston, J.G., et al., *Influence of system and molecular parameters upon fractionation of intracellular proteins from Saccharomyces by aqueous two-phase partition*. *Enzyme and microbial technology*, 1991. **13**(1): p. 24-32.
168. Jyh-Ping, C., *Partitioning and separation of α -lactalbumin and β -lactoglobulin in PEG/potassium phosphate aqueous two-phase systems*. *Journal of Fermentation and Bioengineering*, 1992. **73**(2): p. 140-147.
169. Andrews, B.A. and J.A. Asenjo, *Theoretical and Experimental Evaluation of Hydrophobicity of Proteins to Predict their Partitioning Behavior in Aqueous Two Phase Systems: A Review*. *Separation Science and Technology*, 2010. **45**(15): p. 2165-2170.
170. Mohamadi, H.S., E. Omidinia, and R. Dinarvand, *Evaluation of recombinant phenylalanine dehydrogenase behavior in aqueous two-phase partitioning*. *Process Biochemistry*, 2007. **42**(9): p. 1296-1301.
171. Bekale, L., D. Agudelo, and H.A. Tajmir-Riahi, *The role of polymer size and hydrophobic end-group in PEG-protein interaction*. *Colloids Surf B Biointerfaces*, 2015. **130**: p. 141-8.
172. Wu, J., et al., *Binding characteristics between polyethylene glycol (PEG) and proteins in aqueous solution*. *Journal of Materials Chemistry B*, 2014. **2**(20).
173. Ruiz-Ruiz, F., et al., *Aqueous two-phase affinity partitioning systems: current applications and trends*. *J Chromatogr A*, 2012. **1244**: p. 1-13.
174. Asenjo, J.A., et al., *Model for predicting the partition behaviour of proteins in aqueous two-phase systems*. *Journal of Chromatography A*, 1994. **668**(1): p. 47-54.
175. Zaslavsky, B.Y., *Physicochemical properties of phases in aqueous polymer systems*, in *Aqueous two-phase partitioning: physical chemistry and bioanalytical applications*. 1994, CRC press. p. 155-220.
176. Atefi, E., et al., *Interfacial Tension Effect on Cell Partition in Aqueous Two-Phase Systems*. *ACS Appl Mater Interfaces*, 2015. **7**(38): p. 21305-14.
177. Münchow, G., et al., *Protein Diffusion Across the Interface in Aqueous Two-Phase Systems*. *Langmuir*, 2008. **24**(16): p. 8547-8553.

178. Vijayaragavan, K.S., et al., *Separation of porcine parvovirus from bovine serum albumin using PEG-salt aqueous two-phase system*. J Chromatogr B Analyt Technol Biomed Life Sci, 2014. **967**: p. 118-26.
179. Chow, Y.H., et al., *Characterization of bovine serum albumin partitioning behaviors in polymer-salt aqueous two-phase systems*. J Biosci Bioeng, 2015. **120**(1): p. 85-90.
180. Atefi, E., J.A. Mann, Jr., and H. Tavana, *Ultralow interfacial tensions of aqueous two-phase systems measured using drop shape*. Langmuir, 2014. **30**(32): p. 9691-9.
181. Asenjo, J.A., et al., *Phase separation rates of aqueous two-phase systems: Correlation with system properties*. Biotechnology and Bioengineering, 2002. **79**(2): p. 217-223.
182. Haynes, C.A., et al., *Electrostatic potentials and protein partitioning in aqueous two-phase systems*. AIChE Journal, 1991. **37**(9): p. 1401-1409.
183. Johansson, H.-O., et al., *Driving forces for phase separation and partitioning in aqueous two-phase systems*. Journal of Chromatography B: Biomedical Sciences and Applications, 1998. **711**(1-2): p. 3-17.
184. Pfennig, A., A. Schwerin, and J. Gaube, *Consistent view of electrolytes in aqueous two-phase systems*. Journal of Chromatography B: Biomedical Sciences and Applications, 1998. **711**(1): p. 45-52.
185. Tubío, G., et al., *Liquid-Liquid Equilibria of Aqueous Two-Phase Systems Containing Poly(ethylene glycols) of Different Molecular Weight and Sodium Citrate*. Journal of Chemical & Engineering Data, 2006. **51**(1): p. 209-212.
186. Barani, A., et al., *Influence of the molecular weight of polymer, temperature and pH on phase diagrams of poly (ethylene glycol) + di-potassium tartrate aqueous two-phase systems*. Fluid Phase Equilibria, 2018. **459**: p. 1-9.
187. Lu, Y.-M., et al., *Bovine serum albumin partitioning in polyethylene glycol (PEG)/potassium citrate aqueous two-phase systems*. Food and Bioproducts Processing, 2010. **88**(1): p. 40-46.
188. Iqbal, M., et al., *Aqueous two-phase system (ATPS): an overview and advances in its applications*. Biol Proced Online, 2016. **18**: p. 18.
189. Rosa, P.A., A.M. Azevedo, and M.R. Aires-Barros, *Application of central composite design to the optimisation of aqueous two-phase extraction of human antibodies*. J Chromatogr A, 2007. **1141**(1): p. 50-60.

190. Kalaivani, S. and I. Regupathi, *Partitioning studies of alpha-lactalbumin in environmental friendly poly (ethylene glycol)--citrate salt aqueous two phase systems*. Bioprocess Biosyst Eng, 2013. **36**(10): p. 1475-83.
191. Bastos-González, D., et al., *Ions at interfaces: the central role of hydration and hydrophobicity*. Current Opinion in Colloid & Interface Science, 2016. **23**: p. 19-28.
192. Glyk, A., T. Scheper, and S. Beutel, *Influence of Different Phase-Forming Parameters on the Phase Diagram of Several PEG–Salt Aqueous Two-Phase Systems*. Journal of Chemical & Engineering Data, 2014. **59**(3): p. 850-859.
193. Silvério, S.C., et al., *Effect of Aqueous Two-Phase System Constituents in Different Poly(ethylene glycol)–Salt Phase Diagrams*. Journal of Chemical & Engineering Data, 2012. **57**(4): p. 1203-1208.
194. Silvério, S.C., et al., *The Effect of Salts on the Liquid–Liquid Phase Equilibria of PEG600 + Salt Aqueous Two-Phase Systems*. Journal of Chemical & Engineering Data, 2013. **58**(12): p. 3528-3535.
195. Jacinto, M.J., et al., *Optimization and miniaturization of aqueous two phase systems for the purification of recombinant human immunodeficiency virus-like particles from a CHO cell supernatant*. Separation and Purification Technology, 2015. **154**: p. 27-35.
196. Yoshizawa, S., T. Arakawa, and K. Shiraki, *Effect of counter ions of arginine as an additive for the solubilization of protein and aromatic compounds*. Int J Biol Macromol, 2016. **91**: p. 471-6.
197. Wysoczanska, K., et al., *Cation effect on the (PEG 8000 + sodium sulfate) and (PEG 8000 + magnesium sulfate) aqueous two-phase system: Relative hydrophobicity of the equilibrium phases*. The Journal of Chemical Thermodynamics, 2015. **91**: p. 321-326.
198. Breydo, L., et al., *Effects of osmolytes on protein-solvent interactions in crowded environment: Analyzing the effect of TMAO on proteins in crowded solutions*. Arch Biochem Biophys, 2015. **570**: p. 66-74.
199. Willow, S.Y. and S.S. Xantheas, *Molecular-Level Insight of the Effect of Hofmeister Anions on the Interfacial Surface Tension of a Model Protein*. J Phys Chem Lett, 2017. **8**(7): p. 1574-1577.
200. Light, T.P., et al., *Hofmeister Ion-Induced Changes in Water Structure Correlate with Changes in Solvation of an Aggregated Protein Complex*. Langmuir, 2016. **32**(5): p. 1360-9.

201. Hamzehzadeh, S. and M.T. Zafarani-Moattar, *Phase separation in aqueous solutions of polypropylene glycol and sodium citrate: Effects of temperature and pH*. Fluid Phase Equilibria, 2015. **385**: p. 37-47.
202. Grossman, P.D. and J.L. Gainer, *Correlation of aqueous two-phase partitioning of proteins with changes in free volume*. Biotechnology progress, 1988. **4**(1): p. 6-11.
203. Schloer, G.M. and S.S. Breese Jr, *Purification of African malignant catarrhal fever virus using a two-phase aqueous polymer system*. Journal of General Virology, 1982. **59**(1): p. 101-110.
204. Eiteman, M.A. and J.L. Gainer, *Peptide hydrophobicity and partitioning in poly (ethylene glycol)/magnesium sulfate aqueous two-phase systems*. Biotechnology Progress, 1990. **6**(6): p. 479-484.
205. Eiteman, M.A., C. Hassinen, and A. Veide, *A mathematical model to predict the partitioning of peptides and peptide-modified proteins in aqueous two-phase systems*. Biotechnology progress, 1994. **10**(5): p. 513-519.
206. Andrews, B.A., A.S. Schmidt, and J.A. Asenjo, *Correlation for the partition behavior of proteins in aqueous two-phase systems: Effect of surface hydrophobicity and charge*. Biotechnology and bioengineering, 2005. **90**(3): p. 380-390.
207. Johnson, S.A., et al., *The step-wise framework to design a chromatography-based hydrophobicity assay for viral particles*. J Chromatogr B Analyt Technol Biomed Life Sci, 2017. **1061-1062**: p. 430-437.
208. Arnold, E., et al., *The structure determination of a common cold virus, human rhinovirus 14*. Acta Crystallographica Section A, 1987. **43**(3): p. 346-361.
209. Mi, X., et al., *Virus Isoelectric Point Determination Using Single-Particle Chemical Force Microscopy*. Langmuir, 2020. **36**(1): p. 370-378.
210. Yancey, P.H., et al., *Living with water stress: evolution of osmolyte systems*. Science, 1982. **217**(4566): p. 1214-1222.
211. Yancey, P.H., W.R. Blake, and J. Conley, *Unusual organic osmolytes in deep-sea animals: adaptations to hydrostatic pressure and other perturbants*. Comparative Biochemistry and Physiology Part A: Molecular & Integrative Physiology, 2002. **133**(3): p. 667-676.
212. Bockus, A.B. and B.A. Seibel, *Trimethylamine oxide accumulation as a function of depth in Hawaiian mid-water fishes*. Deep Sea Research Part I: Oceanographic Research Papers, 2016. **112**: p. 37-44.

213. Yancey, P.H., *Organic osmolytes as compatible, metabolic and counteracting cytoprotectants in high osmolarity and other stresses*. J Exp Biol, 2005. **208**(Pt 15): p. 2819-30.
214. Seki, M., et al., *Regulatory metabolic networks in drought stress responses*. Curr Opin Plant Biol, 2007. **10**(3): p. 296-302.
215. Suprasanna, P., G.C. Nikalje, and A.N. Rai, *Osmolyte Accumulation and Implications in Plant Abiotic Stress Tolerance*, in *Osmolytes and Plants Acclimation to Changing Environment: Emerging Omics Technologies*, N. Iqbal, R. Nazar, and N. A. Khan, Editors. 2016, Springer India: New Delhi. p. 1-12.
216. Kumar, R., *Role of naturally occurring osmolytes in protein folding and stability*. Arch Biochem Biophys, 2009. **491**(1-2): p. 1-6.
217. Auton, M., et al., *Osmolyte effects on protein stability and solubility: a balancing act between backbone and side-chains*. Biophys Chem, 2011. **159**(1): p. 90-9.
218. Wlodarczyk, S.R., et al., *Influence and effect of osmolytes in biopharmaceutical formulations*. Eur J Pharm Biopharm, 2018. **131**: p. 92-98.
219. Lampel, A., et al., *The effect of chemical chaperones on the assembly and stability of HIV-1 capsid protein*. PLoS One, 2013. **8**(4): p. e60867.
220. Bye, J.W., L. Platts, and R.J. Falconer, *Biopharmaceutical liquid formulation: a review of the science of protein stability and solubility in aqueous environments*. Biotechnol Lett, 2014. **36**(5): p. 869-75.
221. Lee, J.C., *Biopharmaceutical formulation*. Current opinion in biotechnology, 2000. **11**(1): p. 81-84.
222. Meersman, F., et al., *Counteraction of urea by trimethylamine N-oxide is due to direct interaction*. Biophys J, 2009. **97**(9): p. 2559-66.
223. Miles, A.P., et al., *Montanide ISA 720 vaccines: quality control of emulsions, stability of formulated antigens, and comparative immunogenicity of vaccine formulations*. Vaccine, 2005. **23**(19): p. 2530-9.
224. Flood, A., et al., *Development of a Freeze-Dried, Heat-Stable Influenza Subunit Vaccine Formulation*. PLoS One, 2016. **11**(11): p. e0164692.
225. Street, T.O., D.W. Bolen, and G.D. Rose, *A molecular mechanism for osmolyte-induced protein stability*. Proceedings of the National Academy of Sciences, 2006. **103**(38): p. 13997-14002.

226. Fedotova, M.V. and S.E. Kruchinin, *Hydration and ion-binding of glycine betaine: How they may be involved into protection of proteins under abiotic stresses*. Journal of Molecular Liquids, 2017. **244**: p. 489-498.
227. Auton, M., D.W. Bolen, and J. Rosgen, *Structural thermodynamics of protein preferential solvation: osmolyte solvation of proteins, aminoacids, and peptides*. Proteins, 2008. **73**(4): p. 802-13.
228. Heldt, C.L., et al., *Experimental and computational surface hydrophobicity analysis of a non-enveloped virus and proteins*. Colloids Surf B Biointerfaces, 2017. **153**: p. 77-84.
229. Gencoglu, M.F., E. Pearson, and C.L. Heldt, *Porcine parvovirus flocculation and removal in the presence of osmolytes*. J Biotechnol, 2014. **186**: p. 83-90.
230. Liao, Y.T., et al., *Trimethylamine N-oxide stabilizes proteins via a distinct mechanism compared with betaine and glycine*. Proc Natl Acad Sci U S A, 2017. **114**(10): p. 2479-2484.

3 Tie line framework to optimize non-enveloped virus recovery in aqueous two-phase systems^{1,2}

¹The material in this chapter is published in Journal of Chromatography B.
Full Citation: *Joshi, P.U., Turpeinen, D.G., Weiss, M., Escalante-Corbin, G., Schroeder, M., and Heldt, C.L. Tie Line Framework to Optimize Non-enveloped Virus Recovery in Aqueous Two-Phase Systems. Journal of Chromatography B, 2019, 1126-1127, 121744.*

²The unpublished extension of the work in this chapter is mentioned in Appendix B.

3.1 Introduction

The large number of new vaccines and gene therapy vectors coming to market has spurred growth in viral particle manufacturing. Vaccine manufacturing growth is also shifting to India and China [1], providing an opportunity to redesign currently approved processes for traditional vaccines. Since industries have yet to achieve a platform virus particle process, as has been achieved with antibody manufacturing [2], new unit operations need to be considered for viral products that can provide virus stability, high yields, and increased purity. The ultimate goals are to increase throughput, reduce production cost, and to shift towards continuous processing. Two key attributes are hindering the manufacturing of viral particles, scale-up difficulties, and low yield. In the laboratory, ultracentrifugation produces high purity and high concentration viral stocks [3,4]. However, this extremely manual process is time consuming and expensive. In addition, co-precipitation has made sedimentation processes discouraging to be used for large-scale production of vaccines [5,6].

The current race to develop a robust, easy to scale up, environmentally friendly, and continuous process has led to tremendous research in various chromatography methods for viral particles. Commonly used chromatography modes for virus and viral vector processing include size exclusion [7–9], affinity [10,11] and ion exchange [12,13]. Although chromatography is a widely used method for purification of other biomolecules, low dynamic binding capacities of large biomolecules reduces the throughput and yield [14,15]. The purification of rhinovirus using anion-exchange chromatography (AEX) found that only a fraction of viral particles bound to the column, leading to a high purity but low recovery process [16]. It was also observed that two peaks of virus eluted from the column, suggesting either different sites on the virus binding to the column or different sites on the column binding with different strength to the virus [16]. Issues of yield need to be addressed prior to large scale manufacturing of these viral particles. A few studies have shown a continuous viral downstream process.

Most commonly, a continuous simulated moving bed (SMB) configuration is used [17,18]. Cell culture-derived influenza virus was purified with a three column SMB arrangement and a productivity of 3.8 times higher than batch mode was achieved [17]. However, the yield decreased from 80% in the batch mode to 70% in the SMB configuration and the purity decreased. A two column SMB chromatography system was used to purify adenovirus serotype 5 with size exclusion chromatography in a countercurrent configuration [18]. In this case, a higher yield was achieved in the SMB configuration (86%) as compared to batch mode (57%), with a 6-fold increase in the productivity. Although the integration of continuous chromatography is likely to reduce the overall cost and increase the productivity, the challenges pertaining to maintaining equipment robustness, sterility over long processing times, and real time process analytical technology (PAT) remain [19]. Due to these problems, the use of multiple columns still lack integration to the rest of the downstream processing units and is not currently used commercially [20]. Aqueous two-phase systems (ATPS) are potential candidates for

virus purification to shorten the number of unit operations needed in the downstream processing train and provide simple integration into a continuous process. Unlike other purification methods, ATPS is robust, environmentally friendly, inexpensive, easy to scale up, and can be operated as a continuous process with short processing times [21]. ATPS involves mixing two aqueous solutions which produce two phases when present above a critical concentration. Water is the major constituent of each phase. Contrary to the high cost of chromatography resins and specialty membranes, the inexpensive raw materials used in ATPS, along with lower processing time and energy consumption, makes it a potential method to trim the cost of production for any biotherapeutic product [22]. A previous study of penicillin acylase purification compared ion exchange chromatography with ATPS, concluding that ATPS not only reduced the unit operation number from 7 to 4 but also lowered the gross production cost by 37%. The findings were obtained considering 100 times re-use of the resin [23]. ATPS provides a good alternative for integrating clarification and purification for a more

efficient downstream process. Many types of ATPS have been developed to partition biomolecules.

Examples include polymer/polymer [24], polymer/salt [25,26], ionic liquid/salt [27,28], and quaternary ammonium salt/salt [29] systems. The polymer/polymer system, typically polyethylene glycol (PEG) and dextran, is the classic ATPS. However, high viscosities, the expense of dextran, and the difficulty in polymer recycling led to the development of salt-containing systems. Polymer/salt systems have been extensively studied for protein purification [30–33] and only a few studies have been reported on virus purification in ATPS. Some viruses and virus-like particles recovered by ATPS are shown in **Table 3-1**. Virus-like particles (VLPs) have been studied more often in ATPS to demonstrate a better downstream process for gene therapy vectors or subunit vaccines [25,26,34]. VLPs mimic the viral surface immunogenicity but are void of genomes [35]. Maintaining the infectivity of viruses is one of the major challenges in the downstream processes. This difference can be seen in the higher VLP recoveries as compared to the lower recoveries of infectious virus (**Table 3-1**). ATPS have been run in continuous mode for the processing of protein products [39–41]. The relatively low viscosities and interfacial tension make the PEG-salt systems the preferred ATPS for scale up and continuous operation. Various methods to contact the two phases, such as spray columns, perforated discs, pulsed cap columns, and conventional mixer-settlers have been suggested to perform continuous ATPS [39]. Mixer-settlers have successfully extracted monoclonal antibody (IgG1) [41] and an enzyme from spent yeast [40]. Some processing drawbacks such as flooding and backmixing have been identified [39]. But the problems are outweighed by the easy adaption of ATPS to continuous processes, as compared to chromatography. However, the complex partitioning mechanism of biomolecules has averted the integration of ATPS at an industrial scale. Numerous theories on the mechanism of partitioning of biomolecules in ATPS have been proposed. The two leading theories are that the partitioning is, 1) highly dependent on the excluded volume [30,42–44], or 2) a combination of hydrophobic and electrostatic interactions [38,45–47]. The excluded volume theory suggests that the random distribution of PEG molecules

results in a geometrically saturated solution, excluding biomolecules from the polymer-rich phase due to a lack of space available for the biomolecule to occupy [48]. On the other hand, the hydrophobic and electrostatic interaction theory argues that the partitioning of the biomolecules results from the combined effect of the salting-out from the salt-rich phase and a hydrophobic driving force pulling the biomolecule into the more hydrophobic PEG-rich phase [45]. Our data demonstrated that high MW PEG increased virus partitioning to the PEG-rich phase which supports the hydrophobic and electrostatic theory of partitioning [38]. The PEG and the salt composition and concentration control the hydrophobicity and electrostatics, respectively, in ATPS [49,50]. High MW PEG stay more globular in solution than lower MW PEG, which are more linear in solution [49,51]. Linear PEGs have more interaction with water and are better hydrated, whereas globular PEGs are less hydrated and therefore have more hydrophobic character. Unlike higher MW PEGs, lower MW PEGs have lower capabilities to provide multiple hydrophobic binding sites due to fewer of ethylene monomers [49]. For salts, the Hoffmeister series, which describes the hydration ability of different ions, has been used to describe the effect of different salts in ATPS [38,52]. A lower concentration of salt is required to form the twophase region when multivalent salts are used as compared to monovalent salts [50], demonstrating the importance of ionic strength in the system. However, there are still many questions as to the driving forces within the ATPS that govern partitioning. Without a more systematic characterization of the two-phase region, ATPS will continue to have too many unknown variables that make it too risky to use in an FDA approved process.

Table 3-1. Overview of virus and virus-like particles in PEG/salt ATPS.

Target Biomolecule	System	Recovery	Reference
Rotavirus-like particles	PEG 400/phosphate	90%	[26]
HIV-VLP	PEG 1500/sulfate	4.4*	[34]
Bacteriophage M13	PEG 400/ phosphate	83%	[36]
Bacteriophage T4	PEG 8000/phosphate	38%	[37]
Porcine parvovirus	PEG 12000/citrate	64%	[38]

*partition coefficient

This study aimed to determine the effect of PEG and salt concentration on virus recovery. The model non-enveloped viruses used for this study were porcine parvovirus (PPV), a single stranded DNA virus with a diameter of 18–26 nm [53], and human rhinovirus (HRV), a single stranded RNA virus with a diameter of ~30nm [54]. Both viruses have icosahedral symmetry. Previous work had established that the PEG 12 kDa-citrate system could recover PPV in the PEG-rich phase [38]. This particular study focused on tie line (TL) characterization and its effect on PPV and HRV recovery to create a stronger theory on the mechanism of partitioning for viral particles in ATPS. TLs are thermodynamic equilibrium points that form in the two-phase region. Along a TL, the system separates into phases that have the same concentration, but the volume ratio of the phases changes. This systematic evaluation of the two-phase ATPS space allowed us to understand the balance between the salting-out effect of the citrate-rich phase and the ability of the PEG-rich phase to pull the virus out of the interface and into the PEG-rich phase by hydrophobic interactions. It is difficult to recover biomolecules from the interface, so extracting as much virus into the PEG-rich phase was desired. There was a unique separation behavior observed at each tie line length (TLL). With a matrix containing TLL and TL ratios, we were able to recover the majority of the infectious PPV in a PEG 12 kDa-citrate system with high purity. By comparing the PPV recovery to the HRV recovery, we were able to add to the understanding of viral particle driving forces in ATPS.

3.2 Materials & Methods

3.2.1 Materials

Eagle's minimum essential media (EMEM), sodium bicarbonate, phosphate buffered saline (PBS, pH 7.2), penicillin-streptomycin (10,000 U/ml), and trypsin/EDTA for cell propagation were purchased from Life Technologies (Carlsbad, CA). Fetal bovine serum (FBS, Canada origin) was purchased from HyClone™ GE Healthcare (Pittsburg, PA). 2-(3,5-diphenyltetrazol-2-ium-2-yl)-4,5-dimethyl-1,3thiazole;bromide (MTT, 98%) was purchased from Alfa Aesar™ (Haverhill, MA) and sodium dodecyl sulfate (SDS, BioReagent, ≥98.5%) was purchased from VWR (Radnor, PA). Polyethylene glycol with an average molecular weight of 12,000 (PEG 12 kDa), trisodium citrate dihydrate (ACS reagent grade, ≥99%), citric acid monohydrate (ACS reagent, ≥99%), and sodium phosphate dibasic heptahydrate (ACS reagent grade) were purchased from Sigma-Aldrich (St. Louis, MO). Sodium phosphate monobasic monohydrate (ACS reagent grade) was purchased from Fisher Scientific (Waltham, MA). All solutions were made with Nanopure water (Thermo Scientific, Waltham, MA) at a resistance of ≥18 MΩ and filtered with a 0.2 μm Nalgene (Thermo Scientific) bottle top filter prior to use.

3.2.2 Methods

3.2.2.1 Cell maintenance and virus titration

Porcine kidney cells (PK-13) and H1HeLa cells (HeLa), purchased from ATCC (CRL-6489™ and CRL-1958™ respectively), were grown in EMEM supplemented with 1% penicillin/streptomycin. In addition, the PK-13 cell media was supplemented with 10% FBS and the HeLa cell media was supplemented with 5% FBS. The cells were incubated at 37 °C, 5% CO₂, and 100% humidity. PPV strain NADL-2 was a generous gift from Dr. Ruben Carbonell (North Carolina State University, Raleigh, NC), and was propagated

in PK-13 cells, as described previously [55]. HRV-14 strain 1059 was purchased from ATCC (VR-284™) and propagated in HeLa cells. Briefly, HRV was infected at 0.001 MTT50/cell after 24 h of HeLa incubation at 70–80% confluency. The infected HeLa cells were incubated at 35 °C for HRV propagation. The cell lysis was collected 5 days post-infection.

The titer of PPV and HRV were found by the colorimetric MTT cell viability assay [56]. Briefly, 96-well plates were seeded with PK-13 or HeLa cells at a seeding density of 8×10^4 cells/well. The cells were infected 24 h post-incubation with PPV or HRV and serially diluted at a 1:5 ratio across the plate. PPV infected PK-13 cells were incubated at 37 °C and HRV infected HeLa cells were incubated at 35 °C. After six days, an MTT salt solution was added to each well and both cell lines were incubated at 37 °C. This was followed by addition of an acidic SDS solubilization solution. The absorbance was recorded with a Synergy Mx microplate reader (BioTek, Winooski, VT) after 4–12 h. The 50% infectious dose value of PPV and HRV was determined and reported in the units of MTT50/ml [55].

3.2.2.2 Construction of binodal curves and tie lines

The binodal curve was generated using the turbidity method with appropriate stock PEG and citrate concentrations, as described earlier [38]. Briefly, systems were formed at high concentrations and diluted with water until the turbid systems turned clear. The tie lines were determined by conductivity measurements of the citrate-rich (bottom) phase using a VWR® symphony™ conductivity meter (Radnor, PA), [50] and interpolating the citrate compositions from a standard curve. The endpoints of the tie lines were determined by calculating the remaining amount of citrate in the PEG-rich (top) phase by completing a mass balance of the system. The tie lines were characterized by their tie line length (TLL), calculated as [57],

$$TLL = \sqrt{\Delta x_{PEG}^2 + \Delta x_{cit}^2} \quad (3-1)$$

where Δx_{PEG} is the concentration difference of PEG in the top phase and bottom phase and Δx_{cit} is the concentration difference of citrate in the top phase and bottom phase. TL ratios were calculated as

$$TL\ ratio = \frac{length(\overline{TS})}{length(\overline{SB})} \quad (3-2)$$

where S is the system composition point, T is the top node, and B is the bottom node (see Fig. 1). The volume ratios were calculated as

$$VR = \frac{(Volume)_{top\ phase}}{(Volume)_{bottom\ phase}} \quad (3-3)$$

After determining the tie lines, TLL 15, 25, and 36 w/w% were chosen for the study of virus partitioning. ATPSs were made with stock solutions of 30 w/w% citrate and solutions ranging from 33 to 45 w/w % of PEG. Appropriate amounts of stock solutions, water and 0.1 g of crude PPV were added to a microcentrifuge tube to complete a 1 g system. All systems were mixed with a vortex mixer and the phase separation was carried out in an ST16R Centrifuge (Thermo Scientific, Pittsburg, PA) at ~12,300 xg at 21 °C for 5 min. The recovery of PPV was calculated as

$$\%Recovery = \frac{V_{P/C} * T_{P/C}}{V_i * T_i} * 100 \quad (3-4)$$

where V is the volume of the PEG-rich phase (P), the citrate-rich phase (C) or the initial stock (i) and T is the titer of one phase expressed as MTT50/ml [38]. The partitioning coefficient was calculated as

$$K = \frac{V_P * T_P}{V_C * T_C} \quad (3-5)$$

3.2.2.3 Physical Properties of Systems

The refractive index of the extracted PEG-rich phases was measured with a Digital Brix/RI-Chek refractometer (Reichert Technologies, Depew, NY), with an

accuracy of ± 0.0002 . Densities of the PEG-rich and citrate-rich phases were measured by weighing 1 ml of the phase using a calibrated pipette on a Mettler-Toledo analytical balance (Columbus, OH), with a readability up to 0.1 mg.

3.2.2.4 SDS-PAGE

The partitioning of the contaminant proteins in the crude lysate was measured using sodium dodecyl sulfate-polyacrylamide gel electrophoresis (SDS-PAGE) with a 4–12% Bis-Tris NuPage gel and NuPage MOPS running buffer (Life Technologies, Carlsbad, CA). Benchmark™ protein ladder with a molecular weight range of 10–220 kDa (Life Technologies) was used as the marker. Samples were reduced using β mercaptoethanol (Sigma-Aldrich, St. Louis, MO) at 7% concentration, and heated to 70 °C for 10 min prior to loading onto the gel. The SDS-PAGE was run for 55 min at a constant 200 V. The gel was loaded at a constant volume so that concentrations of contaminating proteins could be compared. The gel was stained with the SilverXpress™ staining kit (Life Technologies, Carlsbad, CA).

3.2.2.5 DNA quantification

DNA content in the PEG-rich phase and citrate-rich phase was measured using the Quant-iT™ PicoGreen® dsDNA kit (ThermoFisher Scientific, Waltham, MA). The PEG-rich phase and citrate-rich phase were diluted in water to have a final concentration of PEG and citrate as ≤ 1 w/w%. The host cell DNA in the crude lysate, PEG-rich and citrate-rich phase was measured, as per manufacturer's instruction. The fluorescent activities (excitation: 480 nm and emission: 520 nm) of the samples were measured using a Synergy™ Mx microplate reader. DNA recovery was calculated similar to virus recovery as:

$$\%DNA\ recovery = \frac{DNA\ concentration_{P/C} * V_{P/C} * DF}{DNA\ concentration_i * V_i * DF} * 100 \quad (3-6)$$

where V denotes volume of the PEG-rich phase (P), citrate-rich phase (C) or initial stock (i) and DF denotes the respective dilution factor.

3.2.2.6 Dynamic Light Scattering (DLS)

Virus aggregates at varying concentrations of citrate were measured by DLS with a Malvern Zetasizer Nano ZS (Westborough, MA). First, virus was dialyzed in Biotech cellulose ester 1000 kDa dialysis tubing (Rancho Dominguez, CA) at 4 °C for two days with two buffer exchanges of 20mM phosphate buffer at pH 7.0 (PB). Then, the dialyzed virus was further purified in an Econo-Pac 10DG desalting column (Hercules, CA). The fraction containing the highest titer was used to mix with sodium citrate solution at pH 7 to give different final concentrations of citrate. The hydrodynamic diameter was measured and the aggregate ratio (AR) was calculated as:

$$AR = \frac{D_{H,18-26 \text{ nm}}}{D_{H,>100 \text{ nm}}} \quad (3-7)$$

where $D_{H,18-26\text{nm}}$ is the maximum intensity of the peak at 18–26 nm (the virus intensity) and $D_{H,>100\text{nm}}$ is the maximum intensity of the aggregate peak, which was >100 nm and became larger as the concentration of citrate increased.

3.3 Results

3.3.1 Model Virus

Porcine parvovirus (PPV) and human rhinovirus (HRV) were chosen as the model non-enveloped viruses to study the partitioning in ATPS and key properties are shown in **Table 3-2**. PPV is a ssDNA virus that is approximately 18–26 nm in diameter [53]. PPV is a pathogenic agent that causes reproductive failure in swine populations [58,59], and is a model for the human B19 parvovirus. The capsid of PPV is composed of three proteins, VP1, VP2, and VP3. VP2 is the major constituent (~80%) of the capsid [60]. Recently, a

comparative study using computational and experimental methods showed that PPV [61] and a closely related murine parvovirus, MVM [62], are more hydrophobic than a panel of proteins. This significant difference in the surface hydrophobicity of PPV and contaminant proteins is an ideal driving force to develop new purification methods for viral particles. HRV is a ssRNA virus that is ~30nm in diameter, composed of VP1, VP2, VP3, and VP4 capsid proteins [64,66]. VP1, VP2, and VP3 are surface exposed antigenic proteins, whereas VP4 is present in the inside of the capsid and assists in anchoring the RNA inside the capsid [64]. HRV is one of the agents causing common cold and exacerbations of asthma in humans, with three main species, namely A, B, and C, and >100 serotypes identified [67–71]. Despite extensive research, there is no effective antiviral drug treatment for HRV infections [72]. This virus was used to show the effect of surface hydrophobicity at net neutral surface charge on virus partitioning in ATPS.

Table 3-2. A brief description and comparison of the model viruses (PPV and HRV)

Model Virus	Genome	Family	Related Virus	pI	Size (nm)	References
PPV	ssDNA	parvoviridae	B19, AAV	5.0	18-26	[60, 63]
HRV	(+)ssRNA	picornaviridae	FMDV, Polio, Hep A	6.9	~30	[64-66]

PPV: porcine parvovirus; HRV: human rhinovirus; B19: B19 parvovirus; AAV: adeno associated virus; FMDV: foot & mouth disease virus; Polio: poliovirus; Hep A: hepatitis A virus

3.3.2 Binodal curves & tie lines

The ATPS binodal phase diagram separates the homogeneous region from the two-phase region, as shown in **Figure 3-1A**. Tie lines were generated to study systems containing the same concentrations of each component in the PEG-rich and citrate-rich phases. Tie lines are thermodynamic equilibrium states in the two-phase region, representing a unique value of Gibb's free energy [57,73]. An increase in the TLL (Eq. (3-1)) increases the Gibb's free energy, which correlates to the thermodynamic driving

force [73] and results in higher PEG and salt concentrations in each phase. Additionally, an increase in TLL also provides elevated hydrophobic interaction from the PEG-rich phase and effective salting-out of proteins from the salt-rich phase [74]. Increasing the TLL is hypothesized to provide a larger hydrophobic driving force for the partitioning of PPV and HRV into the PEG-rich phase. Each system composition is represented by a TL ratio (Eq. (3-2)). The TL ratio is the ratio of a length of the segment from the system point to the top node divided by the length of the segment from the system point to the bottom node of that tie line [57]. The phase volumes change as the TL ratio changes, as shown in **Figure 3-1A**.

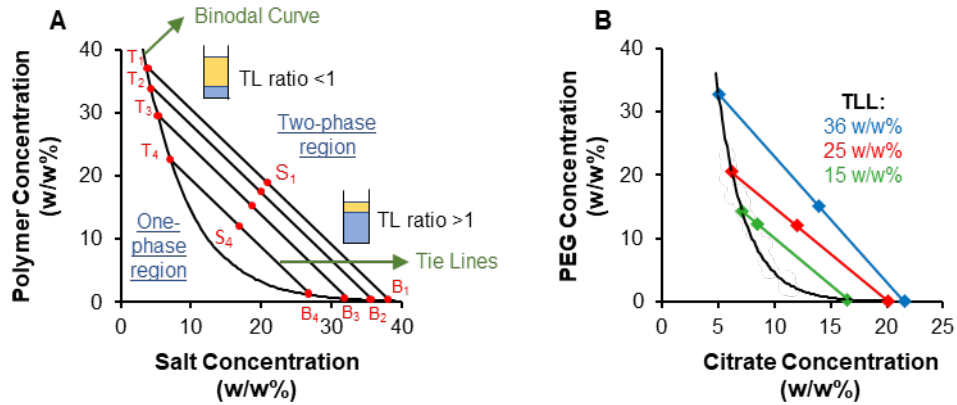


Figure 3-1. Binodal curve and tie lines. (A) Schematic illustration of ATPS showing binodal curve separating one-phase region from the two-phase region and set of systems characterized by tie lines and TL ratios. (B) Experimentally determined binodal curve and tie lines for PEG 12kDa-citrate ATPS at pH 7.

Earlier studies have shown that a PEG 12 kDa-citrate system was able to separate and recover 64% of infectious PPV [38]. This is a higher MW of PEG than typically studied in PEG-salt ATPS. Although higher MW causes an increase in viscosity and interfacial tension [75,76], it also elevates the hydrophobic driving force in the PEG-rich phase, which increased the virus recovery [38]. Hence, it was decided to study the PPV

purification at varying TLL in the PEG 12 kDa-citrate system to better understand the effect of PEG and citrate concentration on virus recovery.

Table 3-3. Comparison of TL ratio (Eq. 3-2) and volume ratio (Eq. 3-3)

System Composition		TLL (w/w%)	TL ratio	Volume ratio
PEG Conc. (w/w%)	Citrate Conc. (w/w%)			
30.0	6.4		0.1	7.7
15.0	14.0	36	1.2	0.9
10.0	16.5		2.3	0.4
18.5	7.5		0.1	3.7
10.3	13.2	25	1.0	0.5
6.2	16.0		2.3	0.3
13.7	7.5		0.1	0.8
7.4	11.8	15	1.0	0.4
4.6	13.6		2.3	0.3

Several groups have generated binodal curves for polymer/salt systems [38,77–80]. The phase diagram was experimentally determined for the PEG 12 kDa-citrate system and can be seen in **Figure 3-1B**. Refractive index and density were also used to confirm the tie lines (see **Tables A.1-1 and A.1-2**). The densities of the PEG-rich phases of systems did not differ much with an increasing TLL. On the other hand, the densities of the citrate-rich phases showed a significant increase with the TLL. Refractive index of the PEG-rich phases increased linearly with TLL. The binodal curve generated was similar to previous work [38] and the tie lines determined were parallel, as expected, and are also shown in **Figure 3-1B**. The tie lines had an average slope of -1.6 ± 0.2 . The PEG concentrations in the PEG-rich phase was measured by generating a standard curve (**Table A.1-3**). The measured PEG concentrations showed a slight deviation from the

previously determined tie lines using conductivity method. However, the standard curve was generated without adding citrate salt, which is present when two-phase systems are formed. Any system composition on a given tie line separates into the same respective PEG and salt compositions [57], only the volume ratio changes of each system. The TL ratios were indirectly proportional to the volume ratios (Eq. (3-3)), as shown in **Table 3-3** thus suggesting an increase in the TL ratio will decrease the volume ratio.

3.3.3 Effect of tie lines & tie line ratios

Three TLLs and at least three TL ratios were chosen to study the recovery of PPV and HRV with respect to phase composition and phase volume. The system matrix also explored the effect of phase composition changes on the partitioning behavior of contaminants, in particular, host-cell proteins and DNA.

The shortest TLL studied was 15 w/w%. TLL 15 w/w% contained the lowest concentration of PEG and citrate of those tested. The lower compositions have relatively low hydrophobic interaction from the PEG-rich phase and low salting-out effect from the citrate-rich phase. It was observed that PPV highly partitioned to the citrate-rich phase and very little PPV was recovered in the PEG-rich phase, as shown in **Figure 3-2A & B**. Recoveries in the citrate-rich phase started at 100% at TL ratio 0.1 and decreased to 20% at TL ratio 2.3. Irrespective of the TL ratio, the contaminant proteins partitioned to the citrate-rich phase, as shown in **Figure 3-2C**. The PPV concentration is too low to be seen on an SDS-PAGE. Since there was not enough preferential partitioning of the PPV particles to the PEG-rich phase, the lower TLL is not suitable for the purification of PPV.

To increase the driving forces (i.e. salting-out of the citrate and hydrophobic interaction of the PEG) and obtain higher recovery of the viral particles in the PEG-rich phase, systems on TLL 25 w/w% were studied. As shown in **Figure 3-2D**, the PPV recovery in the PEG-rich phase increased almost linearly with the TL ratio. A maximum of 52% PPV was recovered in the PEG-rich phase at TL ratio 2.3. This corresponded to a

decrease in recovery in the citrate-rich phase as the TL ratio increased (**Figure 3-2E**). However, the recoveries in the citrate-rich phase remained low at <30%. The remainder of the viral particles are likely aggregated at the interface or have been rendered noninfectious by the system and are not recoverable, as stated previously [38]. It is most likely that the virus has been trapped at the interface, since we do obtain high recoveries at TLLs with both increased and decreased concentrations of PEG and citrate.

Most of the contaminant proteins partitioned to the citrate-rich phase, as shown in **Figure 3-2F**. One contaminant protein partitioned along with PPV in the PEG-rich phase for TLL 25 w/w%, as seen by the band between 50 and 60 kDa. The decreasing band intensity with an increase in the TL ratio was observed in the citrate-rich phase, the cause of which might be the decreasing concentration of the proteins with an increasing volume of the citrate-rich phase, i.e. the citrate is diluting the protein. TLL 25 w/w% provided a better driving force for the preferential partitioning of PPV to the PEG-rich phase than TLL 15 w/w%.

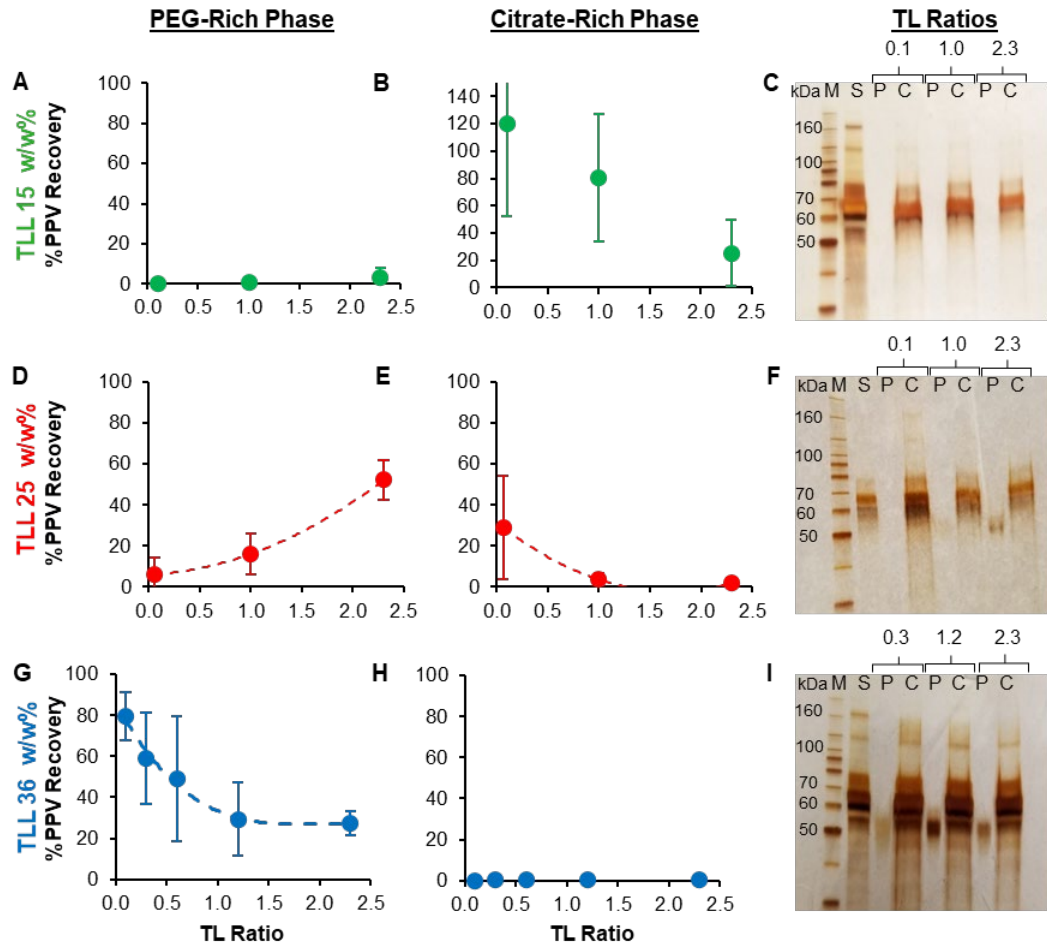


Figure 3-2. PPV recovery in the PEG-rich phase (A, D, and G) and the citrate-rich phase (B, E, and H) at different TLL. SDS-PAGE of marker (M), starting PPV (S) and the PEG-rich phase (P) and the citrate-rich phase (C) at different TLL and TL ratios. The starting titer was \log_{10} 6.5 MTT₅₀/ml. Experiments were done in triplicates and the error bars represent the standard deviation.

Similar studies were performed with HRV to determine the effect of viral surface charge on the partitioning and recovery of the virus. The recovery of HRV in the PEG-rich phase on TLL 15 w/w% remained low, almost 0% (**Figure 3-3A**). This low recovery was similar to PPV for TLL 15 w/w%. At the increased TLL of 25 w/w%, the HRV recovery increased to between 11 and 21%, depending on the TL ratio. Furthermore, TLL 36 w/w% provided an even stronger driving force where the recovery of HRV increased

to 36% at TL ratio 0.3 (**Figure 3-3A**). The recovery of the HRV in the PEG-rich phase showed an opposite trend on TLL 25 w/w% and 36 w/w%. This trend was similar to the PPV behavior at the same TLLs, as shown in **Figure 3-2D & G**. Also, the HRV titers were almost identical to the PPV titers in the PEG-rich phase for all the systems studied (**Table A.1-4**) suggesting that the highly hydrated citrate ions dehydrate the HRV surface which promotes the hydrophobic interaction of PEG-rich phase and dehydrated viral surface.

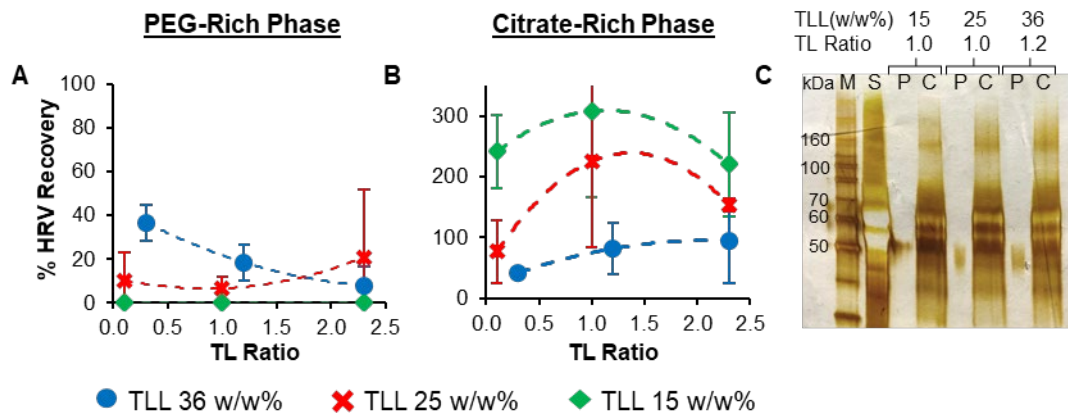


Figure 3-3. HRV recovery in the PEG-rich phase (A) and the citrate-rich phase (B) at different TLL. SDS-PAGE of marker (M), starting HRV (S), PEG-rich phase (P) and the citrate-rich phase (C) at TLL 15, 25, and 36w/w%. %. The starting titer was \log_{10} 6.5 MTT₅₀/ml. Experiments were done in triplicates, and the error bars represent the standard deviation.

The citrate-rich phase titers were strongly affected by the presence of citrate in the samples. This is clearly seen in the citrate-rich phase recoveries, where the recoveries at TLL 15 w/w% and 25 w/w% were >150% at TL ratios >1. These high titers, which then resulted in high recoveries in the citrate-rich phase, were likely due to the interaction of the cells with the citrate. Some groups have shown that citrate reduces cell viability [82] and is cytotoxic to cancer cells [83] at certain concentrations. Reduction of the cell viability increases the titer in the MTT assay as the virus quantification is based on the

cell viability. An increase in the titer increases the recovery. The mass balance of viral particles held true only at TLL 36 w/w% with a total mass balance ranging between 77 and 102%. Overall, the HRV recovery followed the same trends as PPV. At low TLL, the virus remained in the citrate-rich phase and transitioned to the PEG-rich phase at the highest TLL studied.

Similar to PPV, the contaminant proteins present in the HRV solution were found mainly in the citrate rich phase (**Figure 3-3C**). The bands of the PEG-rich phase and citrate-rich phase corresponding to all the systems studied were identical. Hence, only one representative gel comprising of TLL 15, 25, and 36 w/w% at TL ratio 1.2 is shown (**Figure 3-3C**). The purity of the PEG-rich phase was similar to PPV. HRV partitioning demonstrated a high purity but low recovery as compared to the high purity and high recovery found with PPV.

3.3.4 Effect of increased PPV load

To understand the effect of loading, the initial PPV load was increased from 6.5 $\log_{10}(\text{MTT}_{50}/\text{ml})$, used in **Figure 3-2**, to 8 $\log_{10}(\text{MTT}_{50}/\text{ml})$. The loading effect was only performed with PPV as the highest titer of the HRV stock achieved was only 7 $\log_{10} \text{MTT}_{50}/\text{ml}$. The PPV partitioning coefficient, K (Eq. (5)), on all three TLLs showed similar trends for both loadings, as shown in **Figure 3-4A & B**. TLL 15 and 25 w/w% showed increasing K values with respect to an increasing TL ratio and exhibited decreasing K values for TLL 36 w/w%. It was noted that the partitioning coefficient values are similar or lower for the higher load on all the TLLs. However, the virus titer increased in the PEG-rich phase by increasing the initial load for all the systems studied (**Table A.1-5**). But a respective increase of virus titer in the citrate-rich phase suggested that a considerable number of viral particles still remained in the citrate-rich phase. This suggests that all the systems with an initial PPV load of 8 $\log_{10}(\text{MTT}_{50}/\text{ml})$ have higher ability than systems with an initial PPV load of 6.5 $\log_{10}(\text{MTT}_{50}/\text{ml})$ to drive viral particles in the PEG-rich phase, but the distribution of the viral particles is maintained to balance the free energy between the two-phases. In the previous studies, the free energy

has been correlated to the partition coefficient suggesting that for a given system composition the partition coefficient should remain the same [31,84].

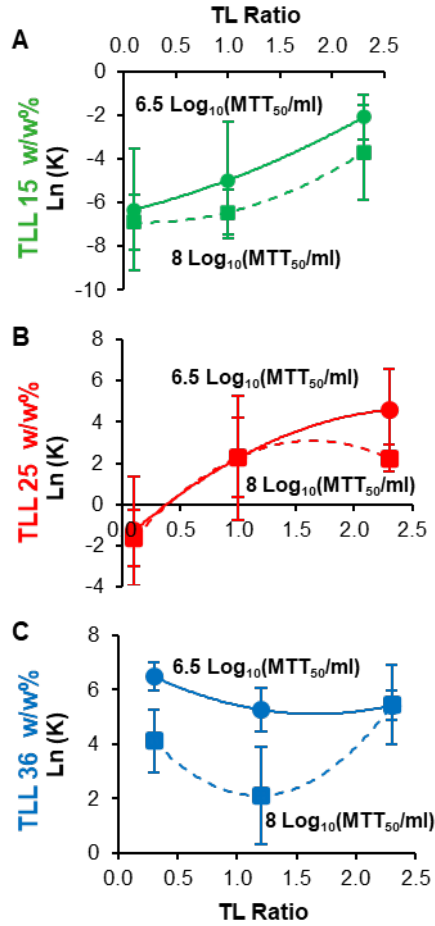


Figure 3-4. Comparison of PPV partitioning at two different loads along (A) TLL 15 w/w%, (B) TLL 25 w/w%, and (C) TLL 36 w/w%. Experiments were repeated in triplicates and error bars represent standard deviation.

3.4 Discussion

This study examined the partitioning of PPV and HRV in an ATPS of PEG 12 kDa-citrate. The goal was to determine the influential driving forces in ATPS partitioning at pH 7. There are two main theories that explain the partitioning of biomolecules in ATPS, 1) the excluded volume effect [30,42–44] and 2) hydrophobic and electrostatic interactions [45–47,74]. A previous study conducted for PPV ATPS partitioning using various molecular weights of PEG, salt types and pHs supported the concept of viral surface and phase hydrophobicity as the main driving forces [38]. This work supports two main conclusions, 1) increasing the PEG and citrate concentration, and therefore increasing the phase hydrophobicity and salting-out effect, increases the PPV and HRV recovery in the PEG-rich phase at a constant pH and 2) the influence of the electrostatic interaction is vital in achieving the high recovery of viruses in the PEG-rich phase. Therefore, the data supports that in a PEG 12 kDa-citrate system, electrostatics and hydrophobic interactions are the dominant forces.

The current theory for the partitioning of virus in ATPS involve the electrostatic interaction of the virus with the salt-rich phase and the hydrophobic interaction of the virus with the water-reduced PEG-rich phase. The first interaction appears to be the salting-out of the virus from the citrate-rich phase. This is due to the charge repulsion of the citrate with the virus. PPV is negatively charged at pH 7, and when the salt concentration is raised from TLL 15 w/w% to TLL 25 w/w%, all of the PPV is salted-out of the salt-rich phase and is likely at the interface. When the PEG-rich phase concentration is increased to TLL 36 w/w%, there is enough hydrophobic interaction driving force from the PEG-rich phase to extract the virus from the interface and have it recovered in the PEG-rich phase. This is illustrated by the recovery map shown in **Figure 3-5**. This theory is also supported by the data from HRV. HRV is neutrally charged at pH 7, and therefore does not experience the same amount of charge repulsion from the citrate-rich phase. Since the virus is not driven to the interface, it is not extracted from the interface by the PEG-rich phase. Therefore, our current hypothesis is that first the virus must be salted-out by charge repulsion from the salt-rich phase to the interface. Then the

PEG-rich phase needs to be strong enough to extract the virus from the interface into the PEG-rich phase. The experiments described here never reached a citrate concentration that salted-out the contaminating proteins so that they could be extracted into the PEG-rich phase. This is preferred because it provides a difference in driving force needed to purify the viral particles.

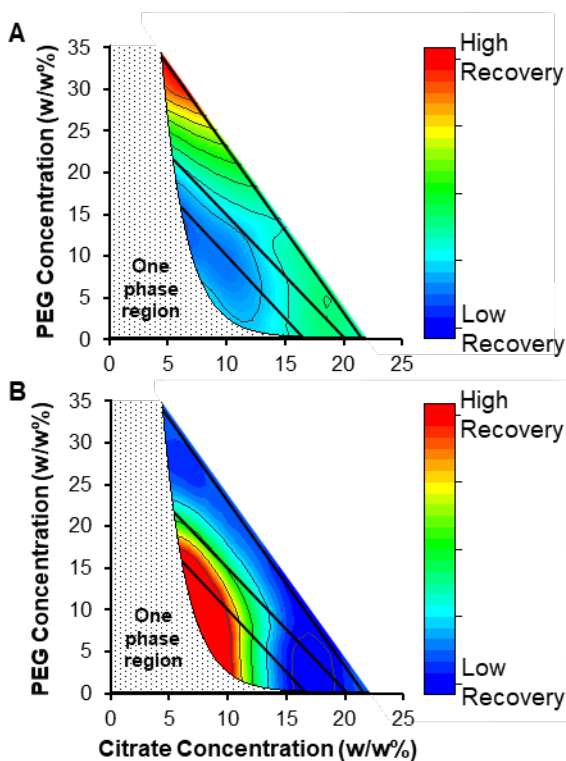


Figure 3-5. Schematic PPV recovery map in the two-phase region for (A) PEG-rich phase and (B) citrate-rich phase.

The salting-out phenomena is the interaction of salt ions (electrolyte), biomolecules (non-electrolyte) and solvent. At lower salt concentrations, the salt ions interact with the biomolecules by forming a layer of counter ions around the charged biomolecule. The counter ion layer increases the water structure stability and decreases the free energy, therefore promoting biomolecule solubility. An increase in the salt

concentration, above a critical concentration, causes a high repulsion force to develop from the development of an electronic double layer and the close proximity of like charged ions near the surface of the biomolecule [85]. This high repulsion force increases the free energy of the biomolecule surface, thereby making the surface thermodynamically unstable [86].

To test the effect of citrate concentration on the aggregation of PPV, DLS was measured for PPV in different citrate concentrations. Due to aggregates that were present in the starting material, an aggregation ratio was used to compare the intensity of the PPV peak and the aggregate peak. The full calculation is described in Eq. (3-7). PPV particles started to aggregate at 15 w/w% citrate, with extensive aggregation occurring at 20 w/w% and above (**Figure A.1-1**). 20 w/w% citrate and above are close to the citrate-rich phase compositions of the TLLs, 25 and 36 w/w%, studied (see **Figure A.1-1**). These results support the hypothesis that PPV is salted-out at high citrate concentration. Without the PEG-rich phase present (i.e. citrate only, as was conducted in the DLS experiments), PPV aggregated. In the presence of the PEG-rich phase, the PPV particles can reduce their free energy by migrating to the PEG-rich phase. Aggregation was not measured for HRV due to the low HRV titer available which was not detectable by DLS measurements.

The proposed theory of hydrophobicity as the main driving force in ATPS was based on recent studies that have shown viral particles to be relatively more hydrophobic than proteins [61,87]. The PPV surface was shown to be more hydrophobic than the model proteins BSA, lysozyme, bovine fibrinogen, and human IgG by studying reverse phase chromatography and ANS fluorescence, and the results were compared with computationally determined solvent exposed surface area [61]. Another team performed hydrophobic interaction chromatography (HIC) studies on a variety of enveloped and non-enveloped mammalian viruses and protein models, where viruses eluted at lower citrate concentrations as compared to the model proteins, suggesting the relatively hydrophobic nature of the viruses studied [87]. One of the viruses studied was MVM. MVM and PPV are both parvoviruses, therefore complementing the idea that PPV is

hydrophobic. Similarly, the ATPS described here was designed to utilize the hydrophobic property of PPV to induce preferential partitioning of the virions to the PEG-rich phase.

A few studies have been reported to measure the hydrophobicity or predict the partitioning behavior based on hydrophobicity of proteins [45], or peptides [47] in ATPS. The hydrophobic interaction in ATPS is driven by the PEG molecular weight and concentration. This growing evidence of the hydrophobic interaction as a vital driving force in ATPS could be reasoned by the molecular composition of PEG. The increase in the PEG molecular weight and/or concentration increases the number of ethyl groups in the polymer chain. Ethyl groups are hydrophobic and optimum number of monomers provide the necessary hydrophobic interaction binding sites to attract proteins or viruses [49]. The minimization of free energy increase of the biomolecules, from the salting-out effect, is compensated by the availability of the free energy provided by the amount of –CH₂-CH₂– groups in the PEG-rich phase. The high recoveries of virus in PEG-citrate ATPS is possible by the right balance of salting-out and hydrophobic interaction.

3.5 Conclusion

This study reported the recoveries of PPV and HRV in a PEG 12 kDa-citrate system at pH 7. The PPV and HRV titers in the PEG-rich phase increased with an increase in TLL. Most of the viral particles were recovered in the citrate-rich phase at TLL 15 w/w%, the lowest TLL studied. The PPV and HRV recovery in the PEG-rich phase increased at TLL 25 w/w%. Across this tie line, the PPV and HRV recovery increased in the PEG-rich phase as the TL ratio increased. TLL 36 w/w% showed the opposite trend; the recovery decreased as the TL ratio increased. The highest PPV recovery of 79% and HRV recovery of 36% was found on TLL 36 w/w% and the lowest TL ratio studied. An increase in the PPV titer yielded higher titers in the PEG-rich phase. Overall, this work supported the hypothesis that the main driving forces in viral particle ATPS are the salting-out from the citrate-rich phase followed by the hydrophobic interaction of the PEG-rich phase. Therefore, a higher TLL, leading to higher

concentrations of salt and PEG, is needed for a high virus recovery in the PEG-rich phase.

The framework in this study achieves high virus recovery in a PEG-citrate system using known surface properties of the virus. The model viruses used, demonstrated a need to understand the virus properties to improve virus recovery. By systematically studying the partitioning and recovery of negatively charged PPV and neutral HRV across tie lines, it was determined that the surface hydrophobicity and the charge at a given pH of the virus were key in the selective partitioning of the virus to the more hydrophobic PEG-rich phase. By combining the study of virus particle surfaces and the experimental ATPS design space, future correlations can be determined that will reduce the number of ATPS experiments needed to find an optimal system.

3.6 References

- [1] WHO, Global Vaccine Action Plan 2011–2020, Global Vaccine Action Plan 2011–2020 (2013).
- [2] A.A. Shukla, J. Thommes, Recent advances in large-scale production of monoclonal antibodies and related proteins, *Trends Biotechnol.* 28 (5) (2010) 253–261.
- [3] S.M. Crosson, P. Dib, J.K. Smith, S. Zolotukhin, Helper-free production of laboratory grade AAV and purification by iodixanol density gradient centrifugation, *Mol. Ther.* 10 (2018) 1–7.
- [4] R.P. Araldi, D.N. Giovanni, T.C. Melo, N. Diniz, J. Mazzuchelli-de-Souza, T.A. Sant'Ana, R.F. Carvalho, W. Becak, R.C. Stocco, Bovine papillomavirus isolation by ultracentrifugation, *J. Virol. Methods* 208 (2014) 119–124.
- [5] L. Besnard, V. Fabre, M. Fettig, E. Gousseinov, Y. Kawakami, N. Laroudie, C. Scanlan, P. Pattnaik, Clarification of vaccines: an overview of filter-based technology trends and best practices, *Biotechnol. Adv.* 34 (1) (2016) 1–13.
- [6] M.A. Robert, P.S. Chahal, A. Audy, A. Kamen, R. Gilbert, B. Gaillet, Manufacturing of recombinant adeno-associated viruses using mammalian expression platforms, *Biotechnol. J.* 12 (3) (2017).

- [7] G. Zhang, R. Deng, M. Zhao, S. Qiao, G. Xing, Y. Yang, Y. Wang, Q. Jin, J. Yang, L. Wang, Q. Li, J. Guo, Y. Zhi, R. Wang, Efficient purification of cell culture-derived classical swine fever virus by ultrafiltration and size-exclusion chromatography, *Front. Agr. Sci. Eng.* 2 (3) (2015).
- [8] J. Transfiguracion, H. Jorio, J. Meghrou, D. Jacob, A. Kamen, High yield purification of functional baculovirus vectors by size exclusion chromatography, *J. Virol. Methods* 142 (1–2) (2007) 21–28.
- [9] L. Bohua, S. Ming, Y. Lu, D. Xiaoyu, L. Baochun, S. Fenqin, Z. Li, C. Xizhao, Purification of porcine reproductive and respiratory syndrome virus using ultrafiltration and liquid chromatography, *J Chromatogr B Analyt Technol Biomed Life Sci* 1017-1018 (2016) 182–186.
- [10] A. Auricchio, E. O'Connor, M. Hildinger, J.M. Wilson, A single-step affinity column for purification of serotype-5 based adeno-associated viral vectors, *Mol. Ther.* 4 (4) (2001) 372–374.
- [11] P. Du, S. Sun, J. Dong, X. Zhi, Y. Chang, Z. Teng, H. Guo, Z. Liu, Purification of footand-mouth disease virus by heparin as ligand for certain strains, *J Chromatogr B Analyt Technol Biomed Life Sci* 1049-1050 (2017) 16–23.
- [12] E.I. Trilisky, A.M. Lenhoff, Sorption processes in ion-exchange chromatography of viruses, *J. Chromatogr. A* 1142 (1) (2007) 2–12.
- [13] B. Kalbfuss, M. Wolff, R. Morenweiser, U. Reichl, Purification of cell culture-derived human influenza A virus by size-exclusion and anion-exchange chromatography, *Biotechnol. Bioeng.* 96 (5) (2007) 932–944.
- [14] P. Nestola, C. Peixoto, R.R. Silva, P.M. Alves, J.P. Mota, M.J. Carrondo, Improved virus purification processes for vaccines and gene therapy, *Biotechnol. Bioeng.* 112 (5) (2015) 843–857.
- [15] P. Kramberger, L. Urbas, A. Strancar, Downstream processing and chromatography based analytical methods for production of vaccines, gene therapy vectors, and bacteriophages, *Hum Vaccin Immunother* 11 (4) (2015) 1010–1021.
- [16] G. Allmaier, D. Blaas, C. Bliem, T. Dechat, S. Fedosyuk, I. Gosler, H. Kowalski, V.U. Weiss, Monolithic anion-exchange chromatography yields rhinovirus of high purity, *J. Virol. Methods* 251 (2018) 15–21.
- [17] T. Krober, M.W. Wolff, B. Hundt, A. Seidel-Morgenstern, U. Reichl, Continuous purification of influenza virus using simulated moving bed chromatography, *J. Chromatogr. A* 1307 (2013) 99–110.

- [18] P. Nestola, R.J. Silva, C. Peixoto, P.M. Alves, M.J. Carrondo, J.P. Mota, Adenovirus purification by two-column, size-exclusion, simulated countercurrent chromatography, *J. Chromatogr. A* 1347 (2014) 111–121.
- [19] A.L. Zydney, Perspectives on integrated continuous bioprocessing - opportunities and challenges, *Curr Opin Chem Eng* 10 (2015) 8–13.
- [20] A.L. Zydney, Continuous downstream processing for high value biological products: a review, *Biotechnol. Bioeng.* 113 (3) (2016) 465–475.
- [21] M. Rito-Palomares, Practical application of aqueous two-phase partition to process development for the recovery of biological products, *J Chromatogr B Analyt Technol Biomed Life Sci* 807 (1) (2004) 3–11.
- [22] S. Chethana, C.A. Nayak, M.C. Madhusudhan, K.S. Raghavarao, Single step aqueous two-phase extraction for downstream processing of C-phycoerythrin from *Spirulina platensis*, *J. Food Sci. Technol.* 52 (4) (2015) 2415–2421.
- [23] O. Aguilar, V. Albiter, L. Serrano-Carreón, M. Rito-Palomares, Direct comparison between ion-exchange chromatography and aqueous two-phase processes for the partial purification of penicillin acylase produced by *E. coli*, *J Chromatogr B Analyt Technol Biomed Life Sci* 835 (1–2) (2006) 77–83.
- [24] L. Philipson, P.Å. Albertsson, G. Frick, The purification and concentration of viruses by aqueous polymer phase systems, *Virology* 11 (3) (1960) 553–571.
- [25] F. Luechau, T.C. Ling, A. Lyddiatt, Recovery of B19 virus-like particles by aqueous two-phase systems, *Food Bioprod. Process.* 89 (4) (2011) 322–327.
- [26] J. Benavides, J.A. Mena, M. Cisneros-Ruiz, O.T. Ramirez, L.A. Palomares, M. RitoPalomares, Rotavirus-like particles primary recovery from insect cells in aqueous two-phase systems, *J Chromatogr B Analyt Technol Biomed Life Sci* 842 (1) (2006) 48–57.
- [27] R.K. Desai, M. Streefland, R.H. Wijffels, M.H.M. Eppink, Extraction and stability of selected proteins in ionic liquid based aqueous two-phase systems, *Green Chem.* 16 (5) (2014) 2670–2679.
- [28] Z. Du, Y.L. Yu, J.H. Wang, Extraction of proteins from biological fluids by use of an ionic liquid/aqueous two-phase system, *Chemistry* 13 (7) (2007) 2130–2137.
- [29] C.X. Zeng, R.P. Xin, S.J. Qi, B. Yang, Y.H. Wang, Aqueous two-phase system based on natural quaternary ammonium compounds for the extraction of proteins, *J. Sep. Sci.* 39 (4) (2016) 648–654.

- [30] S.L. Ho, J.C.-W. Lan, J.S. Tan, H.S. Yim, H.S. Ng, Aqueous biphasic system for the partial purification of *Bacillus subtilis* carboxymethyl cellulase, *Process Biochem.* 58 (2017) 276–281.
- [31] N.R. da Silva, L.A. Ferreira, P.P. Madeira, J.A. Teixeira, V.N. Uversky, B.Y. Zaslavsky, Analysis of partitioning of organic compounds and proteins in aqueous polyethylene glycol-sodium sulfate aqueous two-phase systems in terms of solute-solvent interactions, *J. Chromatogr. A* 1415 (2015) 1–10.
- [32] A. Glyk, T. Scheper, S. Beutel, PEG–salt aqueous two-phase systems: an attractive and versatile liquid–liquid extraction technology for the downstream processing of proteins and enzymes, *Appl. Microbiol. Biotechnol.* 99 (16) (2015) 6599–6616.
- [33] J.A. Asenjo, B.A. Andrews, Aqueous two-phase systems for protein separation: a perspective, *J. Chromatogr. A* 1218 (49) (2011) 8826–8835.
- [34] M.J. Jacinto, R.R.G. Soares, A.M. Azevedo, V. Chu, A. Tover, J.P. Conde, M.R. AiresBarros, Optimization and miniaturization of aqueous two phase systems for the purification of recombinant human immunodeficiency virus-like particles from a CHO cell supernatant, *Sep. Purif. Technol.* 154 (2015) 27–35.
- [35] R. Noad, P. Roy, Virus-like particles as immunogens, *Trends Microbiol.* 11 (9) (2003) 438–444.
- [36] A. González-Mora, F. Ruiz-Ruiz, J. Benavides, R.C. Willson, M. Rito-Palomares, Recovery and primary purification of bacteriophage M13 using aqueous two-phase systems, *J. Chem. Technol. Biotechnol.* 92 (11) (2017) 2808–2816.
- [37] A. Negrete, T.C. Ling, A. Lyddiatt, Aqueous two-phase recovery of bio-nanoparticles: a miniaturization study for the recovery of bacteriophage T4, *J Chromatogr B Analyt Technol Biomed Life Sci* 854 (1–2) (2007) 13–19.
- [38] K.S. Vijayaragavan, A. Zahid, J.W. Young, C.L. Heldt, Separation of porcine parvovirus from bovine serum albumin using PEG-salt aqueous two-phase system, *J Chromatogr B Analyt Technol Biomed Life Sci* 967 (2014) 118–126.
- [39] E. Espitia-Saloma, P. Vázquez-Villegas, O. Aguilar, M. Rito-Palomares, Continuous aqueous two-phase systems devices for the recovery of biological products, *Food Bioprod. Process.* 92 (2) (2014) 101–112.
- [40] P. Vázquez-Villegas, O. Aguilar, M. Rito-Palomares, Continuous enzyme aqueous two-phase extraction using a novel tubular mixer-settler in multi-step countercurrent arrangement, *Sep. Purif. Technol.* 141 (2015) 263–268.

- [41] J. Muendges, A. Zalesko, A. Gorak, T. Zeiner, Multistage aqueous two-phase extraction of a monoclonal antibody from cell supernatant, *Biotechnol. Prog.* 31 (4) (2015) 925–936.
- [42] F. Luechau, T.C. Ling, A. Lyddiatt, Selective partition of plasmid DNA and RNA in aqueous two-phase systems by the addition of neutral salt, *Sep. Purif. Technol.* 68 (1) (2009) 114–118.
- [43] G.A. Gomes, A.M. Azevedo, M.R. Aires-Barros, D.M.F. Prazeres, Purification of plasmid DNA with aqueous two phase systems of PEG 600 and sodium citrate/ ammonium sulfate, *Sep. Purif. Technol.* 65 (1) (2009) 22–30.
- [44] O. Annunziata, N. Asherie, A. Lomakin, J. Pande, O. Ogun, G.B. Benedek, Effect of polyethylene glycol on the liquid-liquid phase transition in aqueous protein solutions, *Proc. Natl. Acad. Sci. U. S. A.* 99 (22) (2002) 14165–14170.
- [45] B.A. Andrews, J.A. Asenjo, Theoretical and experimental evaluation of hydrophobicity of proteins to predict their partitioning behavior in aqueous two phase systems: a review, *Sep. Sci. Technol.* 45 (15) (2010) 2165–2170.
- [46] A.L. Grilo, M. Raquel Aires-Barros, A.M. Azevedo, Partitioning in aqueous twophase systems: fundamentals, applications and trends, *Sep. Purif. Rev.* 45 (1) (2014) 68–80.
- [47] M.A. Eiteman, J.L. Gainer, Peptide hydrophobicity and partitioning in poly (ethylene glycol)/magnesium sulfate aqueous two-phase systems, *Biotechnol. Prog.* 6 (6) (1990) 479–484.
- [48] Y. Guan, T.H. Lilley, T.E. Treffry, A new excluded volume theory and its application to the coexistence curves of aqueous polymer two-phase systems, *Macromolecules* 26 (15) (1993) 3971–3979.
- [49] J. Wu, C. Zhao, W. Lin, R. Hu, Q. Wang, H. Chen, L. Li, S. Chen, J. Zheng, Binding characteristics between polyethylene glycol (PEG) and proteins in aqueous solution, *J. Mater. Chem. B* 2 (20) (2014).
- [50] S.C. Silvério, A. Wegrzyn, E. Lladosa, O. Rodríguez, E.A. Macedo, Effect of aqueous two-phase system constituents in different poly(ethylene glycol)–salt phase diagrams, *J. Chem. Eng. Data* 57 (4) (2012) 1203–1208.
- [51] H.S. Mohamadi, E. Omidinia, R. Dinarvand, Evaluation of recombinant phenylalanine dehydrogenase behavior in aqueous two-phase partitioning, *Process Biochem.* 42 (9) (2007) 1296–1301.

- [52] M.J. Hey, D.P. Jackson, H. Yan, The salting-out effect and phase separation in aqueous solutions of electrolytes and poly(ethylene glycol), *Polymer* 46 (8) (2005) 2567–2572.
- [53] T.W. Molitor, H.S. Joo, M.S. Collett, Porcine parvovirus: virus purification and structural and antigenic properties of virion polypeptides, *J. Virol.* 45 (2) (1983) 842–854.
- [54] E. Arnold, G. Vriend, M. Luo, J.P. Griffith, G. Kamer, J.W. Erickson, J.E. Johnson, M.G. Rossmann, The structure determination of a common cold virus, human rhinovirus 14, *Acta Crystallogr. Sect. A: Found. Crystallogr.* 43 (3) (1987) 346–361.
- [55] C.L. Heldt, R. Hernandez, U. Mudiganti, P.V. Gurgel, D.T. Brown, R.G. Carbonell, A colorimetric assay for viral agents that produce cytopathic effects, *J. Virol. Methods* 135 (1) (2006) 56–65.
- [56] M.F. Tafur, K.S. Vijayaragavan, C.L. Heldt, Reduction of porcine parvovirus infectivity in the presence of protecting osmolytes, *Antivir. Res.* 99 (1) (2013) 27–33.
- [57] R. Hatti-Kaul, Aqueous two-phase systems_ methods and protocols, in: J.M. Walker (Ed.), *Methods in Biotechnology*, vol. 11, Springer Science & Business Media, 2000.
- [58] J. Nielsen, L. Rønsholt, K.J. Sørensen, Experimental in utero infection of pig fetuses with porcine parvovirus (PPV), *Vet. Microbiol.* 28 (1) (1991) 1–11.
- [59] H.S. Joo, C.R. Donaldson-Wood, R.H. Johnson, Observations on the pathogenesis of porcine parvovirus infection, *Arch. Virol.* 51 (1) (1976) 123–129.
- [60] A.A. Simpson, B. Hebert, G.M. Sullivan, C.R. Parrish, Z. Zadori, P. Tijssen, M.G. Rossmann, The structure of porcine parvovirus: comparison with related viruses, *J. Mol. Biol.* 315 (5) (2002) 1189–1198.
- [61] C.L. Heldt, A. Zahid, K.S. Vijayaragavan, X. Mi, Experimental and computational surface hydrophobicity analysis of a non-enveloped virus and proteins, *Colloids Surf B* 153 (2017) 77–84.
- [62] S. Johnson, K.A. Brorson, D.D. Frey, A.K. Dhar, D.A. Cetlin, Characterization of noninfectious virus-like particle surrogates for viral clearance applications, *Appl. Biochem. Biotechnol.* 183 (1) (2017) 318–331.
- [63] W.S. Weichert, J.S. Parker, A. Wahid, S.-F. Chang, E. Meier, C.R.J.V. Parrish, Assaying for structural variation in the parvovirus capsid and its role in infection, *Virology* 250 (1) (1998) 106–117.
- [64] S.E. Jacobs, D.M. Lamson, K. St George, T.J. Walsh, Human rhinoviruses, *Clin. Microbiol. Rev.* 26 (1) (2013) 135–162.

- [65] T.J. Smith, M.J. Kremer, M. Luo, G. Vriend, E. Arnold, G. Kamer, M.G. Rossmann, M.A. McKinlay, G.D. Diana, M.J. Otto, The site of attachment in human rhinovirus 14 for antiviral agents that inhibit uncoating, *Science* 233 (4770) (1986) 1286–1293.
- [66] M.G. Rossmann, E. Arnold, J.W. Erickson, E.A. Frankengerger, J.P. Griffith, H.J. Hecht, J.E. Johnson, G. Kamer, M. Luo, A.G.J.N. Mosser, Structure of a human common cold virus and functional relationship to other picornaviruses, *Nature* 317 (6033) (1985) 145.
- [67] S.L. Johnston, P.K. Pattemore, G. Sanderson, S. Smith, F. Lampe, L. Josephs, P. Symington, S.O. Toole, S.H. Myint, D.A.J. Tyrrell, S.T. Holgate, Community study of role of viral infections in exacerbations of asthma in 9–11 year old children, *BMJ* 310 (1995) 1225–1229.
- [68] M. Yamaya, H. Sasaki, Rhinovirus and asthma, *Viral Immunol.* 16 (2) (2003) 99–109.
- [69] S.L. Friedlander, W.W. Busse, The role of rhinovirus in asthma exacerbations, *J. Allergy Clin. Immunol.* 116 (2) (2005) 267–273.
- [70] A.C. Palmenberg, J.E. Gern, Classification and evolution of human rhinoviruses, *Methods Mol. Biol.* 1221 (2015) 1–10.
- [71] T. Heikkinen, A. Järvinen, The common cold, *Lancet* 361 (9351) (2003) 51–59. [72] S.R. Kim, J.H. Song, J.H. Ahn, G.S. Lee, H. Ahn, S.I. Yoon, S.G. Kang, P.H. Kim, S.M. Jeon, E.J. Choi, S. Shin, Y. Cha, S. Cho, D.E. Kim, S.Y. Chang, H.J. Ko, Antiviral and anti-inflammatory activity of budesonide against human rhinovirus infection mediated via autophagy activation, *Antivir. Res.* 151 (2018) 87–96.
- [73] K. Wysoczanska, H.T. Do, C. Held, G. Sadowski, E.A. Macedo, Effect of different organic salts on amino acids partition behaviour in PEG-salt APTS, *Fluid Phase Equilib.* 456 (2018) 84–91.
- [74] A. Goja, H. Yang, M. Cui, C. Li, Aqueous two-phase extraction advances for bioseparation, *J. Bioprocess Biotech.* 04 (01) (2013).
- [75] C.C. de Oliveira, J.S.d.R. Coimbra, A.D.G. Zuniga, J.P. Martins, A.M.d.O. Siqueira, Interfacial tension of aqueous two-phase systems containing poly(ethylene glycol) and potassium phosphate, *J. Chem. Eng. Data* 57 (6) (2012) 1648–1652.
- [76] M. Perumalsamy, T. Murugesan, Phase compositions, molar mass, and temperature effect on densities, viscosities, and liquid–liquid equilibrium of polyethylene glycol and salt-based aqueous two-phase systems, *J. Chem. Eng. Data* 54 (4) (2009) 1359–1366.
- [77] A. Chakraborty, K. Sen, Impact of pH and temperature on phase diagrams of different aqueous biphasic systems, *J. Chromatogr. A* 1433 (2016) 41–55.

- [78] K. Wysoczanska, E.A. Macedo, Influence of the molecular weight of PEG on the polymer/salt phase diagrams of aqueous two-phase systems, *J. Chem. Eng. Data* 61 (12) (2016) 4229–4235.
- [79] J.G. Huddleston, H.D. Eillauer, R.D. Rogers, Phase diagram data for several PEG+salt aqueous biphasic systems, *J. Chem. Eng. Data* 48 (5) (2003) 1230–1236.
- [80] G. Tubío, L. Pellegrini, B.B. Nerli, G.A. Picó, Liquid–liquid equilibria of aqueous two-phase systems containing poly(ethylene glycols) of different molecular weight and sodium citrate, *J. Chem. Eng. Data* 51 (1) (2006) 209–212.
- [81] B. Nazer, M.R. Dehghani, B. Goliaei, Plasmid DNA affinity partitioning using polyethylene glycol - sodium sulfate aqueous two-phase systems, *J Chromatogr B Analyt Technol Biomed Life Sci* 1044-1045 (2017) 112–119.
- [82] E.M. Garland, J.M. Parr, D.S. Williamson, S.M. Cohen, In vitro cytotoxicity of the sodium, potassium and calcium salts of saccharin, sodium ascorbate, sodium citrate and sodium chloride, *Toxicol. in Vitro* 3 (3) (1989) 201–205.
- [83] Y. Lu, X. Zhang, H. Zhang, J. Lan, G. Huang, E. Varin, H. Lincet, L. Poulain, P. Icard, Citrate induces apoptotic cell death: a promising way to treat gastric carcinoma? *Anticancer Res.* 31 (3) (2011) 797–805.
- [84] D.P. de Barros, S.R. Campos, A.M. Azevedo, A.M. Baptista, M.R. Aires-Barros, Predicting protein partition coefficients in aqueous two phase system, *J. Chromatogr. A* 1470 (2016) 50–58.
- [85] M. Bostrom, F.W. Tavares, S. Finet, F. Skouri-Panet, A. Tardieu, B.W. Ninham, Why forces between proteins follow different Hofmeister series for pH above and below pI, *Biophys. Chem.* 117 (3) (2005) 217–224.
- [86] J.A. Queiroz, C.T. Tomaz, J.M.S. Cabral, Hydrophobic interaction chromatography of proteins, *J. Biotechnol.* 87 (2) (2001) 143–159.
- [87] S.A. Johnson, A. Walsh, M.R. Brown, S.C. Lute, D.J. Roush, M.S. Burnham, K.A. Brorson, The step-wise framework to design a chromatography-based hydrophobicity assay for viral particles, *J Chromatogr B Analyt Technol Biomed Life Sci* 1061-1062 (2017) 430–437.

4 Osmolyte enhanced Aqueous two-phase systems for virus purification^{3, 4}

³The material contained in the chapter is in preparation for submission to a peer-reviewed journal

⁴The extension of the material in this chapter is mentioned in Appendix B

4.1 Introduction

Downstream purification of viral vaccines needs to address the challenges of yield, purity, scale-up, and robust processing. In addition, continuous processing is also a future target. To accomplish these goals, we are studying the use of aqueous two-phase systems (ATPSs) to purify viral particles. The biphasic systems are formed by mixing two aqueous solutions above certain critical compositions with different phase-forming components. Typical phase-forming components are polymer-polymer and polymer-salt, due to their superior biocompatibility and mild, water-based environment. ATPSs have been mostly studied for therapeutic proteins [1-3] and plasmid DNA [4, 5] purification in the biotherapeutic area over the decades, with a limited focus on viruses. Viral purification using ATPS has only recently gained attention, as the onset of new vaccines and gene therapy modalities create a need to increase capacity and throughput for viral processing methods. However, this technique still requires extensive study to understand viral behavior in these types of biphasic systems. Traditionally, viral partitioning has been studied in a polyethylene glycol (PEG)-dextran system [6-8] and more recent studies have focused on PEG-salt systems [9-12]. This study explores a PEG-salt system and ways to enhance virus partitioning to the PEG-rich phase and contaminant retention in the salt-rich phase by addition of a third component.

Numerous studies have tried to understand the characteristics of ATPSs that lead to biomolecule partitioning. A comprehensive review suggests that the partitioning of biomolecules is synergistically influenced by the excluded volume theory, electrostatic interaction, and hydrophobic interaction [13]. However, recent reports have demonstrated critical contributions from the electrostatic and hydrophobic interactions in a PEG-salt system for virus purification [12, 14], with a contradictory contribution of the excluded volume theory. The virus prefers the PEG-rich phase once it is salted out of the salt-rich phase. This is accomplished by employing a stronger kosmotropic salt, such as citrate, for salting out, and a higher molecular weight PEG to provide hydrophobic interaction. One could also operate the ATPS at higher system compositions, which will create a higher ionic strength of the salt-rich phase and an increase in relative hydrophobicity of the

PEG-rich phase, thus promoting virus separation [12]. However, the hydrophobic interactions are relatively weak in a PEG-salt system as compared to a conventional hydrophobic interaction chromatography using phenyl-based resins. Due to this, a higher ionic strength might be detrimental to the virus structure and functional stability. On the other hand, higher compositions of the PEG-rich phase, needed to achieve high recoveries, generate a viscous solution which pose a processing challenge. Moreover, with an increasing array of viruses used in biotherapeutics that have a wide variety of surface characteristics and stability, there is a need to look for driving force enhancers that will preferentially increase the virus partitioning at milder system compositions.

Osmolytes are a class of molecules that occur naturally and are used by cells to compensate for changes in osmotic stress [15, 16]. Osmolytes have been divided into two groups based on the nature of their interaction with the protein backbone; 1) osmoprotectants or protecting osmolytes and 2) denaturing osmolytes. Osmoprotectants, such as betaine and trimethylamine N-oxide (TMAO), help in stabilizing protein structures [17]. Denaturing osmolytes, such as urea and guanidinium chloride, have been shown to unfold and destabilize protein structures [18, 19]. Numerous applications of osmoprotectants have been reported in the life sciences and biomanufacturing. Osmolytes function as water structure modulators, either to maintain osmotic balance [20, 21] or induce intramolecular or intermolecular interactions that stabilize proteins during osmotic stress [22]. Osmoprotectants have been utilized to induce intramolecular interactions to stabilize biologics in the formulation of biomolecules [23, 24]. Conversely, osmolytes have been shown to induce intermolecular interactions to flocculate viruses [25], which aided in the development of filtration-based method for virus purification. The exact mechanism of osmolyte function in protein stabilization or viral flocculation, however, is not clearly understood.

A few studies have used osmolytes as additives in ATPS. However, most of them have reported the effects in polymer-polymer systems on small organic molecules or protein partitioning (Ferreira, Fan [26], [27, 28]). This study explores the effect of osmolytes on two virus models in a PEG 12kDa-citrate system. Our previous study

showed that negatively charged non-enveloped viral particles partition to the PEG-rich phase only at higher system compositions [14]. It was hypothesized that a high salt concentration was needed to salt-out the virus to the interface. Then a high PEG concentration was needed to draw the virus out of the interface and into the more hydrophobic PEG-phase. To decrease the concentration of salt and PEG needed in the system, we added osmolytes and explored the partitioning of two viruses. The use of additives demonstrated preferential enhancement of partitioning at lower system compositions. This was likely by improving the hydrophobic interaction of virus and VLP with the PEG-rich phase. Moreover, the efficiency of osmolyte type to improve virus recover in the hydrophobic PEG-rich phase has led to theories on the mechanism of osmolyte action. Understanding the mechanism driving partitioning has direct correlation not only in the viral purification, but also in understanding the differential action of osmolyte towards biomolecules.

4.2 Materials and Methods

4.2.1 Materials

Eagle's minimum essential media (EMEM), sodium bicarbonate, phosphate buffered saline (PBS, pH 7.2), penicillin-streptomycin (pen-strep) (10,000 U/ml), fetal bovine serum (FBS, USDA approved) and trypsin/EDTA for cell propagation were purchased from Life Technologies (Carlsbad, CA). 2-(3,5-diphenyltetrazol-2-ium-2-yl)-4,5-dimethyl-1,3thiazole;bromide (MTT, 98%) was purchased from Alfa AesarTM (Haverhill, MA) and sodium dodecyl sulfate (SDS, BioReagent, $\geq 98.5\%$) was purchased from Sigma Aldrich (Radnor, PA). Polyethylene glycol with an average molecular weight of 12,000 Da (PEG 12 kDa), trisodium citrate dihydrate (ACS reagent grade, $\geq 99\%$), citric acid monohydrate (ACS reagent, $\geq 99\%$) were a generous gift from MilliporeSigma (Burlington, MA). Osmolytes glycine (BioUltra, $\geq 99.0\%$), betaine (BioUltra, $\geq 99.0\%$), trimethylamine N-oxide (TMAO) dihydrate, D-mannitol, and urea were purchased from Sigma-Aldrich (St. Louis, MO). Stable isotopes glycine (1-¹³C, 99%), betaine (D-11, 98%), TMAO (D9, 98%), and D-mannitol (U-¹³C6, 99%) were purchased from

Cambridge Isotope Laboratory (Tewksbury, MA). All solutions were made with Nanopure water (Thermo Scientific, Waltham, MA) at a resistance of ≥ 18 M Ω and filtered with a 0.2 μm Nalgene (Thermo Scientific) bottle top filter or 0.22 μm cellulose acetate syringe filters (VWR, Radnor, PA) prior to use.

HIV-VLP crude stock was a generous gift from Esperovax (Plymouth, MI). HIV-VLP with genetically infused green fluorescent protein (GFP) were expressed in *Saccharomyces cerevisiae* with a proprietary method.

4.2.2 Methods

4.2.2.1 Cell maintenance, virus propagation and virus titration

Porcine kidney cells (PK-13, CRL-6489TM) purchased from ATCC were cultured in EMEM pH 7.1 supplemented with 10 v/v% FBS and 1 v/v% pen-strep. The cell cultures were grown by incubating at 37°C, 5% CO₂, and 100% humidity. Porcine parvovirus (PPV) strain NADL-2, gifted by Dr. Ruben Carbonell (North Carolina State University, Raleigh, NC), was propagated in PK-13 cells as described previously [29]. PPV titration was performed by a colorimetric cell viability assay using MTT salt as described previously [14].

4.2.2.2 Generation of binodal curve and tie lines

Binodal curves were generated using the turbidity method [12] with 50 w/w% PEG and 35 w/w% citrate, and 0.5 M osmolyte stocks. Titration was done using 0.5 M osmolyte solutions to maintain the osmolyte concentration in the systems until the systems turned clear.

The tie lines were determined using the conductivity measurements of the citrate-rich phases as described previously [14]. The conductivity contribution of osmolytes was measured and determined to be negligible as compared to the conductivity of citrate. The osmolyte concentration was disregarded in the calculation of the citrate concentrations in

the citrate-rich phase. The tie line length (TLL) and tie line ratios (TLR) were calculated as mentioned previously [14].

4.2.2.3 *Osmolyte detection and quantification*

Osmolyte in the citrate-rich phases were quantified using LC-MS. A Thermo Scientific™ UltiMate™ 3000 HPLC (Thermo Fisher Scientific, Waltham, MA) was coupled with an Orbitrap Elite mass spectrometer (Thermo Fisher Scientific) with an electrospray ionization capability. Separate LC-MS/MS methods were developed for detection and quantification of glycine, betaine, TMAO, and urea. For each method, a corresponding isotope was added to all the calibration solutions and samples at the same concentration as the internal standard were used to compensate for instrument fluctuations. The analytical column used was an Ascentis Express HILIC 15 cm x 2.1 mm, 2.7 micron (Sigma Aldrich). Eluent A was acetonitrile (HPLC grade, Fisher Scientific) and eluent B was 0.1 v/v% formic acid (98-100%, Sigma Aldrich) in HPLC grade H₂O (Fisher Scientific). The LC-MS/MS conditions used for each osmolyte are listed in the **Table A.2-1** in the appendix. For quantifications, standard curves were generated by with the measuring the elution curve area of osmolyte and corresponding internal standard at different concentrations detected by the mass spectrometry. For mass spectrometry, selected ion monitoring (SIM) of the parent ion $[M+H]^+$, or the selected reaction monitoring (SRM) of the suitable fragmentation ion were used. For SRM, the transitions used for parent ion and fragment ion used for each osmolyte are reported in the **Table A.2-1**.

4.2.2.4 *Virus and virus-like particle partitioning*

Two phase systems were prepared with 50 w/w% PEG and 35 w/w% citrate. Appropriate stock concentration of each osmolyte was used to maintain a concentration of 0.5 M in the total system. Appropriate amounts of stocks with 0.1 g crude virus were added to a microcentrifuge tube to total 1g systems. The rest of the procedure was similar to our study reported earlier [14]. The virus and VLP recoveries and partition coefficient (K) were calculated using equations 4-1 and 4-2, respectively.

$$\% \text{ Recovery} = \frac{V_{P/C} * T_{P/C}}{V_i * T_i} * 100 \quad (4-1)$$

$$K = \frac{V_P * T_P}{V_C * T_C} \quad (4-2)$$

where V refers to the volume of either PEG-rich phase (P), citrate-rich phase (C), or initial stock (i) and T refers to the titer of the virus or virus-like particle in either phases or initial stock. PPV titer was expressed as MTT₅₀/mL. HIV-VLP titers were expressed as relative fluorescent unit (RFU)/0.1 mL, as measured with a Synergy Mx microplate reader (BioTek, Winooski, VT) at an excitation wavelength of 485 ± 9 nm and emission wavelength 509 ± 9 nm with 80% sensitivity and 10 mm probe offset in black 96-well plates (VWR).

4.2.2.5 SDS-PAGE for protein detection

The contaminant protein partitioning was detected using sodium dodecyl sulfate-polyacrylamide gel electrophoresis (SDS-PAGE) with a 4–12% Bis-Tris NuPage gel and NuPage MOPS running buffer (Life Technologies, Carlsbad, CA). SeeBlue Plus2 pre-stained protein ladder (molecular weight range: 14–191 kDa, Life Technologies) was used as the marker. Samples were reduced using 7 v/v% β mercaptoethanol (Sigma-Aldrich, St. Louis, MO) and heated to 90 °C for 10 minutes prior to loading onto the gel. The SDS-PAGE was run for 55 min at a constant 200 V. The gel was loaded with a same volume of the samples. The gel was stained with the SimplyBlue Safe stain (Life Technologies, Carlsbad, CA) as per the manufacturer's protocol.

4.2.2.6 DNA Quantification

Host cell dsDNA content was measured using the Quant-iT™ PicoGreen® dsDNA kit (ThermoFisher Scientific, Waltham, MA) as per the manufacturer's protocol. The PEG-rich phase and citrate-rich phase were diluted in water to a final concentration of PEG and citrate ≤ 1 w/w% to reduce the interference with the assay. The fluorescence (excitation: 480 nm and emission: 520 nm) of the samples were measured using a

Synergy™ Mx microplate reader. A DNA partition coefficient was calculated similar to virus partitioning using equation 4-3

$$K = \frac{V_P * DNA\ concentration_P * DF}{V_C * DNA\ concentration_C * DF} \quad (4-3)$$

where V denotes volume of respective phases and DF denotes respective dilution factor.

4.3 Results

4.3.1 Effect of osmolytes on two-phase behavior

In this study, both protecting and denaturing osmolytes were used to study the partitioning of viruses in ATPS. Protecting osmolytes modulate the water structure in the solution due to their strong solvation ability, denoted by the hydration number. The classification and characteristic hydration number of osmolytes in the concentration range used in this study is listed in **Table 4-1**. The osmolytes affected the two-phase systems by changing the threshold compositions of immiscibility and/or altering the equilibrium phase compositions.

Table 4-1. Osmolytes and their characteristics

Osmolyte	Class	Molecular mass (g/mol)	Hydration number (Concentration, mol/L)*	References
Glycine	Amino acid	75.07	7	[28, 30]
Betaine	Modified amino acid	117.15	31 (0.1 - 1)	[31]
Mannitol	Sugar alcohol	182.17	NA	
TMAO	Amine oxide	75.11	22.6 - 23 (0.9 - 0.46)	[27, 32]
Urea	Carbamide	60.06	~1 - 1.8 (0.5 - 1)	[33]

*Values in the parenthesis denote the range of concentrations for which the hydration numbers were determined

Binodal curves generated with the addition of 0.5 M osmolyte in the PEG-citrate system changed the two-phase formation. Osmoprotectants demonstrated a shift of the two-phase region (**Figure 4-1A**), whereas the denaturant urea did not show considerable change in the separation between the homogeneous and heterogeneous region. The addition of osmoprotectants shifted the binodal curve towards the citrate axis, indicating an increase in the salting-out behavior of the citrate-rich phase. The incompatibility of the phases is driven by the salting-out ability of salt-rich phase towards the ethylene oxide groups in the PEG chains [34]. On the other hand, the system formed with urea did not demonstrate a significant shift in the binodal curve as compared to the osmolyte-free binodal curve. It is likely that a high concentration of urea is required to make significant change in the phase behavior as studied previously [35].

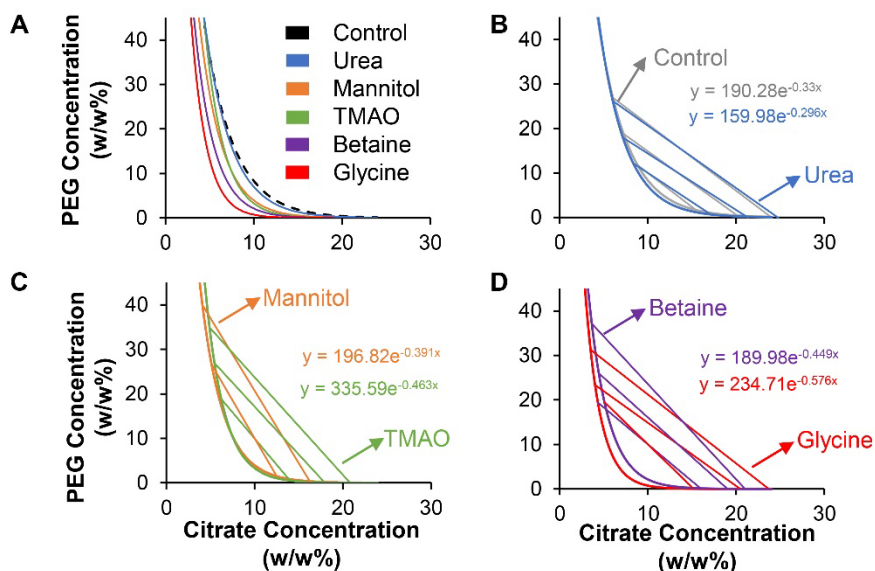


Figure 4-1. (A) Binodal curves and (B, C, D) tie lines for PEG 12kDa – citrate systems in presence of various 0.5 M osmolytes. Denaturing osmolyte – (B) urea and protecting osmolytes – (C) mannitol, TMAO, (D) betaine, and glycine.

The other important characteristic of two-phase systems are tie-lines, representing the set of systems at thermodynamic equilibrium with identical final phase compositions. The slope of a tie-line determines the equilibrium system compositions. The change in the TL slopes due to addition of osmolytes is compared to the osmolyte-free system in **Table 4-2** and shown in **Figures 4-1(B-D)**. Osmoprotectants betaine, TMAO, and mannitol showed a negative change in the TL slope (in that order) as compared to the osmolyte-free system, thus showing an increase in the PEG concentration and a decrease in citrate concentration as compared to a common point on that TL for the no osmolyte control. Glycine did not significantly change the slope. The denaturant urea demonstrated a positive change in the slope. If the altered equilibrium compositions generate an optimum balance between the hydrophobic and electrostatic interaction for the preferential partitioning of biomolecules, higher recovery and yield could be achieved. In this regard, mannitol, a polyol, demonstrated the largest increase in the PEG-rich phase composition and the largest decrease in the citrate-rich phase composition followed by TMAO (see **Figure 4-1** and **Table 4-2**).

Table 4-2. Changes in the TLL and TL slope with addition of osmolytes

Osmolyte	Δ TLL	Average TL Slope	Δ TL Slope	t-test values of Δ TL Slope
	(w/w%)	Deg (rad)	Deg (rad)	<i>P</i>
-		-1.48 ± 0.05		
Glycine	10.4	-1.54 ± 0.12	-0.06	0.4688
Betaine	9.5	-1.95 ± 0.18	-0.47	0.0121
TMAO	7.8	-2.23 ± 0.11	-0.75	0.0004
Mannitol	13.8	-3.33 ± 0.11	-1.85	0.0001
Urea	2.3	-1.33 ± 0.07	+0.16	0.0392

Note: Mannitol was not used to generate TL at high TLL

Δ = control - osmolyte

The osmolytes affected the interactions by variably partitioning between the two phases. Osmoprotectants preferred the citrate-rich phase, whereas the urea highly partitioned to the PEG-rich phase (**Figure 4-2A**). Almost 100% of the glycine was recovered in the citrate-rich phase at all TLL. Glycine partitioning to the citrate-rich phase shifted the binodal curve towards the citrate axis and increased the length of tie-lines, without affecting the tie-line slope, as compared to the osmolyte-free system. Betaine, TMAO, and mannitol demonstrated similar partitioning behavior. 60% recovery was observed for these osmolytes in the citrate-rich phase at the lowest TLL and increased up to 80% recovery at the higher TLLs (**Figure 4-2B**). Only 40% of urea was recovered in the citrate-rich phase at all TLL. Overall, the degree of osmolyte partitioning to the citrate-rich corresponded to the shift of binodal curve away from the osmolyte-free system.

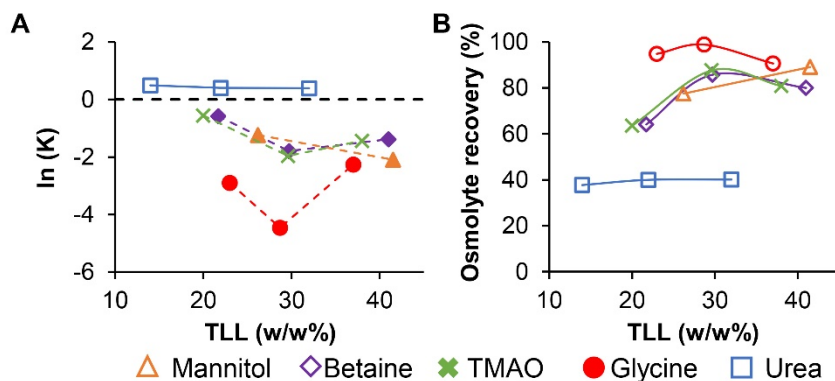


Figure 4-2. Partitioning of the osmolytes at common compositions of ATPS with increasing TLL represented as (A) ln(K) and (B) % recovery in the corresponding citrate-rich phases.

4.3.2 Model viruses

Two virus models - porcine parvovirus (PPV) and human immunodeficiency virus-group specific antigens virus-like particles (HIV-gag VLP) were used to determine the effect of osmolytes on the partitioning within an aqueous two-phase system. The structural and

physiochemical characteristics of PPV and HIV-gag VLPs are compiled in **Table 4-3**. Essentially, PPV used in this study is a non-enveloped infectious virus and comprises of three capsomeres VP1, VP2, and VP3, assembled in an icosahedral geometry [36]. HIV-gag VLP is an enveloped, non-infectious, virus-like particle comprised of Gag polyproteins self-assembled in spherical particles and enclosed in the envelope derived from *S. cerevisiae* cell membrane [37] These two models were used to determine the osmolyte action to modulate the partitioning of both non-enveloped and enveloped virus/VLP in the PEG-citrate system.

Table 4-3. Biophysical and biochemical characteristics of model virus/VLP

Model	family	Cell origin	pI	Size (nm)	genome	Structure	Ref
PPV	Parvoviridae	Mammalian	5	18-26	ssDNA	Non-enveloped	[36, 38]
HIV-gag VLP	Retroviridae (Original virus)	Yeast	?	80-120	-	Enveloped	proprietary

PPV: porcine parvovirus; HIV-gag-VLP: human immunodeficiency virus-group specific antigen-virus like particle

4.3.3 Influence of osmolyte class on virus partitioning

Initially, three global compositions having similar osmolyte concentrations were studied to understand the efficacy of different osmolyte classes to modulate virus partitioning in the PEG-citrate system at pH 7. Previous studies have shown that the negatively charged PPV partitions to the PEG-rich phase only at high system compositions. This is hypothesized to be due to the need to salt-out the virus from the citrate-rich phase to the interface. Then, the virus is pulled from the interface at high PEG concentrations due to the hydrophobic interaction between the amphiphilic PEG [14]. Here, the objective is to determine the additive that could enhance the purification at lower PEG and citrate concentrations, thus reducing viscosity and ionic strength of the system.

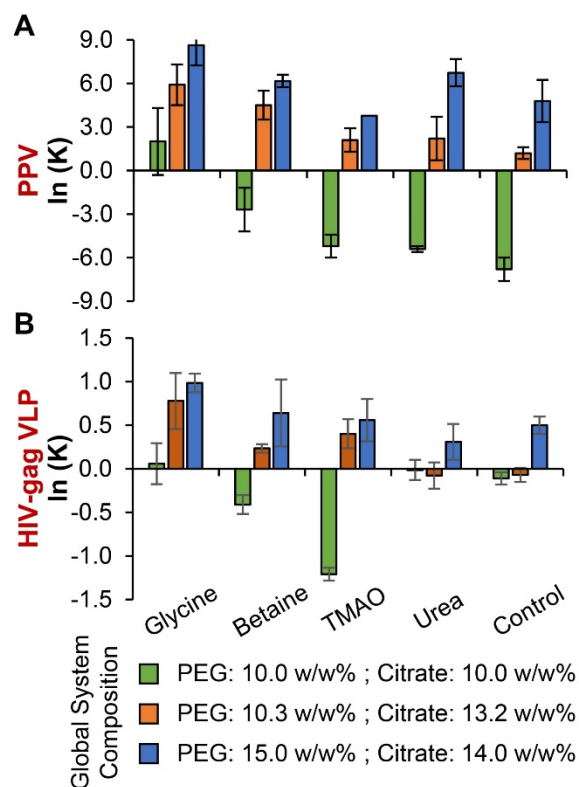


Figure 4-3. Effect of different osmolytes on (A) PPV and (B) HIV-gag VLP partitioning. Biomolecule partitioning upon addition of 0.5 M protecting (glycine, betaine, and TMAO) and non-protecting (urea) osmolytes are compared to osmolyte-free (control) system. Experiments were performed in triplicates and the error bars represent standard deviation.

The zwitterionic osmolytes glycine and betaine had most significantly altered the binodal curve as compared to the other osmolytes used (**Figure 4-1A**), indicating elevated driving forces for phase separation. A similar effect was observed for the viral partitioning, whereas addition of glycine and betaine significantly improved the PPV and HIV-VLP partitioning to the PEG-rich phase (**Figure 4-3**). Glycine-containing systems were able to enhance the partitioning of PPV at the lowest composition studied, yielding about 95% PPV recovery in the PEG-rich phase as compared to ~0% with the osmolyte-free systems (**Figure A.2-11A in Appendix**). The other two higher systems compositions

both yielded ~100 % recovery of PPV when glycine was added. Betaine improved the PPV partitioning slightly at the lowest composition studied, whereas TMAO did not change the partitioning behavior as compared to osmolyte-free system. However, most of the viral particles still partitioned to the citrate-rich phase in both betaine and TMAO-containing systems, exhibiting a lack of salting-out (**Figure 4-3**). Interestingly, urea-containing systems demonstrated a similar effect on the partitioning behavior of PPV as TMAO. It should be noted here that most of urea partitioned to the PEG-rich phase as compared to the citrate-rich phase partitioning of TMAO (**Figure 4-2**).

A similar study was performed to determine the effect of osmolytes on the enveloped HIV-VLP. At the lowest system composition, the glycine-containing system demonstrated an insignificant increase in the partition coefficient and betaine and TMAO reduced the partitioning of the VLP in the PEG-rich phase, as compared to the control (**Figure 4-3B**). The partition coefficient elevated significantly at the mid-system composition containing glycine, betaine, and TMAO, yielding 92% VLP recovery in the PEG-rich phase (**Figure 4-3B and Figure A.2-11C**). The highest system composition containing glycine demonstrated an increase in the partition coefficient as compared to the osmolyte-free system but yielded 83% recovery (**Figure 4-3B and Figure A.2-11C**). On the other hand, betaine and TMAO-containing systems did not show any significant differences in the partition coefficients (**Figure 4-3B**).

In both model viruses, osmolyte systems with betaine and TMAO recovered a lower number of viral particles in the PEG-rich phase when compared to glycine-containing systems of the same composition. This difference is likely due to the osmolyte partition in the citrate-rich phase, where glycine is recovered at >80%, and betaine/TMAO are recovered at ~60% (**Figure 4-2**). Although the hydration number of glycine is almost three-fold lower than betaine and TMAO (see **Table 4-2**), it is likely that the higher concentration of glycine in the citrate-rich phase compensates for the lower hydration number. It has been also shown that glycine is more kosmotropic as compared to betaine and TMAO [39]. Now, the same study suggested that betaine is less kosmotropic than TMAO which also correlated with the change in the TL slopes in our

study (**Table 4-2**). However, this kosmotropic difference was not translated to the virus partitioning, which showed similar salting-out effect by betaine and TMAO, but higher hydrophobic interaction to draw the virus into the PEG-rich phase by betaine than TMAO (**Figure A.2-11A & B**). Secondly, as the TLL increases with osmolyte-containing systems, the recovery is lower at low TLL compared to higher TLL. However, at the mid-TLL, the system reaches a maximum PEG-rich phase virus recovery meaning the addition of more osmolyte no longer increases virus recovery. This is hypothesized to be due to the salting-out effect of the citrate itself being the dominant driving force to salt-out virus from the citrate-rich phase, regardless of osmolyte concentration. A common trend of driving force enhancement for non-enveloped PPV and enveloped HIV-VLP recovery appears to follow the order glycine > betaine > TMAO > Urea ~ osmolyte-free.

4.3.4 Influence of osmolyte class on protein and HC-DNA partitioning

Depending on the class, the osmolytes in the previous section demonstrated an elevated partitioning of virus and VLP. It is essential to see if a similar effect is observed on the proteins which would lower the purity of the virus recovered PEG-rich phase.

As glycine and betaine had demonstrated the most improvement in the virus partitioning, host cell proteins (HCP) and host cell DNA (HC-DNA) were tracked only in these systems. The HCP were only detected in the citrate-rich phase, except at the highest TLL in which one band at 51 kDa appeared in the PEG-rich phase (**Figure 4A & B**). Also, all the contaminant proteins from HIV-VLP crude partitioned to the citrate-rich phase (data not shown). It is noted that the lower TLLs were of primary interest, as the glycine and betaine additions were able to recover most of the viral particles in the PEG-rich phase (**Figure A.2-11**). The partitioning of proteins in the citrate-rich phase is likely because the osmolytes stabilize the protein structure. Stabilization causes intraparticle interactions [22, 25] and likely does not induce interaction between the proteins and the PEG-rich phase. These results correlate with the previous studies that have shown osmolytes to induce only structural changes in the flexible proteins, whereas the

comparatively rigid viral particles experience interparticle interactions or flocculation in a single-phase solution [25, 40].

The HC-DNA partitioned to the citrate-rich phase at the lower TLLs of both the glycine and betaine-added systems (**Figure 4-4C & D**). At the highest TLL, glycine, but not betaine, enhanced the HC-DNA partitioning to the PEG-rich phase. This indicates that either glycine enhances the hydrophobic interaction of DNA with the PEG-rich phase or induces interaction between viral particles and DNA causing DNA to attach to the viral particles and co-partition in the PEG-rich phase. Overall, the lower TLLs with lower PEG and citrate compositions achieved a very high yield and purification of the viruses in the PEG-rich phases when glycine or betaine were used as additives.

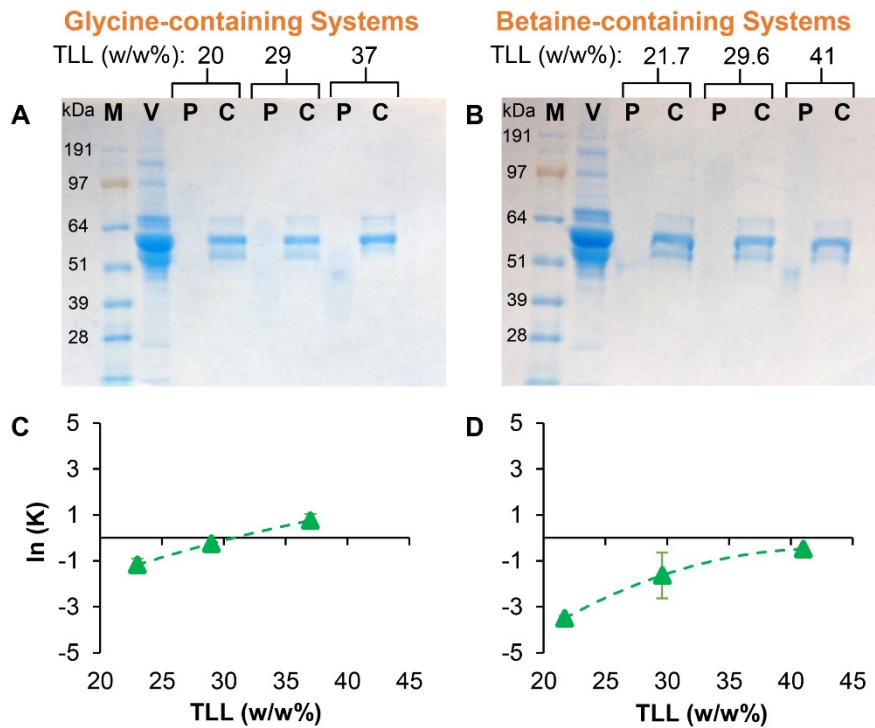


Figure 4-4. Contaminant protein (A & B) and HC-DNA (C & D) partitioning at varying TLL in presence of 0.5 M glycine or betaine. Contaminant protein partitioning were visualized on Coomassie stained SDS-PAGE and HC-DNA were quantified using Quant-iT™ PicoGreen® dsDNA assay. The error bars in the DNA partitioning figures represent standard deviations from the experiments done in triplicates.

4.3.5 Effect of tie-line framework on virus partitioning

Tie-lines guide the volume ratio of the phases, providing opportunity to recover viral particles in the PEG-rich phase having low volume. However, the system characteristic changes at the phase inversion point where the dispersed phase changes from the citrate-rich phase to PEG-rich phase as the TL ratio increases [41]. The phase inversion dictates if the viral particles directly partition to the bulk PEG-rich phase or accumulates at the interface of the dispersed PEG-rich phase to coalesce. This study was performed only with PPV to evaluate the phase inversion effects. The partition coefficient of PPV increased with the increasing TL ratio at lower TLLs and remained constant at the highest TLL (**Figure 4-5A**). This indicates that at the lower TL ratio, where the citrate-rich phase is the dispersed phase, there is no salting out of the viral particles. The increase in the TL ratio, where the PEG-rich phase is the dispersed phase, resulted in a slightly higher partition coefficient. PPV still partitioned to the citrate-rich phase at the lower TLL. However, more PPV was in the PEG-rich phase than the citrate-rich phase at the mid-TLL which indicates that the salting-out effect caused the viral particles to partition at the interface and coalition of the PEG-rich phase droplets collected the viral particles from the interface. At the highest TLL studied, PPV clearly exhibited hydrophobic interaction with the PEG-rich phase as the partitioning trend flattened. The PPV partitioning not only demonstrated a flat trendline in the systems containing glycine but also demonstrated that most of the viral particles partitioned to the PEG-rich phase at all TLLs (**Figure 4-5B**). This trend was observed at the mid and highest-TLL in the systems containing betaine or TMAO (**Figure 4-5C&E**). Interestingly, urea containing systems demonstrated similar trend as osmoprotectants (**Figure 4-5D**). However, the partition coefficients were lower than glycine and close to betaine and TMAO (**Figure 4-5B-E**). The systems containing mannitol demonstrated a reverse trendline as compared to the osmolyte-free system where the partitioning coefficient decreased with the TL ratios (**Figure 4-5F**). The overall trend of PPV partition coefficients implies that the osmolytes, except mannitol, provide consistent partitioning of viral particles across the tie line on contrary to the osmolyte-free systems.

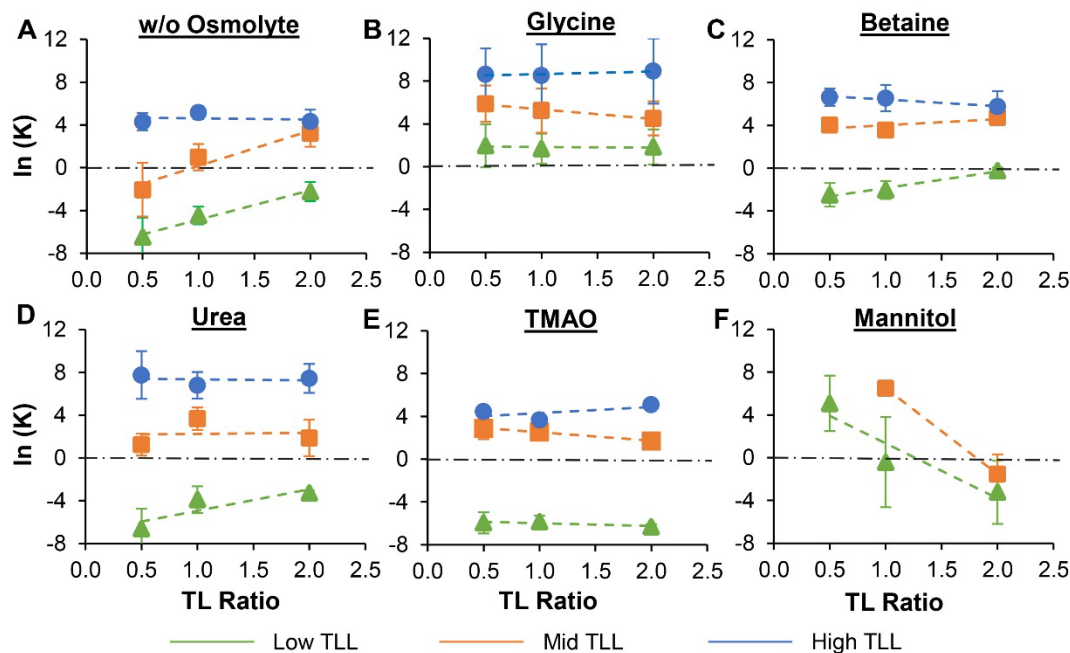


Figure 4-5. Partition coefficient of PPV in the systems (A) without osmolyte and systems enhanced with 0.5 M protecting osmolytes (B) glycine (C) betaine (D) TMAO (E) mannitol. Experiments were done in triplicates and the error bars represent the standard deviation.

The effect of osmolytes on the interaction of PPV and either phases is too complex to just be explained by the partition coefficients. Glycine containing systems yielded high PPV titers in the PEG-rich phase at all the TLL and TL ratio (**Table A.2-2**). However, the titers dropped with the increasing TLL in the citrate-rich phase. Similar trend was observed for betaine-containing systems, except the PPV titers in the PEG-rich phase were slightly lower than glycine. On the other hand, both TMAO and urea-containing systems demonstrated an increasing PPV titer with increasing TLLs, but the actual titers were much lower than glycine and betaine. The significantly different titers in the PEG-rich phase followed a decreasing order as glycine > betaine > TMAO > urea.

4.3.6 Effect of pH on virus partitioning

Surface charge of the viruses plays a vital role in the partitioning between the PEG-rich and citrate-rich phases. Negatively charged viruses experience repulsion effects by citrate ions, causing the salting-out effect. The repulsion effect decreases at the isoelectric point of the virus, causing the majority of viruses to partition to the citrate-rich phase [14, 38]. PPV has a pI near 5, thus it has a net neutral charge at that pH [38]. The systems containing the osmolytes glycine, betaine, or TMAO at pH 5 seem to have no effect on the interaction between PPV and the PEG-rich phase, as the systems infused with either of these osmolytes resulted in similar partitioning (**Figure 4-6**). However, an increase in the TLL increased the partitioning of the PPV, which is likely due to an increase in the ionic strength of the citrate-rich phase. This is a preliminary, yet significant observation, and more studies need to be performed to fully understand the effect of osmolytes on biomolecules at their pI.

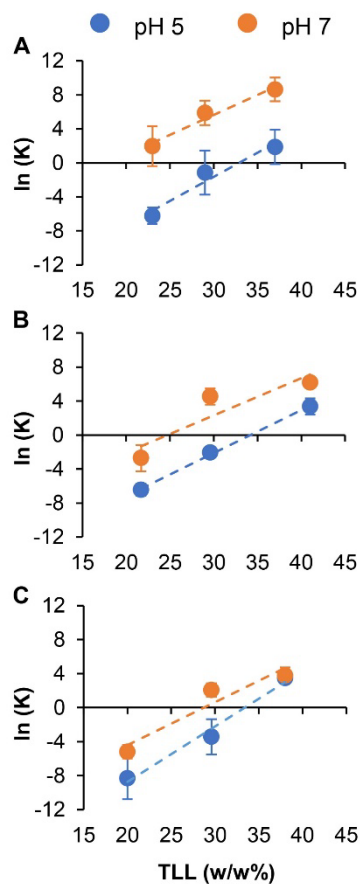


Figure 4-6. PPV partitioning at varying TLL in presence of (A) 0.5 M glycine, (B) 0.5 M betaine, and (C) 0.5 M TMAO maintained at pH 5 and 7. The error bars represents standard deviation of experiments done in triplicates.

4.4 Discussion

The partitioning of biomolecules in the PEG-salt systems is suggested to be highly affected by the balance of electrostatic and/or hydrophobic interactions [42]. The goal of this study was to improve the virus recovery in the PEG-rich phase at lower TLL where high recoveries were not achieved without additives. Osmolytes are known to modulate solvent properties and induce hydrophobic interactions in aqueous solutions [43, 44]. Changes in electrostatic and hydrophobic interactions can result in either intraparticle or interparticle interactions. The flexible smaller proteins are known to undergo conformational changes (intraparticle interactions) in the presence of

osmoprotectants [17, 18] and comparatively rigid viruses have been shown to flocculate (interparticle interactions) [25] in the presence of similar osmolytes. In this study, the osmolytes induced interfacial interactions between virus particles and the PEG-rich phase to improve virus recovery. This is an interesting observation in that the addition of protecting osmolytes yielded a high selectivity, as there was no interaction between the contaminant proteins and PEG-rich phase. It is likely that the osmolytes only affected the conformation of proteins.

The mechanism of protecting osmolytes glycine, betaine, and TMAO to stabilize the proteins structures and flocculate viruses is still unclear. In one study, the stabilizing effect of glycine and betaine disrupted the hydrogen bond network of elastin-like polypeptide with water [39]. The changes in the water structure was caused by osmolytes partitioning away from the polypeptide. On the other hand, TMAO was observed to favorably interact with the backbone of a collapsed protein and a hydrophobic homopolymer [39, 45]. Among the three osmolytes, TMAO was least recovered in the citrate-rich phase and this might indicate an interaction with the globular PEG molecules in the PEG-rich phase. Moreover, in this study, glycine and betaine (in that order) induced hydrophobic interactions between the virus models and PEG-rich phase to improve the partition coefficient (**Figure 4-3**). TMAO did not seem to improve the hydrophobic interaction, as previously shown [46] and shown here.

The enhancement of the driving forces at lower TLL also signifies comparatively easier processability of the phases, as the high recovery of biomolecules are obtained at lower phase compositions. The concentrated PEG-rich phase is viscous, which might pose challenges towards phase handling. The osmolytes recovered viruses at lower compositions that have lower viscosities of the PEG-rich phase as compared to osmolyte-free systems (**Table A.2-3**). Also, lower ATPS concentrations have a lower ionic strength. A lower ionic strength is highly preferred to maintain the stability of the viral particle function for use as a vaccine or gene therapy.

4.5 Conclusion

This study reports the use of osmolytes to modify the partitioning behavior of PPV and HIV-gag-VLP. Glycine followed by betaine, among the zwitterionic osmolytes, demonstrated an increase in the salting-out ability of the citrate-rich phase and an increase in the phase hydrophobicity of the PEG-rich phase. The elevated driving forces improved the recoveries of viruses at lower TLLs, where the systems without osmolytes are insufficient to induce the needed electrostatic and hydrophobic interactions to cause preferential virus partitioning. TMAO increased the ability of two-phase formation at lower system compositions, but it did not increase the hydrophobic interaction of viruses with the PEG-rich phase at lower TLL. ~100% of PPV and 90% of HIV-gag-VLP were recovered using glycine at the lowest TLL studies. The order of efficiency of osmolytes to enhance the driving forces was determined to be glycine > betaine > TMAO > urea.

High recovery and purity of viral modalities in the PEG-rich phase implied that osmolyte addition enhances the interfacial interactions for comparatively hydrophobic and rigid viruses as compared to the intramolecular interactions for flexible proteins. The HC-DNA partitioned to the citrate-rich phase at low TLL but increased towards the PEG-rich at higher TLL in presence of glycine and betaine. This study provides evidence that osmolyte addition not only improves the recovery, but also alleviate the challenges of high concentration ATPS processing. Moreover, this study showed that the effect of osmolytes on virus is drastically different than a protein, which is essential to develop a robust and versatile downstream process for viral particle manufacturing.

4.6 References

1. Azevedo, A.M., et al., *Partitioning of human antibodies in polyethylene glycol–sodium citrate aqueous two-phase systems*. Separation and Purification Technology, 2009. **65**(1): p. 14-21.

2. Platis, D. and N.E. Labrou, *Development of an aqueous two-phase partitioning system for fractionating therapeutic proteins from tobacco extract*. Journal of chromatography A, 2006. **1128**(1-2): p. 114-124.
3. Rosa, P.A., et al., *Aqueous two-phase systems: A viable platform in the manufacturing of biopharmaceuticals*. J Chromatogr A, 2010. **1217**(16): p. 2296-305.
4. Johansson, H.O., et al., *Plasmid DNA partitioning and separation using poly(ethylene glycol)/poly(acrylate)/salt aqueous two-phase systems*. J Chromatogr A, 2012. **1233**: p. 30-5.
5. Trindade, I.P., et al., *Purification of plasmid DNA vectors by aqueous two-phase extraction and hydrophobic interaction chromatography*. Journal of Chromatography A, 2005. **1082**(2): p. 176-184.
6. Norrby, E.C.J. and P. Albertsson, *Concentration of poliovirus by an aqueous polymer two-phase system*. Nature, 1960. **188**(4755): p. 1047-1048.
7. Philipson, L., P.Å. Albertsson, and G. Frick, *The purification and concentration of viruses by aqueous polymer phase systems*. Virology, 1960. **11**(3): p. 553-571.
8. Nakai, H., *Concentration of Japanese Encephalitis Virus by Aqueous Polymer Two-Phase System*. Acta virologica, 1965. **9**(1): p. 89-91.
9. Benavides, J., et al., *Rotavirus-like particles primary recovery from insect cells in aqueous two-phase systems*. J Chromatogr B Analyt Technol Biomed Life Sci, 2006. **842**(1): p. 48-57.
10. Guo, P., et al., *A simplified purification method for AAV variant by polyethylene glycol aqueous two-phase partitioning*. Bioengineered, 2013. **4**(2): p. 103-6.
11. Jue, E., et al., *Using an aqueous two-phase polymer-salt system to rapidly concentrate viruses for improving the detection limit of the lateral-flow immunoassay*. Biotechnol Bioeng, 2014. **111**(12): p. 2499-507.
12. Vijayaragavan, K.S., et al., *Separation of porcine parvovirus from bovine serum albumin using PEG-salt aqueous two-phase system*. J Chromatogr B Analyt Technol Biomed Life Sci, 2014. **967**: p. 118-26.
13. Grilo, A.L., M. Raquel Aires-Barros, and A.M. Azevedo, *Partitioning in Aqueous Two-Phase Systems: Fundamentals, Applications and Trends*. Separation & Purification Reviews, 2014. **45**(1): p. 68-80.

14. Joshi, P.U., et al., *Tie line framework to optimize non-enveloped virus recovery in aqueous two-phase systems*. J Chromatogr B Analyt Technol Biomed Life Sci, 2019. **1126-1127**: p. 121744.
15. Yancey, P.H., et al., *Living with water stress: evolution of osmolyte systems*. Science, 1982. **217**(4566): p. 1214-1222.
16. Yancey, P.H., W.R. Blake, and J. Conley, *Unusual organic osmolytes in deep-sea animals: adaptations to hydrostatic pressure and other perturbants*. Comparative Biochemistry and Physiology Part A: Molecular & Integrative Physiology, 2002. **133**(3): p. 667-676.
17. Auton, M., et al., *Osmolyte effects on protein stability and solubility: a balancing act between backbone and side-chains*. Biophys Chem, 2011. **159**(1): p. 90-9.
18. Street, T.O., D.W. Bolen, and G.D. Rose, *A molecular mechanism for osmolyte-induced protein stability*. Proceedings of the National Academy of Sciences, 2006. **103**(38): p. 13997-14002.
19. Bennion, B.J. and V. Daggett, *The molecular basis for the chemical denaturation of proteins by urea*. Proceedings of the National Academy of Sciences, 2003. **100**(9): p. 5142.
20. Sleator, R.D. and C. Hill, *Bacterial osmoadaptation: the role of osmolytes in bacterial stress and virulence*. FEMS microbiology reviews, 2002. **26**(1): p. 49-71.
21. Kinne, R.K.H., *The role of organic osmolytes in osmoregulation: from bacteria to mammals*. Journal of Experimental Zoology, 1993. **265**(4): p. 346-355.
22. Kumar, R., *Role of naturally occurring osmolytes in protein folding and stability*. Arch Biochem Biophys, 2009. **491**(1-2): p. 1-6.
23. Wlodarczyk, S.R., et al., *Influence and effect of osmolytes in biopharmaceutical formulations*. Eur J Pharm Biopharm, 2018. **131**: p. 92-98.
24. Lee, J.C., *Biopharmaceutical formulation*. Current opinion in biotechnology, 2000. **11**(1): p. 81-84.
25. Heldt, C.L., et al., *A generalized purification step for viral particles using mannitol flocculation*. Biotechnol Prog, 2018. **34**(4): p. 1027-1035.
26. Ferreira, L.A., et al., *Analyzing the effects of protecting osmolytes on solute-water interactions by solvatochromic comparison method: II. Globular proteins*. RSC Adv., 2015. **5**(73): p. 59780-59791.

27. Ferreira, L.A., et al., *How to manipulate partition behavior of proteins in aqueous two-phase systems: Effect of trimethylamine N-oxide (TMAO)*. Fluid Phase Equilibria, 2017. **449**: p. 217-224.
28. Ferreira, L.A., et al., *Analyzing the effects of protecting osmolytes on solute–water interactions by solvatochromic comparison method: I. Small organic compounds*. RSC Adv., 2015. **5**(74): p. 59812-59822.
29. Heldt, C.L., et al., *A colorimetric assay for viral agents that produce cytopathic effects*. J Virol Methods, 2006. **135**(1): p. 56-65.
30. Parsons, M.T. and Y. Koga, *Hydration number of glycine in aqueous solution: an experimental estimate*. J Chem Phys, 2005. **123**(23): p. 234504.
31. Shikata, T., *Dielectric Relaxation Behavior of Glycine Betaine in Aqueous Solution*. The Journal of Physical Chemistry A, 2002. **106**(34): p. 7664-7670.
32. Fedotova, M.V., S.E. Kruchinin, and G.N. Chuev, *Hydration structure of osmolyte TMAO: concentration/pressure-induced response*. New Journal of Chemistry, 2017. **41**(3): p. 1219-1228.
33. Agieienko, V. and R. Buchner, *Urea hydration from dielectric relaxation spectroscopy: old findings confirmed, new insights gained*. Phys Chem Chem Phys, 2016. **18**(4): p. 2597-607.
34. Hey, M.J., D.P. Jackson, and H. Yan, *The salting-out effect and phase separation in aqueous solutions of electrolytes and poly(ethylene glycol)*. Polymer, 2005. **46**(8): p. 2567-2572.
35. Rämisch, C., et al., *Aqueous Two-Phase Systems Containing Urea: Influence on Phase Separation and Stabilization of Protein Conformation by Phase Components*. Biotechnology Progress, 1999. **15**(3): p. 493-499.
36. Simpson, A.A., et al., *The structure of porcine parvovirus: comparison with related viruses*. J Mol Biol, 2002. **315**(5): p. 1189-98.
37. Sakuragi, S., et al., *HIV type 1 Gag virus-like particle budding from spheroplasts of Saccharomyces cerevisiae*. Proceedings of the National Academy of Sciences, 2002. **99**(12): p. 7956.
38. Mi, X., et al., *Virus Isoelectric Point Determination Using Single-Particle Chemical Force Microscopy*. Langmuir, 2020. **36**(1): p. 370-378.
39. Liao, Y.T., et al., *Trimethylamine N-oxide stabilizes proteins via a distinct mechanism compared with betaine and glycine*. Proc Natl Acad Sci U S A, 2017. **114**(10): p. 2479-2484.

40. Gencoglu, M.F., E. Pearson, and C.L. Heldt, *Porcine parvovirus flocculation and removal in the presence of osmolytes*. J Biotechnol, 2014. **186**: p. 83-90.
41. Merchuk, J.C., B.A. Andrews, and J.A. Asenjo, *Aqueous two phase system for protein separation studies on phase inversion*. Journal of Chromatography B, 1998. **711**(1-2): p. 285-293.
42. Asenjo, J.A. and B.A. Andrews, *Aqueous two-phase systems for protein separation: a perspective*. J Chromatogr A, 2011. **1218**(49): p. 8826-35.
43. Ferreira, L.A., et al., *Effects of osmolytes on solvent features of water in aqueous solutions*. J Biomol Struct Dyn, 2017. **35**(5): p. 1055-1068.
44. Athawale, M.V., S. Sarupria, and S. Garde, *Enthalpy–Entropy Contributions to Salt and Osmolyte Effects on Molecular-Scale Hydrophobic Hydration and Interactions*. The Journal of Physical Chemistry B, 2008. **112**(18): p. 5661-5670.
45. Mondal, J., et al., *How osmolytes influence hydrophobic polymer conformations: A unified view from experiment and theory*. Proc Natl Acad Sci U S A, 2015. **112**(30): p. 9270-5.
46. Athawale, M.V., J.S. Dordick, and S. Garde, *Osmolyte trimethylamine-N-oxide does not affect the strength of hydrophobic interactions: origin of osmolyte compatibility*. Biophys J, 2005. **89**(2): p. 858-66.

5 Affinity aqueous two-phase system using multimodal peptide ligand for virus partitioning⁵

⁵The content of this chapter is in preparation for submission to a peer-reviewed journal

5.1 Introduction

Aqueous two-phase systems (ATPS) formed by partially miscible aqueous solutions (polyethylene glycol-salt) have shown a great potential to be used in the downstream processing of viral vaccines and biotherapeutics [1-3]. However, our previous studies have shown that higher viral recoveries are obtained in the systems that have higher PEG-rich phase volume [4]. When the PEG-rich phase volumes are higher than the salt-rich phase volume, the PEG-rich phase acts as a continuous phase with the dispersed salt-rich phase [5]. The PEG-rich phase being viscous, the processing of ATPS becomes difficult. Moreover, the separation of viral particles from the PEG-rich phase is challenging. The possible strategy to reduce the processing burden is to operate the two-phase systems with the compositions that yield continuous salt-rich phase and dispersed PEG-rich phase is limited by the virus partitioning at the interface [4, 6]. This problem of lower virus recovery with lower PEG-rich phase volumes needs to be addressed by developing novel systems that improve the affinity of the PEG-rich phase to allow higher virus partitioning.

ATPS composed of different phase forming components such as polymer-polymer (polyethylene glycol-dextran) and polymer-salt (polyethylene glycol-sulfate/citrate/phosphate) have found numerous applications in bioprocessing and biotechnology. The common application of ATPS in biotherapeutic field has been in the recovery and purification of cells [7-9], antibodies [10, 11], viruses [12-14], and nucleic acids [15, 16]. The advantages of ATPS as a potential alternative to the conventional downstream processing unit operations are high target biomolecule yield, inexpensive, easy-to-scale up, and continuously processable unit operation. However, in the early days, the unambiguity in understanding the partitioning behavior of biomolecules between the two phases hindered the potential use of the mild biphasic systems. Various studies point to the following factors affecting the partitioning behavior: hydrophobicity, electrostatics, and volume-exclusion [17, 18]. These interactive forces are influenced by the phase-forming component and biomolecule structural and physicochemical properties. The insight into the driving forces has been used to investigate ATPS as a tool

in the surface physicochemical characterization of biomolecules [19, 20], developing assays for molecular recognition [21-23], and producing microspheres for protein and drug encapsulation [24, 25].

There has been a significant advancement in designing and synthesizing molecules to enhance the affinity for biomolecules. The affinity ligands are made from peptides [26, 27], aptamers [28, 29], proteins [30], and polysaccharides [31]. These ligands have been utilized in the affinity and multimodal chromatography for purification of a target biomolecule. Protein A, used for the affinity purification of immunoglobulin G (IgG), is expensive, labile, and requires harsh elution conditions. One way to alleviate the disadvantages of Protein A is to design short peptides to mimic the protein A binding to IgG [32, 33]. A hybrid ligand composed of a trimeric peptide FYE conjugated with a hydrophobic charge-induction group provided a comparable purity and recovery of IgG with a milder elution condition than protein A [34]. The design of appropriate ligands to alleviate harsh processing conditions has helped to improve the downstream processing of biologics [35, 36].

While similar strategies have been used to select ligands with a high affinity towards viral particles, the diversity in the viral surface composition and physicochemical characteristics makes the use of appropriate ligands difficult. Ligands for viral processing has come in the form of antibodies [37, 38], protein-based lectin [36, 39], metal ions [40, 41], and polysaccharide-based heparin and heparan sulfate [42, 43]. A more robust method suggests the use of multimodal ligands that use a combination of electrostatic interaction, hydrophobic interaction, and hydrogen bonding mechanisms [44, 45]. Synthetic peptide libraries are also being explored as the potential sources of multimodal ligands. Zheng and coworkers (2017) demonstrated that the peptide motif YHDCFSAGFCIG presented a high affinity with a dissociation constant of 98 nM towards porcine circovirus type 2 Cap protein [46]. The other study found that the peptide sequence CAAALAKPHTENHLLT, selected by phage-display, was able to bind to retrovirus virus-like particle expressing Ampho4070A protein and recovered 90% viral particles with a mild elution condition [47]. However, such peptides not only depend on

the amino acid sequence to harness the molecular interactions but also on the spatial orientation of the peptide to dock in a targeted pocket of the viral proteins [48]. The peptide ligands could also be designed to preferentially interact with viral proteins based only on the molecular interactions without requiring a constrained structural conformation of amino acid residues. This was achieved previously by limiting the number of residues where trimeric peptides were found to bind porcine parvovirus and the binding was not improved by adding more amino acids, which likely resulted in secondary structure of the ligand [49].

Affinity ligands have also been used in ATPS to improve the specificity and processing abilities for biomolecule partitioning. The affinity ligands are generally conjugated with the polymer and attract the target biomolecule to the polymer-rich phase. Polyethylene glycol has been modified to present electrophilic, nucleophilic, or hydrophobic end groups [50]. Ligands were either small organic molecules, such as benzoyl or dinitrophenyl, or biospecific proteins or enzymes such as avidin or antibody-horse radish peroxidase. However, there have been hardly any studies performed with the inclusion of small peptide ligands in affinity ATPS. The challenge of using a PEGylated ligand is the long PEG tail may hinder the accessibility of the active site of the ligand [51]. The conjugation of a small antimicrobial peptide with PEG inhibited the antimicrobial activity and was hypothesized that the PEG chain interfered with the functioning of the active sites [52]. The presence of PEG functionalized with the cell adhesion domain (RGD) did not induce cell adhesion as the peptide was surrounded by a PEG shell [53]. However, the masking of the active domains by PEG chain could be averted by utilizing an optimum molecular weight of PEG that increases the flexibility of the polymer and provides steric hindrance for nonspecific interactions [54].

In this study, a non-enveloped porcine parvovirus (PPV) partitioning behavior was studied in the PEG-citrate system in the presence of peptides conjugated to PEG 10kDa. A trimeric multimodal affinity region WRW was chosen due to its high affinity towards PPV [55]. With the growing interest of determining if the active sites of ligands are accessible upon conjugation, the target peptide with the WRW region was

characterized using the fluorescence quenching method. High solvent accessibility of the target multimodal region favored the PPV partitioning into the PEG-rich phase. The improved PPV partitioning was suggested to be the result of either direct binding with the PPV capsids or enhancing the hydrophobicity and electrostatic potential of the PEG-rich phase. The use of multimodal peptide ligand demonstrated that the virus partitioning could be enhanced at lower phase composition and lower volumes of the PEG-rich phase.

5.2 Materials & Methods

5.2.1 Materials

Eagle's minimum essential media (EMEM), sodium bicarbonate, phosphate buffer saline (PBS, pH 7.2), penicillin-streptomycin (pen-strep) (10,000 U/ml), fetal bovine serum (FBS, USDA approved) and trypsin/EDTA for cell propagation were purchased from Life Technologies (Carlsbad, CA). 2-(3,5-diphenyltetrazol-2-ium-2-yl)-4,5-dimethyl-1,3thiazole;bromide (MTT, 98%) was purchased from Alfa Aesar™ (Haverhill, MA) and sodium dodecyl sulfate (SDS, BioReagent, ≥98.5%) was purchased from Sigma Aldrich (Radnor, PA). Polyethylene glycol with an average molecular weight of 12,000 Da (PEG 12 kDa), trisodium citrate dihydrate (ACS reagent grade, ≥99%), and citric acid monohydrate (ACS reagent, ≥99%) were a generous gift by Millipore Sigma (Burlington, MA). Monofunctional methoxy-polyethylene glycol-vinyl sulfone (mPEG-VS) (PEG molecular weight: 10000 Da) was purchased from Creative PEGworks (Chapel Hill, NC). Peptide ligands GRCDGGWRW, GRCDGGGGG, and GRCDGGAAA (98% purity) were purchased from Peptide 2.0 Inc. (Chantilly, VA). Acrylamide solution (40% w/v) was purchased from Bio-Rad Laboratories (Hercules, CA). Triethanolamine (TEA) was purchased from Thermo Fisher Scientific (St. Louis, MO). Phosphate buffer saline (PBS) was obtained from HyClone Laboratories (South Logan, UT). Dialysis tubing (MW cutoff 3.5 kDa) and black-walled, glass-bottom 96-well plates were purchased from Thermo Fisher Scientific (Waltham, MA). Solutions were prepared with Nanopure water (Thermo Scientific, Waltham, MA) at a resistance of

$\geq 18 \text{ M}\Omega$ and filtered with either a 0.2 μm Nalgene (Thermo Scientific) bottle top filter or 0.22 μm cellulose acetate syringe filters (VWR, Radnor, PA) before use.

5.2.2 Methods

5.2.2.1 Cell culture, virus propagation, and titration

Porcine kidney cells (PK-13, CRL-6489) purchased from ATCC (Manassas, VA) were maintained in EMEM pH 7.1 mixed with 10 v/v% FBS and 1 v/v% pen-strep as described previously [4]. Porcine parvovirus strain NADL-2 (PPV) was a generous gift from Dr. Ruben Carbonell (North Carolina State University, Raleigh, NC) and was propagated in PK-13 cells, as described previously [56]. PPV was quantified by titration using MTT salt-based colorimetric cell viability assay [4].

5.2.2.2 Functionalized PEG conjugation and purification

The functionalization of PEG with peptide ligands was carried out by reacting vinyl sulfone on mPEG(10 kDa)-VS with the thiol group of cysteine on the peptide sequence GRCDGGXXX, where XXX represents GGG, AAA, or WRW (**Figure 5-1**). Each peptide (WRW, GGG or AAA at 12 mM) was reacted via Michael-type addition with mPEG-VS (10 mM) in 0.3 M triethanolamine (TEA) pH 7.4 at a molar ratio of 1.2 peptide:1 PEG in an incubator at 37 °C for 30 minutes. The solution was removed from the incubator and dialyzed in dialysis tubing of molecular weight cut-off 3.5 kDa in deionized water with convective mixing at 200 RPM. The water was replaced 3 times in the first hour and once a day for two more days. The solution was then aliquoted, frozen at -80 °C for ~1 hour and lyophilized overnight. The resulting functionalized mPEGVS-peptide was stored in a desiccated container at -20 °C until use. The average product yield was ~90% and the average derivatization was >95% as confirmed by proton nuclear magnetic resonance (^1H NMR): the product was dissolved in deuterated chloroform (CDCl_3) and the disappearance of peaks at 6, 6.5, and 7 ppm confirmed successful mPEG-VS functionalization.

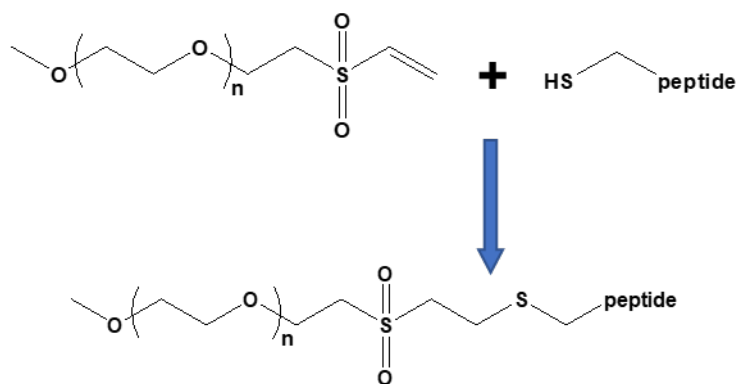


Figure 5-1. Synthesis flow diagram of functionalized PEG-peptide conjugates. A linear PEG-vinyl sulfone is covalently functionalized with a cysteine terminated peptide.

5.2.2.3 Steady-state fluorescence quenching

To determine whether derivatization with PEG ‘buried’ the peptide, GRCDWRW peptide and mPEGVS-WRW were dissolved in PBS at a final concentration of 1200 nM. Acrylamide solutions of 0.8 M, 0.6 M, 0.4 M, and 0.2 M were prepared in PBS by serial dilution. Next, 50 μ L of GRCDWRW or mPEGVS-WRW solutions were added in triplicate to a black-walled, glass-bottom 96-well plate and 50 μ L of acrylamide solution was added to each well for a total of 100 μ L volume per well. Fluorescence of the tryptophan amino acid (W; excitation at 280 nm/emission at 350 nm) was then recorded using a spectrophotometer (SpectraMax i3, Molecular Devices, Sunnyvale, CA). Fluorescence quenching experiments were performed by measuring the fluorescence intensity loss of the free GRCDWRW peptide or conjugated mPEGVS-WRW as a function of acrylamide concentration. Acrylamide quenches the fluorescence of W, where quenching kinetics depends on W accessibility. Fluorescence quenching data were fitted to the Stern-Volmer equation [57]:

$$F_0/F = 1 + K_{SV}[Q] \quad (5-1)$$

where F_0 and F are the fluorescence intensities in the absence and presence of the quencher, Q , and K_{SV} is the Stern-Volmer quenching constant.

5.2.2.4 Virus Partitioning and Recovery

1 g two-phase systems were prepared by mixing appropriate amounts of 45 w/w% PEG and 35 w/w% citrate stocks along with 0.1 g crude PPV stock to a non-stick 1.5 mL microcentrifuge tube (VWR, Radnor, PA) for systems without affinity ligands [4]. The systems with affinity ligands were prepared by maintaining a 7:3 mass ratio of PEG to PEG-peptide, and the rest of the components remaining identical to the ligand-free systems. A 7:3 mass ratio of unfunctionalized and functionalized PEG was maintained by an appropriate amount of 45 w/w% PEG-peptide stock. The virus partitioning procedure was similar to the previously described study [4]. The PPV partitioning (K) and recovery were calculated using equations 2 and 3, respectively.

$$K = \frac{V_P * T_P}{V_C * T_C} \quad (5-2)$$

$$\% \text{ Recovery} = \frac{V_{P/C} * T_{P/C}}{V_i * T_i} * 100 \quad (5-3)$$

where V and T are the volume and PPV titers of the PEG-rich phase (P), citrate-rich phase (C), or initial stock virus (i). PPV titers are expressed as MTT_{50}/mL

5.3 Results

5.3.1 Virus partitioning in the presence of affinity ligand

Aqueous two-phase systems are defined by a binodal curve and tie lines (see **Figure 5-2A**). The binodal curve defines the two-phase region and tie lines represent the thermodynamic equilibrium of the system, where any system on a tie line will separate into two phases containing the concentrations found by the intersection of the tie line and the binodal curve. Previous work has shown that high PEG and salt concentrations (i.e.

longer tie line lengths) are needed to partition viral particles to the PEG-rich phase [3, 4]. Also, virus partitioning increases with higher volume ratios or lower tie-line ratios (TLR) [4]. Since partitioning is an equilibrium process, virus titers in each phase were similar at different volume ratios, but when taking volume into account, yield was higher in the PEG-rich phase when there was more PEG-rich phase volume (i.e. lower TLR). A non-enveloped porcine parvovirus (PPV) comprised of capsid proteins VP1, VP2, and VP3 is used as a model virus in this study [58]. A multimodal peptide-based affinity ligand was used in this study to enhance the PPV partitioning at lower volume ratios in the PEG 12kda-citrate systems at pH 7.

Two TLR at three different tie-line lengths were selected (**Figure 5-2A**) such that the volume ratios of the equilibrium PEG-rich phase to the citrate-rich phase volumes were < 1 (**Table A.3-1**). These represent cases where there is low virus partitioning to the PEG-rich phase without affinity ligands present. WRW peptide has been shown to display high affinity towards PPV with a combined hydrophobic and electrostatic interaction of WRW with the PPV capsids [49]. Thus, this peptide was used as the primary affinity ligand in this study. As controls to the multimodal WRW ligand, GGG and AAA were used to evaluate the specificity of the virus partitioning. The effect of a 30 w/w% replacement of PEG with functionalized PEG can be found in **Figure 5-2B & C**. At the TLR of 1 (**Figure 5-2C**), PEG-WRW increased the PPV partitioning to the PEG-rich phase significantly at all tie-line lengths, as compared to the unmodified systems (ligand-free systems). However, most of the PPV particles still partitioned to the citrate-rich phase at the tie-line length 15 w/w%, and the significant increase by was observed at the tie-line length 36 w/w%. On the other hand, control ligands demonstrated the opposite trend. The PPV partitioning was not significantly affected by GGG and AAA at the tie-line lengths 15 and 36 w/w%. The PPV partitioning was pushed to the citrate-rich phase at tie length 25 w/w%. The WRW ligand is likely attracting viral particles to the PEG-rich phase if the viral particles are at the interface, and the control ligands seem to push the viruses away from the interface to the citrate-rich. An increase in the TLR to 2.3 only increased the partition coefficient at the tie-line length 15 w/w% of the PEG-WRW

containing systems, whereas, the other two tie-line lengths did not show any significant change in the virus partitioning (**Figure 2C**). Even though the equilibrium PEG-rich phase composition remains the same for each tie line length, a lower number of affinity ligands were added to the system due to the overall lower PEG mass in the system. On the other hand, the control ligands (GGG and AAA) had no significant effect on the virus partitioning at the tie-line length 15 w/w%. However, the control ligands reduced the virus partitioning at tie-line length 25 and 36 w/w% even more than the addition of PEG-WRW. It is likely that PEG-WRW makes the PEG-rich phase more hydrophobic and positively charged than the unmodified systems, thereby elevating the negatively charged virus partitioning towards the PEG-rich phase. The control polymers PEG-GGG and PEG-AAA may make the PEG-rich phase more hydrophilic, thereby suppressing the virus partitioning to the PEG-rich phase.

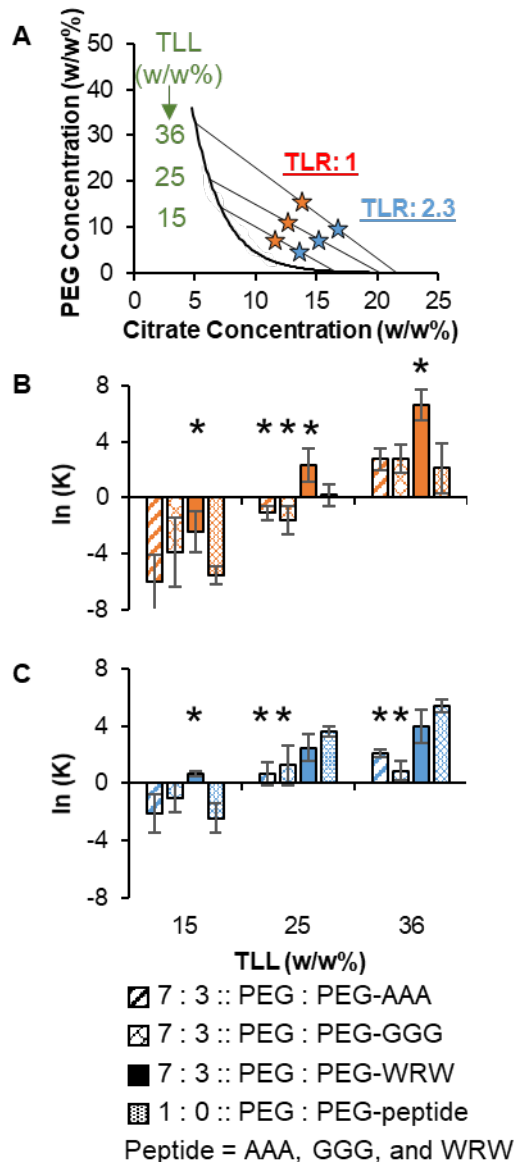


Figure 5-2. Effect of TLL and TL ratios on PPV partitioning with an inclusion of affinity ligand mPEGVS-WRW. (A) Six systems were selected on three different tie-lines and two TLR. The partitioning coefficients in the presence of 30% PEG-peptide doping are demonstrated at (B) TLR:1 and (C) TLR:2.3 on all the three TLL along with systems without the affinity ligand doping. Experiments were conducted in triplicates and the error bar represents standard deviation. *p-value < 0.05 using Student's t-test as compared to the ligand-free system.

Another way to assess the effect of viral behavior at the interface and determine the ligand efficiency is to explore the recoveries of the viral particles in each equilibrium phase. The viral transport through the interface was traced by determining the viral recovery (**Figure 5-3A and B**) in the PEG-rich and citrate-rich phases of the systems studied in **Figure 5-2**. The PPV recovery in the PEG-rich phase was higher at the TLR 2.3 as compared to the TLR 1 with the inclusion of PEG-WRW (**Figure 5-3C and D**). It is likely that the increased volume of the citrate-rich phase was able to induce an interaction of additional number of the viral particles with the PEG-rich phase, as a lower PPV recovery was observed in the citrate-rich phase of the TLR 2.3 compared to the TLR 1 (see **Figure 5-3E and F**). The PEG-WRW containing system at the TLR 2.3 was able to recover the virus at the interface in the PEG-rich phase due to the high affinity towards PPV. The ligand-free system was incapable of transporting a similar number of salted-out PPV to the PEG-rich phase. The system at TLR 1 was able to recover only 10% of PPV as most of the viral particles were not salted-out (**Figure 5-3C and F**). However, this effect is more prominently observed at the tie-line length 15 w/w% because the citrate-rich phase composition is insufficient for the driving force to act upon all the viral particles. The tie line lengths 25 and 36 w/w% demonstrated that most of the viral particles salted-out of the citrate-rich phase at both the TLRs. The PPV recoveries in the citrate-rich phases ranged between 0-5% in the unmodified and PEG-WRW systems (See **Figure 5-3E and F**). A similar effect was observed in the PEG-rich phase at the tie line length 25 w/w% where the system at TLR 2.3 was able to recover more PPV as compared to the TLR 1 (**Figure 5-3C and D**). The control ligands GGG and AAA demonstrated a similar high PPV recovery of 80-90% in the citrate-rich phase at TLR 1 of the tie line length 15 w/w% as compared to the ligand-free system (**Figure 5-3E**). However, similar viral particles were still recovered in the citrate-rich phase as compared to a relatively lower recovery in the ligand-free and PEG-WRW systems at the TLR 2.3. On the other hand, the PPV recoveries in the PEG-rich phases were minimal, indicating that the viruses do interact with the PEG-rich phases. The increased concentration of control ligands in the systems at tie-line length 25 w/w% showed a comparatively higher PPV recovery in the citrate-rich phase at TLR 1 and a similar recovery at TLR 2.3 as the

ligand-free systems (**Figure 5-3E and F**). A slight increase in the PPV recovery was seen at the TLR 2.3 than the TLR 1, but most of the PPV appears to be stuck at the interface (**Figure 5-3C and D**). The tie line length 36 w/w% demonstrated a similar low PPV recovery in both the citrate-rich phase and PEG-rich phase as the ligand-free system indicating that the viruses partitioning to the interface. In general, PEG-WRW enhanced the virus recovery at TLR 2.3 on all the tie lengths and likely improved the virus partitioning by directly attaching to PPV capsids or increasing the affinity of the PEG-rich phase for PPV partitioning.

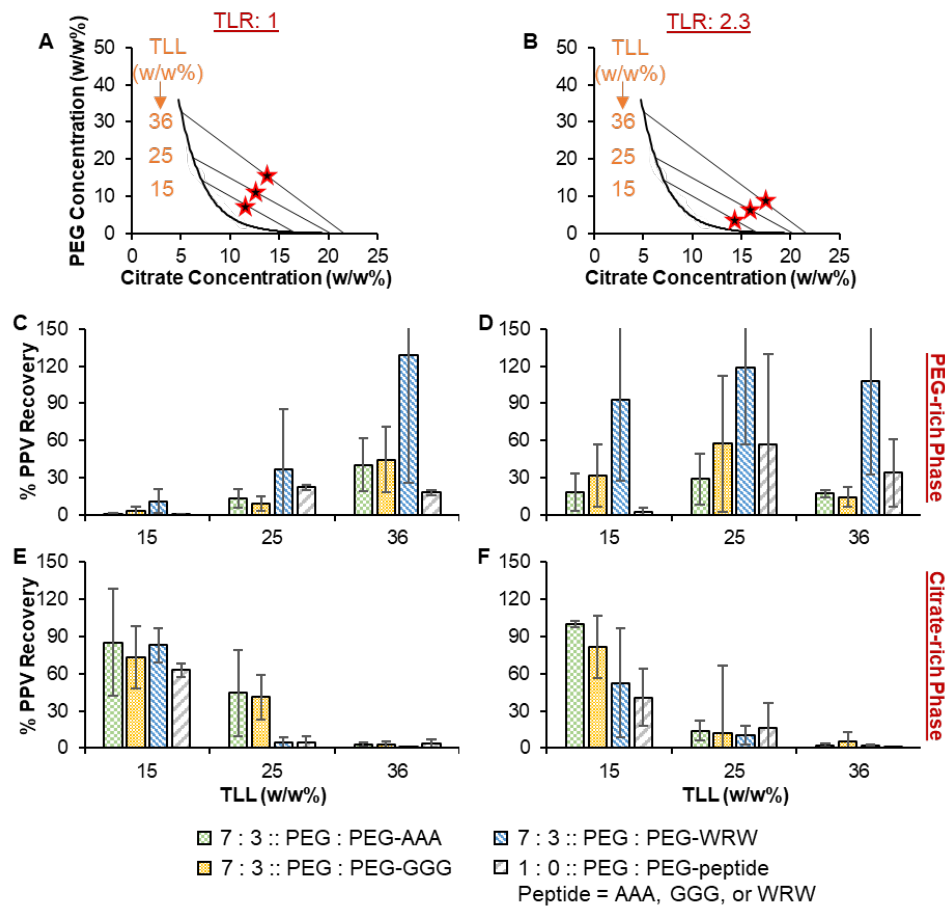


Figure 5-3. PPV recovery comparison at (A&B) the three TLL and two TLRs in the (C&D) PEG-rich phase and (E&F) citrate-rich phase. Three separate ligands (AAA, GGG, and WRW) were added individually in each system at a 7:3 ratio of PEG 12 kDa to PEG-peptide conjugate and compared with the ligand-free control systems. The error bars represent the standard deviations from three individual experiments.

5.3.2 Efficiency and characterization of PEG-peptide conjugation

The conjugation of PEG-peptide was confirmed using the ^1H NMR spectra of the polymers. The disappearance of the peaks at 6, 6.5, and 7 ppm (orange box) after functionalization of mPEG-VS indicates that functionalization had successfully occurred (Figure 5-5A-D). This absence of peaks, which corresponded to the unreacted VS group, indicated a successful conjugation of PEGVS and peptide at the thiol group of the cystine terminal [59]. The conjugation of PEG-WRW was further confirmed as PEG-peptide and free WRW peptide demonstrated a similar fluorescence profile with a peak at 310 nm (Figure A.3-1A). Lastly, a high absorbance of PEG-WRW between 210-280 nm as compared to a no absorbance of unfunctionalized PEGVS further confirmed successful conjugation (Figure A.3-1B).

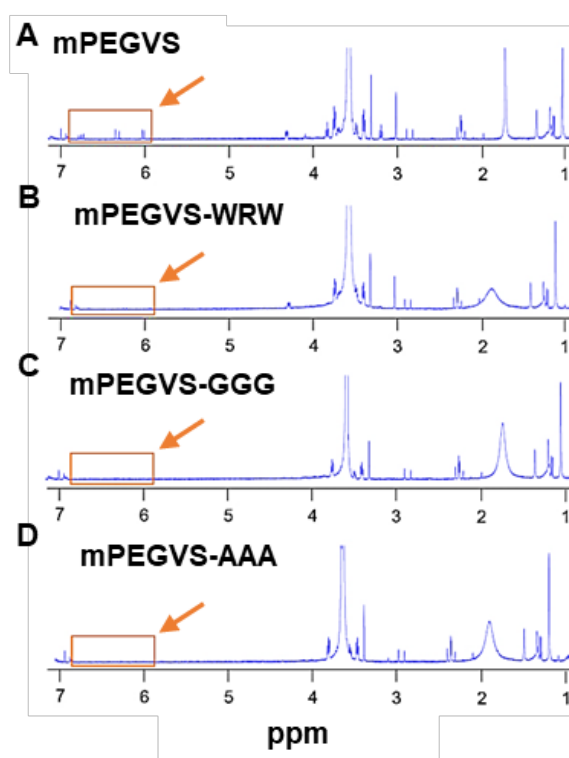


Figure 5-4. Conjugation confirmation of mPEGVS and peptides represented as ^1H NMR spectra of (A) mPEGVS, (B) mPEGVS-AAA, (C) mPEGVS-GGG, and (D) mPEGVS-WRW. The orange box at 6, 6.5, and 7 ppm indicates the vinyl sulfone peaks, whose disappearance shows that the reaction between the mPEGVS and the peptides had occurred.

The affinity of WRW towards PPV was possible only if the target peptide was accessible in the aqueous solution. It was possible that the WRW peptide would be buried by the PEG polymer. However, WRW was found to be accessible as acrylamide highly quenched the fluorescence intensity of PEG-WRW as compared to the unconjugated WRW peptide (**Figure 5-6**). The Stokes-Volmer coefficient (K_{SV}) was found to be 13.5 for PEG-WRW as compared to only 5.1 for the free WRW. This indicated that the PEG conjugation made the peptide more accessible to the quencher as opposed to less accessible.

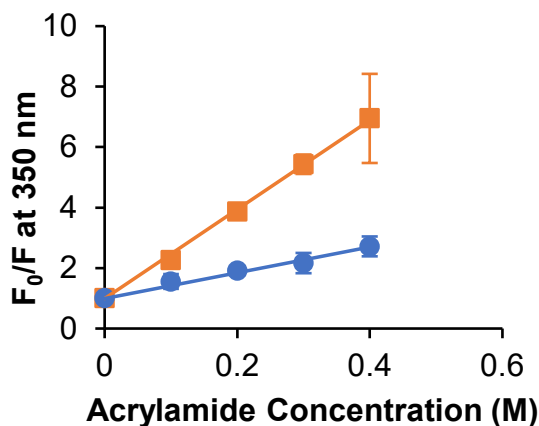


Figure 5-5. Acrylamide quenching of free WRW peptide and mPEGVS-WRW fluorescence. Fitting of data points to the Stern-Volmer equation yields K_{SV} values of 5.1 ± 0.8 and 13.5 ± 1.1 M^{-1} for free WRW and mPEGVS-WRW, respectively. Experiments were conducted in triplicates and the error bars represent standard deviations.

5.4 Discussion

Aqueous two-phase systems have been widely utilized for developing an alternative to the conventional downstream processing unit operations. The new generation applications have focused on the various biotechnology applications such as

drug encapsulation, delivery, and model bio-compartmentalization [24, 60, 61]. These applications have recognized the potential of affinity ligands to improve the specificity and partitioning of target biomolecules [50, 61, 62]. In this study, PEG conjugated with the multimodal affinity ligand WRW demonstrated an enhancement in the virus partitioning, which provides an opportunity for various applications stated above. However, the changes to virus partitioning depended on the bioavailability of the peptide upon conjugation. The PEGylation of peptides has shown to alter the peptide conformations depending on the physicochemical characteristics of the peptide and the PEG chain length [63, 64]. A molecular simulation study showed that the cationic residues of the peptides interacted favorably with the PEG oxygen atoms and the hydrophobic residues interacted with non-polar ethyl regions of the PEG subunits [64]. The favorable interactions of the peptide residues with the PEG chain led to a shielding effect by PEG, thereby reducing the solvent-accessible surface area of α -helical peptides. A similar study showed that charged and polar smaller peptides had higher solvent-exposed structures than hydrophobic peptides [63]. The same study demonstrated that PEG has an insignificant effect on the conformation of neutral peptides. In another study, a specific PEG chain length has shown to display a shielding effect for peptides with a specific amino acid number [65]. Specifically, PEG 10kDa has shown to have the shielding of the electrostatic potential of the peptide with a maximum of eight amino acid residues. In this study, the biologically active region WRW of the nine amino acids peptide, with both hydrophobic and positively charge amino acids at physiological pH (**Table 5-1**), was found to be solvent accessible upon conjugation (**Figure 5-6**). It is highly possible that the tendency of hydrophobic residues to avoid exposure to the polar solvent was comprised of the highly charged peptide or the hydrophilic PEG chain length resisted the structural change of small peptide due to the hydrophilic and neutral spacer region (GRCDGG). It has been shown previously that the preferential partitioning of PPV to the PEG-rich phase in a PEG-salt system is driven by electrostatic and hydrophobic interactions [3, 4]. The accessible bioactive region WRW likely improved the virus partitioning through the charge and hydrophobic interactions with the PPV capsid. It is also possible that the WRW increased the biospecific affinity of the PEG-rich

phase towards negatively charged PPV by increasing the positive charge density of the phase as the neutrally charged slightly hydrophobic ligand AAA did not improve the virus partitioning (**Figure 5-2**).

Previous studies have shown that the high virus partitioning is achieved at lower TLR where the PEG-rich phase volumes are higher than the salt-rich phase volumes [4, 6]. The addition of hydrophobic and positively charged peptide containing WRW residues improved the virus recovery in the PEG-rich phase at the higher TLR with lower volumes of the PEG-rich phases. The enhanced recovery at higher TLR is beneficial for the downstream processing of biomolecules. The high TLR systems fall in the regime of continuous citrate-rich phases, which have higher settling kinetics, lower dependence of viscosity, and low volume of target biomolecule containing PEG-rich phase [5]. Further, the high partitioning of the viruses in low PEG-rich phase volumes may be desired to generate droplet hydrogels or microgels for drug encapsulation and compartmentalization studies. Overall, the two-phase system designs with conjugated multimodal affinity peptides, having balanced physicochemical characteristics to preserve the accessibility for a target biomolecule, suggests various advantages in bioprocessing and biomedical applications.

Table 5-1. Hydrophobic and charge characteristics of peptides

Peptide use	Peptide sequence	Avg. molecular weight (g/mol)	Theoretical pI	Hydrophobicity	Attributes at pH 7
Spacer	GRCDGG	563.59	6.1	1.28	Hydrophilic and neutral charge
	GRCDGGWRW	1092.21	9.0	20.70	Hydrophobic and positive charge
This study	GRCDGGAAA	776.32	6.1	2.93	Hydrophobic and neutral charge
	GRCDGGGGG	734.75	6.1	1.37	Hydrophilic and neutral charge
	EEGEEG	648.58	3.0	1.16	Hydrophilic and negative charge
Adapted from [63]	KKGKG	644.81	11.0	0.86	Hydrophilic and positive charge
	YGSLPQ	663.73	5.9	12.30	Hydrophobic and negative charge
	VFVVFV	708.42	6.0	33.13	Hydrophobic and negative charge

The pI and hydrophobicity measures were determined using the peptide analyzer tool from ThermoFisher Scientific [66].

5.5 Conclusions

This study demonstrates the potential use of peptides as multimodal affinity ligands in the PEG-salt system for virus purification. The partitioning behavior of PPV significantly improved in the presence of the multimodal ligand GRCDGGWRW. The affinity ligand-induced biospecific affinity through hydrophobic interaction and charge to

drive the PPV particles to the PEG-rich phase at lower TLR generating lower PEG-rich phase volumes than the citrate-rich phases. The control hydrophobic peptide containing AAA residues with a neutral charge did not improve the virus partitioning, confirming that the multimodal effects of WRW were influential in the virus partitioning. The inclusion of affinity ligand did not seem to affect the salting-out ability but only the ability to extract the viral particles residing at the interface into the PEG-rich phase. This suggests that the multimodal ligand only changes the physicochemical environment of the PEG-rich phase.

The conjugation of peptides with PEG generally affects the bioactivity of the peptides by either increasing or decreasing the accessibility of the biologically active domain [67]. Through fluorescence quenching, we demonstrated that the accessibility of the WRW domain was retained upon the conjugation to PEG. This unique combination of ligand accessibility and high virus partitioning improve the downstream processing of the viral vaccines and biotherapeutics.

5.6 References

1. Ladd Effio, C., et al., *Downstream processing of virus-like particles: single-stage and multi-stage aqueous two-phase extraction*. J Chromatogr A, 2015. **1383**: p. 35-46.
2. Jacinto, M.J., et al., *Optimization and miniaturization of aqueous two phase systems for the purification of recombinant human immunodeficiency virus-like particles from a CHO cell supernatant*. Separation and Purification Technology, 2015. **154**: p. 27-35.
3. Vijayaragavan, K.S., et al., *Separation of porcine parvovirus from bovine serum albumin using PEG-salt aqueous two-phase system*. J Chromatogr B Analyt Technol Biomed Life Sci, 2014. **967**: p. 118-26.
4. Joshi, P.U., et al., *Tie line framework to optimize non-enveloped virus recovery in aqueous two-phase systems*. J Chromatogr B Analyt Technol Biomed Life Sci, 2019. **1126-1127**: p. 121744.

5. Asenjo, J.A. and B.A. Andrews, *Aqueous two-phase systems for protein separation: phase separation and applications*. J Chromatogr A, 2012. **1238**: p. 1-10.
6. Benavides, J., et al., *Rotavirus-like particles primary recovery from insect cells in aqueous two-phase systems*. J Chromatogr B Analyt Technol Biomed Life Sci, 2006. **842**(1): p. 48-57.
7. Albertsson, P.-A., *Partition of cell particles and macromolecules in polymer two phase systems*. Advances in protein chemistry, 1970. **24**: p. 309-341.
8. Yamada, M., et al., *Continuous cell partitioning using an aqueous two-phase flow system in microfluidic devices*. Biotechnol Bioeng, 2004. **88**(4): p. 489-94.
9. Gonzalez-Gonzalez, M., M. Rito-Palomares, and O. Mendez Quintero, *Partition behavior of CD133(+) stem cells from human umbilical cord blood in aqueous two-phase systems: In route to establish novel stem cell primary recovery strategies*. Biotechnol Prog, 2014. **30**(3): p. 700-7.
10. Azevedo, A.M., et al., *Partitioning of human antibodies in polyethylene glycol–sodium citrate aqueous two-phase systems*. Separation and Purification Technology, 2009. **65**(1): p. 14-21.
11. Rosa, P.A., A.M. Azevedo, and M.R. Aires-Barros, *Application of central composite design to the optimisation of aqueous two-phase extraction of human antibodies*. J Chromatogr A, 2007. **1141**(1): p. 50-60.
12. Schloer, G.M. and S.S. Breese Jr, *Purification of African malignant catarrhal fever virus using a two-phase aqueous polymer system*. Journal of General Virology, 1982. **59**(1): p. 101-110.
13. Philipson, L., P.Å. Albertsson, and G. Frick, *The purification and concentration of viruses by aqueous polymer phase systems*. Virology, 1960. **11**(3): p. 553-571.
14. González-Mora, A., et al., *Recovery and primary purification of bacteriophage M13 using aqueous two-phase systems*. Journal of Chemical Technology & Biotechnology, 2017. **92**(11): p. 2808-2816.
15. Gomes, G.A., et al., *Purification of plasmid DNA with aqueous two phase systems of PEG 600 and sodium citrate/ammonium sulfate*. Separation and Purification Technology, 2009. **65**(1): p. 22-30.
16. Johansson, H.O., et al., *Plasmid DNA partitioning and separation using poly(ethylene glycol)/poly(acrylate)/salt aqueous two-phase systems*. J Chromatogr A, 2012. **1233**: p. 30-5.

17. Grilo, A.L., M. Raquel Aires-Barros, and A.M. Azevedo, *Partitioning in Aqueous Two-Phase Systems: Fundamentals, Applications and Trends*. Separation & Purification Reviews, 2014. **45**(1): p. 68-80.
18. Albertsson, P.-Å., *Aqueous Biphasic Systems. Properties and Applications in Bioseparation*, in *Aqueous Biphasic Separations: Biomolecules to Metal Ions*, R.D. Rogers and M.A. Eiteman, Editors. 1995, Springer US: Boston, MA. p. 21-30.
19. Mi, X., et al., *Virus Isoelectric Point Determination Using Single-Particle Chemical Force Microscopy*. Langmuir, 2020. **36**(1): p. 370-378.
20. Umakoshi, H., R. Kuboi, and I. Komasa, *Control of partitioning of bacterial cells and characterization of their surface properties in aqueous two-phase systems*. Journal of fermentation and bioengineering, 1997. **84**(6): p. 572-578.
21. Jue, E., et al., *Using an aqueous two-phase polymer-salt system to rapidly concentrate viruses for improving the detection limit of the lateral-flow immunoassay*. Biotechnol Bioeng, 2014. **111**(12): p. 2499-507.
22. Mashayekhi, F., et al., *Enhancing the lateral-flow immunoassay for viral detection using an aqueous two-phase micellar system*. Anal Bioanal Chem, 2010. **398**(7-8): p. 2955-61.
23. Frampton, J.P., et al., *Aqueous two-phase system patterning of detection antibody solutions for cross-reaction-free multiplex ELISA*. Sci Rep, 2014. **4**: p. 4878.
24. Mytnyk, S., et al., *Compartmentalizing Supramolecular Hydrogels Using Aqueous Multi-phase Systems*. Angew Chem Int Ed Engl, 2017. **56**(47): p. 14923-14927.
25. Watanabe, T., I. Motohiro, and T. Ono, *Microfluidic Formation of Hydrogel Microcapsules with a Single Aqueous Core by Spontaneous Cross-Linking in Aqueous Two-Phase System Droplets*. Langmuir, 2019. **35**(6): p. 2358-2367.
26. Ho, K.L., et al., *Selection of high affinity ligands to hepatitis B core antigen from a phage-displayed cyclic peptide library*. J Med Virol, 2003. **69**(1): p. 27-32.
27. Trasatti, J.P., et al., *Rational design of peptide affinity ligands for the purification of therapeutic enzymes*. Biotechnol Prog, 2018. **34**(4): p. 987-998.
28. Perret, G. and E. Boschetti, *Aptamer affinity ligands in protein chromatography*. Biochimie, 2018. **145**: p. 98-112.
29. Percze, K., et al., *Aptamers for respiratory syncytial virus detection*. Sci Rep, 2017. **7**: p. 42794.

30. Reyes-del Valle, J. and R.M. del Angel, *Isolation of putative dengue virus receptor molecules by affinity chromatography using a recombinant E protein ligand*. J Virol Methods, 2004. **116**(1): p. 95-102.
31. Mejía-Manzano, L.A., et al., *Optimized purification of mono-PEGylated lysozyme by heparin affinity chromatography using response surface methodology*. Journal of Chemical Technology & Biotechnology, 2017. **92**(10): p. 2554-2562.
32. Kruljec, N. and T. Bratkovic, *Alternative Affinity Ligands for Immunoglobulins*. Bioconjug Chem, 2017. **28**(8): p. 2009-2030.
33. Fassina, G., et al., *Protein a mimetic peptide ligand for affinity purification of antibodies*. Journal of Molecular Recognition, 1996. **9**(5-6): p. 564-569.
34. Zou, X., et al., *Development of a hybrid biomimetic ligand with high selectivity and mild elution for antibody purification*. Chemical Engineering Journal, 2019. **368**: p. 678-686.
35. Fang, Y.M., D.Q. Lin, and S.J. Yao, *Review on biomimetic affinity chromatography with short peptide ligands and its application to protein purification*. J Chromatogr A, 2018. **1571**: p. 1-15.
36. Opitz, L., et al., *Lectin-affinity chromatography for downstream processing of MDCK cell culture derived human influenza A viruses*. Vaccine, 2007. **25**(5): p. 939-47.
37. Brgles, M., et al., *Nonspecific native elution of proteins and mumps virus in immunoaffinity chromatography*. Journal of Chromatography A, 2016. **1447**: p. 107-114.
38. Elkana, Y., A. Thornton, and A.J. Zuckerman, *Purification of hepatitis A virus by affinity chromatography*. Journal of immunological methods, 1979. **25**(2): p. 185-187.
39. Olofsson, S., S. Jeansson, and E. Lycke, *Unusual lectin-binding properties of a herpes simplex virus type 1-specific glycoprotein*. Journal of virology, 1981. **38**(2): p. 564-570.
40. Opitz, L., et al., *Purification of cell culture-derived influenza virus A/Puerto Rico/8/34 by membrane-based immobilized metal affinity chromatography*. J Virol Methods, 2009. **161**(2): p. 312-6.
41. Jiang, C., et al., *Immobilized cobalt affinity chromatography provides a novel, efficient method for herpes simplex virus type 1 gene vector purification*. J Virol, 2004. **78**(17): p. 8994-9006.

42. del Cañizo, A.A.N., et al., *Foot and mouth disease virus concentration and purification by affinity chromatography*. Applied biochemistry and biotechnology, 1997. **61**(3): p. 399-409.
43. Du, P., et al., *Purification of foot-and-mouth disease virus by heparin as ligand for certain strains*. J Chromatogr B Analyt Technol Biomed Life Sci, 2017. **1049-1050**: p. 16-23.
44. Nestola, P., et al., *Improved virus purification processes for vaccines and gene therapy*. Biotechnol Bioeng, 2015. **112**(5): p. 843-57.
45. Kallberg, K., H.O. Johansson, and L. Bulow, *Multimodal chromatography: an efficient tool in downstream processing of proteins*. Biotechnology journal, 2012. **7**(12): p. 1485-1495.
46. Zheng, G., et al., *Selection of affinity peptides for the purification potential of porcine circovirus type 2 (PCV2) Cap virus-like particles (VLPs)*. RSC Advances, 2017. **7**(62): p. 38911-38914.
47. Fernandes, C.S., et al., *Retroviral particles are effectively purified on an affinity matrix containing peptides selected by phage-display*. Biotechnol J, 2016. **11**(12): p. 1513-1524.
48. Menegatti, S., A.D. Naik, and R.G. Carbonell, *The hidden potential of small synthetic molecules and peptides as affinity ligands for bioseparations*. Pharmaceutical Bioprocessing, 2013. **1**(5): p. 467-485.
49. Heldt, C.L., et al., *Porcine parvovirus removal using trimer and biased hexamer peptides*. Biotechnol J, 2012. **7**(4): p. 558-65.
50. Ruiz-Ruiz, F., et al., *Aqueous two-phase affinity partitioning systems: current applications and trends*. J Chromatogr A, 2012. **1244**: p. 1-13.
51. Veronese, F.M., *Peptide and protein PEGylation: a review of problems and solutions*. Biomaterials, 2001. **22**(5): p. 405-417.
52. Guiotto, A., et al., *PEGylation of the antimicrobial peptide nisin A: problems and perspectives*. Il Farmaco, 2003. **58**(1): p. 45-50.
53. Castelletto, V., et al., *Self-assembly and bioactivity of a polymer/peptide conjugate containing the RGD cell adhesion motif and PEG*. European Polymer Journal, 2013. **49**(10): p. 2961-2967.
54. Chiu, K., et al., *Effects of Polymer Molecular Weight on the Size, Activity, and Stability of PEG-Functionalized Trypsin*. Biomacromolecules, 2010. **11**(12): p. 3688-3692.

55. Heldt, C.L., et al., *Identification of Trimeric Peptides That Bind Porcine Parvovirus from Mixtures*. Biotechnology Progress, 2008. **24**(3): p. 554-560.
56. Heldt, C.L., et al., *A colorimetric assay for viral agents that produce cytopathic effects*. J Virol Methods, 2006. **135**(1): p. 56-65.
57. Lakowicz, J.R., et al., *Measurement of subnanosecond anisotropy decays of protein fluorescence using frequency-domain fluorometry*. Journal of Biological Chemistry, 1986. **261**(5): p. 2240-2245.
58. Simpson, A.A., et al., *The structure of porcine parvovirus: comparison with related viruses*. J Mol Biol, 2002. **315**(5): p. 1189-98.
59. Zustiak, S.P., R. Durbal, and J.B. Leach, *Influence of cell-adhesive peptide ligands on poly(ethylene glycol) hydrogel physical, mechanical and transport properties*. Acta Biomater, 2010. **6**(9): p. 3404-14.
60. Pereira, J.F.B., M.G. Freire, and J.A.P. Coutinho, *Aqueous two-phase systems: Towards novel and more disruptive applications*. Fluid Phase Equilibria, 2020. **505**.
61. Ma, Q., et al., *Affinity Partitioning-Induced Self-Assembly in Aqueous Two-Phase Systems: Templating for Polyelectrolyte Microcapsules*. ACS Macro Letters, 2016. **5**(6): p. 666-670.
62. Lin, C.C. and K.S. Anseth, *Controlling Affinity Binding with Peptide-Functionalized Poly(ethylene glycol) Hydrogels*. Adv Funct Mater, 2009. **19**(14): p. 2325.
63. Xue, Y., et al., *Effect of poly(ethylene glycol) (PEG) spacers on the conformational properties of small peptides: a molecular dynamics study*. Langmuir, 2011. **27**(1): p. 296-303.
64. Hamed, E., T. Xu, and S. Keten, *Poly(ethylene glycol) conjugation stabilizes the secondary structure of alpha-helices by reducing peptide solvent accessible surface area*. Biomacromolecules, 2013. **14**(11): p. 4053-60.
65. Thi Nguyen, N.T., et al., *Shielding effect of a PEG molecule of a mono-PEGylated peptide varies with PEG chain length*. Prep Biochem Biotechnol, 2018. **48**(6): p. 522-527.
66. Mishra, R., D. Sjolander, and P. Hammarstrom, *Spectroscopic characterization of diverse amyloid fibrils in vitro by the fluorescent dye Nile red*. Molecular Biosystems, 2011. **7**(4): p. 1232-1240.

67. Veronese, F.M. and A. Mero, *The impact of PEGylation on biological therapies*. *BioDrugs*, 2008. **22**(5): p. 315-329.

6 Conclusions and future work

6.1 Conclusions

Aqueous two-phase systems (ATPS) have emerged as potential alternatives for the purification of biomolecules that is easy-to-scale-up and can be run continuously. A few studies performed on the separation of viruses using ATPS have shown discrepancies in the proposed partitioning mechanism. Some argue that the main driving force is volume exclusion [1-3], while others interpret the mechanism to be a mixture of intermolecular interactions based on hydrophobicity and electrostatics [4]. The lack of understanding of the viral behavior and interactions with the phases have led to a large experimental design to optimize the virus purification. The tie-line framework (chapter 3) presented in this dissertation supported the intermolecular interaction theory. The combination of high PEG-rich phase hydrophobicity combined with the salting-out ability of the salt-rich phase could achieve the high virus recoveries. However, the tie line framework demonstrated the desired virus recovery in the higher system compositions that are not optimal for processing. The motivation to reduce the system concentrations led to the use of osmolytes in the systems (chapter 4). The osmolytes enhanced the driving forces to achieve higher virus recoveries at lower system compositions. Along with the osmolytes, multimodal peptides were explored as the alternatives to improve the specificity and affinity of the PEG-rich phase to viruses (chapter 5). The affinity peptide demonstrated the potential to recover viruses at lower system compositions having lower PEG-rich phase volumes.

The optimization of virus recoveries was performed in the PEG 12kDa-citrate system using a tie-line framework. Non-enveloped porcine parvovirus (PPV) and human rhinovirus 14 (HRV) were used as model viruses. The framework comprising of three tie-line lengths (TLL) and tie-line ratios (TLR) were used to study the viral partitioning behavior. The negatively charged PPV (pI ~5) at pH 7 demonstrated that the virus partitioning shifts from the citrate-rich phase to the PEG-rich phase with an increasing TLL. The PPV partitioning at the highest TLL demonstrated similar virus titers in the PEG-rich phase irrespective of the TLR leading to lower recoveries in the PEG-rich phase with the increasing TLR. Overall, 80% PPV recovery and high purity were

achieved at the lower TLR. An increased PPV load demonstrated a similar pattern of virus partitioning along the TLL and across TLR. However, a lower recovery of ~40% was achieved in the system that yielded a high recovery with a lower load. The PPV partitioning behavior strongly supported the intermolecular interactions (hydrophobicity and charge) to be the dominant forces in the virus partitioning. The neutrally charged HRV (pI~6.9-7) in the systems operated at pH 7 demonstrated a high recovery in the citrate-rich phase leading to a low recovery in the PEG-rich phase at all the TLL. Overall, 36% HRV recovery was achieved in the PEG-rich phase in the system that yielded a high PPV recovery. The HRV behavior suggested inefficiency of the citrate-rich phase in salting-out and inducing hydrophobic interaction with the PEG-rich phase for viruses with a net neutral charge. Overall, the framework aids in the high-throughput optimization of virus recovery.

Naturally occurring osmolytes were used as the additives in the PEG 12kDa-citrate systems to enhance the driving forces for virus partitioning. The objective was to improve the virus recovery at higher virus loadings, and system compositions that yield lower PEG-rich phase compositions and volume. PPV and human immunodeficiency virus-group specific antigen virus-like particles (HIV-gag-VLP) were used as the model viruses. Different osmolytes, glycine, betaine, TMAO, mannitol, and urea were added to the system components. The effect of each osmolyte on the system characteristics was analyzed by the changes in the phase diagrams comprising of the binodal curve and tie lines. The effect of osmolytes on the binodal shift away from the control system was observed in the order of glycine > betaine > mannitol > TMAO > urea. A similar effect on the virus partitioning was observed. The highest recoveries of PPV and HIV-gag-VLP were observed in the systems-containing glycine and betaine. ~ 100% PPV and 80% HIV-gag-VLP recoveries were obtained in the PEG-rich phase with glycine and betaine containing-systems. The high recoveries were obtained in the lower system compositions that yield a lower PEG-rich phase composition and viscosity. The contaminant partitioning was unaffected upon the addition of osmolytes. Overall, the use of osmolytes

not only enhances the virus recovery but also will reduce the processing challenges in scaled-up manufacturing.

The affinity of the PEG-rich phase towards viruses was enhanced using a multimodal peptide ligand. The goal was to improve virus recovery in the PEG-rich phase of the systems at lower volume ratios of the PEG-rich phase to citrate-rich phase. Systems were chosen that would have virus partition to the interface or citrate-rich phase when the affinity peptide was not present. The multimodal affinity peptide WRW was used in conjugation with PEG 10kDa to drive PPV to the PEG-rich phase. A 30% replacement of the unfunctionalized PEG with PEG-WRW showed a significant increase in the PPV recovery in the PEG-rich phase at higher TLR. The control hydrophobic trimer AAA did not show improvement in the PPV partitioning; instead, it decreased the partitioning. The multimodal nature of WRW displaying hydrophobic and positive charge characteristics was regarded as the driving force to capture hydrophobic and negatively charged viral particles in the PEG-rich phase. Moreover, the citrate-rich phase being the continuous phase at the higher TLR provides an ATPS that is easier to process as the system viscosity decreases as compared to the lower TLR with continuous PEG-rich phase. The PEG-conjugate structure analyzed by acrylamide quenching demonstrated the accessibility of WRW, supporting the enhanced specificity of the PEG-rich phase towards PPV. Overall, this was the first study reported in the ATPS literature to utilize affinity peptides to enhance virus partitioning.

The framework demonstrated in this dissertation allows for the rapid optimization of viral product purification. The reduced experimental framework will aid in faster process development of vaccines and viral biotherapeutic. Moreover, the high-throughput recovery of ATPS will help in producing higher number of vaccine doses required for global outreach. The rationale of selecting the phase parameters and the use of specific enhancers will help platform the ATPS as the unit operation for viral processing in the near future.

6.2 Future work

6.2.1 Viral behavior at interface and mathematical model validation

The partitioning of viruses to the PEG-rich phase from the citrate-rich phase depends on the viral ability to crossover the interface. Very few studies have been reported characterizing the biomolecule behavior at the interface [5, 6]. The transition of biomolecules from the interface to the PEG-rich phase has been shown to be related to the surface energy of the biomolecules [6]. The surface energy of the viral particles can be determined through a single particle measurement technique using atomic force spectroscopy (AFM) [7]. The AFM setup could include a two-phase droplet system, and the force measured to pull or push the virus through the interface could be translated to the free energy transfer of viral particle across the interface.

A bulk method using a microfluidic device can be used to determine the diffusion coefficient of viral particles across the interface [8]. Relating the equilibrium phase properties such as viscosity, electrochemical potential difference, and interfacial tension with the diffusion coefficient will yield a better understanding of the local effects of the interface as compared to the bulk phases. Moreover, previous studies have proposed empirical models to predict protein and peptide partitioning by relating biomolecule surface properties and phase properties [9-11]. The ability to measure single particle and bulk surface characteristics of viruses could be potentially used to validate the models for prediction of the partitioning.

6.2.2 Expanding the viral database

The current work showed a proof-of-concept for the optimization of viral recovery in the PEG-salt system. A database of model viruses with different viral surface characteristics and their partitioning behavior needs to be studied. The enveloped viruses are comparatively more prone to aggregation and inactivation than non-enveloped viruses due to high ionic strength of citrate-rich phase and osmotic pressure of the PEG-rich phase. Different enveloped viruses such as herpes simplex virus (HSV), bovine viral

diarrhea virus (BVDV), and influenza B virus need to be evaluated for the deviation in the partitioning behavior and stability to design appropriate systems. Novel ATPS needs to be developed with lower phase compositions and higher driving forces, as shown with the osmolyte addition (chapter 4). The diversity in viral surfaces has been characterized based on morphology [12], hydrophobicity [13], and charge [14]. The relation between viral surface and phase characteristics will help generate a hierarchical model that will help in generalizing the systems for a group of virus models. Neither a single combination of the system parameter nor the extensive variation in the optimized systems is the solutions for platforming ATPS in biotherapeutic manufacturing. The database generated might be used to predict and narrow the search for the virus recovery optimization.

6.2.3 Back-extraction of viral product

The inclusion of ATPS in the DSP train would require a follow-up back extraction stage to separate viral products from the PEG-rich phase. Various methods to extract viral particles from the PEG-rich phase needs to be evaluated for their applicability in the high-throughput production and continuous operation strategy. Some of the methods considered for this process are ultrafiltration, ATPS re-extraction, and steric exclusion chromatography. Ultrafiltration with a membrane pore size ranging from 50 kDa to 500 kDa MWCO needs to be evaluated to retain the viral product and allowing PEG chains in the permeate. The tie-line framework showed that the viral particles partition to the citrate-rich phase at lower TLL (chapter 3). This information can be used to develop a system by mixing a fresh citrate stock with the virus-containing PEG-rich phase to shift from the high TLL to low TLL, which will promote virus partition to the citrate-rich phase. A novel chromatography method using the steric exclusion principle can be used by loading the column at high PEG concentration (PEG-rich phase) and eluting at low PEG concentration [15].

6.2.4 Scale-up and sustainability analysis of ATPS

The implementation of ATPS at an industrial scale needs extensive expertise in the hydrodynamic behavior of the phases [16], and their effects on viral partitioning. We are currently exploring the challenges of the ATPS scale-up and its implementation of the continuous operation for viral processing. The shear effects of mixing hydrodynamics on viral stability need to be evaluated. The viral partitioning effects on the phase separation kinetics need to be assessed.

There is a green manufacturing initiative call for the biomanufacturing industry to prevent environmental risk posed by a high process mass intensity (PMI) [17]. PMI is the mass ratio of consumables to active pharmaceutical ingredient. A previous study has shown that increasing the number of chromatography steps increases the PMI, mainly due to the high consumption of water. PMI needs to be assessed for the proposed DSP train with the inclusion of ATPS and back extraction. The relative intensity index could be assessed by comparing an industry-standard DSP train with the optimized ATPS-included DSP train on a case-by-case basis. The evaluation will guide the industrial implementation of ATPS in the viral vaccine and biotherapeutic manufacturing.

6.3 Dissertation Summary

The work presented in this dissertation helped gain crucial insights into the viral partitioning behavior in the PEG-salt ATPS. The framework to narrow down the experimental space for optimization, and enhancers to aid in the higher throughput of viral particles suggested a promising future of ATPS to improve viral based vaccines and biotherapeutic manufacturing. However, additional knowledge is still needed before commercial implementation. Partitioning behavior of an extensive virus library, interaction of viruses with the phase components at molecular level, and hydrodynamic behavior of phases at large scales are some of the missing pieces to the puzzle. The

deeper understanding of these pieces would elevate the confidence in implementing the ATPS in the industrial processes.

6.4 References

1. Benavides, J., et al., *Rotavirus-like particles primary recovery from insect cells in aqueous two-phase systems*. J Chromatogr B Analyt Technol Biomed Life Sci, 2006. **842**(1): p. 48-57.
2. Luechau, F., T.C. Ling, and A. Lyddiatt, *Recovery of B19 virus-like particles by aqueous two-phase systems*. Food and Bioproducts Processing, 2011. **89**(4): p. 322-327.
3. González-Mora, A., et al., *Recovery and primary purification of bacteriophage M13 using aqueous two-phase systems*. Journal of Chemical Technology & Biotechnology, 2017. **92**(11): p. 2808-2816.
4. Vijayaragavan, K.S., et al., *Separation of porcine parvovirus from bovine serum albumin using PEG-salt aqueous two-phase system*. J Chromatogr B Analyt Technol Biomed Life Sci, 2014. **967**: p. 118-26.
5. Zaslavsky, B.Y., L.A. Ferreira, and V.N. Uversky, *Driving Forces of Liquid-Liquid Phase Separation in Biological Systems*. Biomolecules, 2019. **9**(9).
6. Atefi, E., et al., *Interfacial Tension Effect on Cell Partition in Aqueous Two-Phase Systems*. ACS Appl Mater Interfaces, 2015. **7**(38): p. 21305-14.
7. Drelich, J., G.W. Tormoen, and E.R. Beach, *Determination of solid surface tension from particle-substrate pull-off forces measured with the atomic force microscope*. J Colloid Interface Sci, 2004. **280**(2): p. 484-97.
8. Münchow, G., et al., *Protein Diffusion Across the Interface in Aqueous Two-Phase Systems*. Langmuir, 2008. **24**(16): p. 8547-8553.
9. de Barros, D.P., et al., *Predicting protein partition coefficients in aqueous two phase system*. J Chromatogr A, 2016. **1470**: p. 50-58.
10. Eiteman, M.A., C. Hassinen, and A. Veide, *A mathematical model to predict the partitioning of peptides and peptide-modified proteins in aqueous two-phase systems*. Biotechnology progress, 1994. **10**(5): p. 513-519.

11. Johansson, H.-O., et al., *Driving forces for phase separation and partitioning in aqueous two-phase systems*. Journal of Chromatography B: Biomedical Sciences and Applications, 1998. **711**(1-2): p. 3-17.
12. Norrby, E., *The morphology of virus particles. Classification of viruses*. Textbook of Medical Virology, 1983: p. 4-16.
13. Johnson, S.A., et al., *The step-wise framework to design a chromatography-based hydrophobicity assay for viral particles*. J Chromatogr B Analyt Technol Biomed Life Sci, 2017. **1061-1062**: p. 430-437.
14. Michen, B. and T. Graule, *Isoelectric points of viruses*. J Appl Microbiol, 2010. **109**(2): p. 388-97.
15. Marichal-Gallardo, P., et al., *Steric exclusion chromatography for purification of cell culture-derived influenza A virus using regenerated cellulose membranes and polyethylene glycol*. Journal of Chromatography A, 2017. **1483**: p. 110-119.
16. Nestola, P., et al., *Improved virus purification processes for vaccines and gene therapy*. Biotechnol Bioeng, 2015. **112**(5): p. 843-57.
17. Budzinski, K.L., et al., *A call for industry to embrace green biopharma*. Nat Biotechnol, 2016. **34**(3): p. 234-5.

A Supplementary information

A.1 Tie-line framework for virus optimization

Table A.1-1. Physical Properties (density and refractive index) of the systems at TLL 15, 25, and 36 w/w%

TLL (w/w%)	TL Ratio	PEG-rich phase density (g/mL)		Citrate-rich phase density (g/mL)		Refractive index	
		Average	Std Dev	Average	Std Dev	Average	Std Dev
15	0.3	1.0675	0.0080	1.0889	0.0142	1.3690	0.0030
	1.2	1.0627	0.0051	1.0895	0.0040	1.3709	0.0029
	2.3	1.0667	0.0125	1.0939	0.0092	1.3731	0.0008
25	0.3	1.0685	0.0044	1.1071	0.0056	1.3755	0.0017
	1.2	1.0630	0.0131	1.1115	0.0033	1.3799	0.0020
	2.3	1.0741	0.0055	1.1248	0.0120	1.3828	0.0012
36	0.1	1.0646	0.0099	1.1456	0.0140	1.3902	0.0058
	0.3	1.0671	0.0066	1.1413	0.0129	1.3897	0.0048
	0.6	1.0755	0.0091	1.1507	0.0096	1.3879	0.0049
	1.2	1.0700	0.0182	1.1459	0.0148	1.3889	0.0034
	2.3	1.0513	0.0361	1.1366	0.0114	1.3886	0.0024

Experiments were conducted in triplicate and the standard deviations were calculated for those three trials

Table A.1-2. PEG concentration in the PEG-rich phase at different TLL using refractive index

TLL (w/w%)	Refractive Index (RI)		PEG concentration (w/w%)
	Average	Std Dev	
36	1.3891	0.0009	36
25	1.3784	0.0037	30
15	1.3710	0.0020	26

PEG concentrations in the PEG-rich phase were calculated from known PEG concentrations found in **Table S3**. Experiments were conducted in triplicate and the standard deviations were calculated for those three trials.

Table A.1-3. Standard Refractive Index of increasing concentration of PEG

PEG Conc. (w/w%)	Refractive Index (RI)		Density (g/mL)		Citrate Conc. (w/w%)	Density (g/mL)	
	Average	Std Dev	Average	Std Dev		Average	Std Dev
0	1.3330	0.0017	0.9933	0.0036			
5	1.3386	0.0055	1.0144	0.0088	5	1.0255	0.0014
10	1.3456	0.0009	1.0189	0.0104	10	1.0417	0.0151
15	1.3517	0.0012	1.0166	0.0120	15	1.0876	0.0169
20	1.3585	0.0028	1.0398	0.0155	20	1.1132	0.0077
25	1.3662	0.0023	1.0152	0.0113	25	1.1467	0.0010
30	1.3735	0.0028	1.0410	0.0142	30	1.1817	0.0043
50	1.4159	0.0006	1.0785	0.0136			

Experiments were conducted in triplicate and the standard deviations were calculated for those three trials

Table A.1-4. HRV titer in the PEG-rich phase and citrate-rich phase as a function of TLL and TL ratio

Initial Titer		$6.7 \pm 0.4 \log_{10} \text{MTT}_{50}/\text{mL}$	
TLL (w/w%)	TL ratio	PEG-rich phase titer	Citrate-rich phase titer
15	0.3	3.4 ± 0.4	6.4 ± 0.4
	1.2	3.3 ± 0.5	6.4 ± 0.4
	2.3	3.7 ± 0.9	6.2 ± 0.3
25	0.1	4.4 ± 0.5	6.2 ± 0.0
	1.2	4.9 ± 0.8	6.2 ± 0.2
	2.3	5.2 ± 1.3	6.0 ± 0.4
36	0.3	5.4 ± 0.4	5.8 ± 0.5
	1.2	5.3 ± 0.6	5.8 ± 0.3
	2.3	5.1 ± 0.6	5.7 ± 0.2

Data is the average of experiments performed in triplicates and the error represents the standard deviation

Table A.1-5. PPV titer in the PEG-rich phase and citrate-rich phase as a function of TLL and TL ratio

TLL (w/w%)	Initial Titters TL ratio	PEG-rich phase titer		Citrate-rich phase titer	
		6.4 ± 0.2	8.3 ± 0.2	6.4 ± 0.2	8.3 ± 0.2
15	0.3	3.1 ± 0.9	4.8 ± 0.4	5.7 ± 0.4	7.7 ± 0.3
	1	3.7 ± 1.1	5.1 ± 0.3	5.4 ± 0.1	7.4 ± 0.2
	2.3	4.4 ± 0.4	6.1 ± 0.9	5.1 ± 0.3	7.2 ± 0.1
25	0.1	4.1 ± 0.8	5.2 ± 0.3	5.3 ± 1.0	6.5 ± 0.3
	1	5.2 ± 0.6	6.7 ± 0.3	3.9 ± 1.0	5.4 ± 0.9
	2.3	5.9 ± 0.1	7.4 ± 0.6	3.4 ± 0.8	5.9 ± 0.8
36	0.3	5.2 ± 0.2	7.1 ± 0.7	*2.8 ± 0.1	5.7 ± 0.2
	1.2	5.2 ± 0.3	7.0 ± 0.5	*2.7 ± 0.0	5.9 ± 0.3
	2.3	5.3 ± 0.2	7.5 ± 0.1	*2.6 ± 0.1	4.8 ± 0.6

*limit of detection. All the titers are expressed $\log_{10}(\text{MTT}_{50}/\text{mL})$

Data is the average of experiments performed in triplicates and the error represents the standard deviation

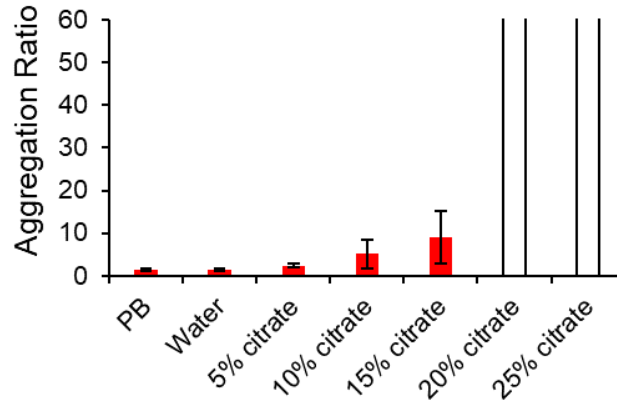


Figure A.1-1. Aggregate ratio of 8 \log_{10} MTT₅₀/ml PPV at varying citrate concentration. Aggregate ratio compares the intensity of the PPV peak to the intensity of the aggregate peak in DLS and can be found in Eq. 3-7. The open bars represent the lack of a PPV peak. Experiments were conducted in triplicate and the error bars represent the standard deviation.

A.2 Osmolyte-containing aqueous two-phase systems

Table A.2-1. Description of the LC-MS method development parameters for osmolyte detection and quantification. Corresponding stable isotopes of each osmolyte was used as the internal standard.

Osmolyte Internal standard	LC Gradient	MS polarity	Quantification Ion
Glycine	85/15 to 50/50 A/B in 6 min at 0.4 mL/min	positive	SIM of m/z 76
Glycine-C13		positive	SIM of m/z 77
Betaine	85/15 to 50/50 A/B in 6 min at 0.4 mL/min	positive	SRM of m/z 118 --> 59
Betaine-D11		positive	SRM of m/z 129 --> 68
TMAO	85/15 to 50/50 A/B in 6 min at 0.6 mL/min	positive	SRM of m/z 76 --> 59
TMAO-D9		positive	SRM of m/z 85 --> 68
Mannitol	85/15 to 60/40 A/B in 4 min at 0.4 mL/min	negative	SRM of m/z 181 --> 101
Mannitol-U-13C6		negative	SRM of m/z 187 --> 105
Urea	85/15 to 70/30 A/B in 5 min at 0.2 mL/min	positive	SIM of m/z 61
Urea-C13-2N15		positive	SIM of m/z 64

SIM: selected ion monitoring; SRM: selected reaction monitoring

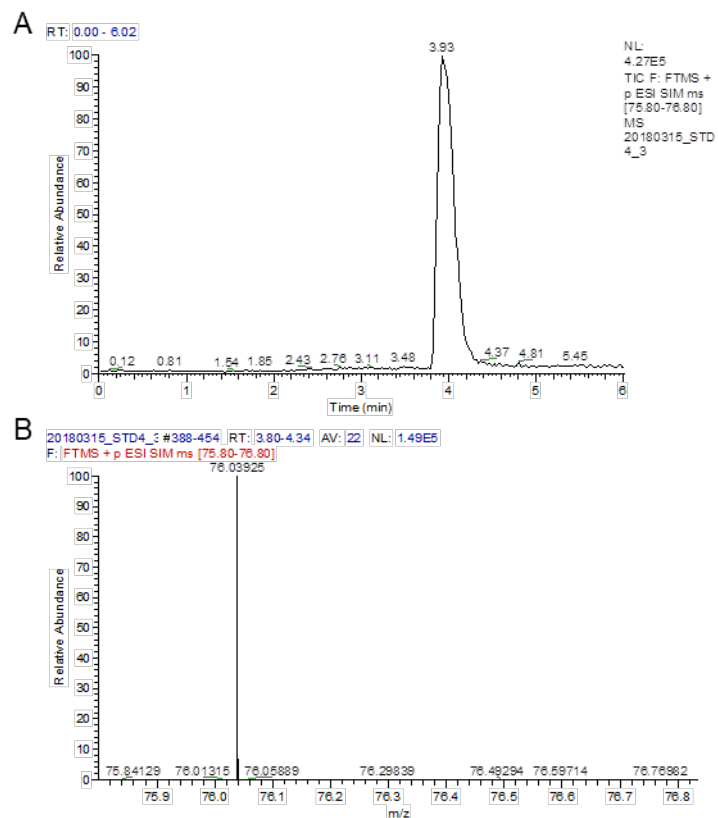


Figure A.2-1. LC-MS profile of glycine. (A) The area under the elution curve of showing(A) was used in relation to the elution area of glycine-C13 internal standard (Figure A.2-2) to form a standard curve and (B) MS peak used to detect glycine, operated with conditions shown in table A.2-1.

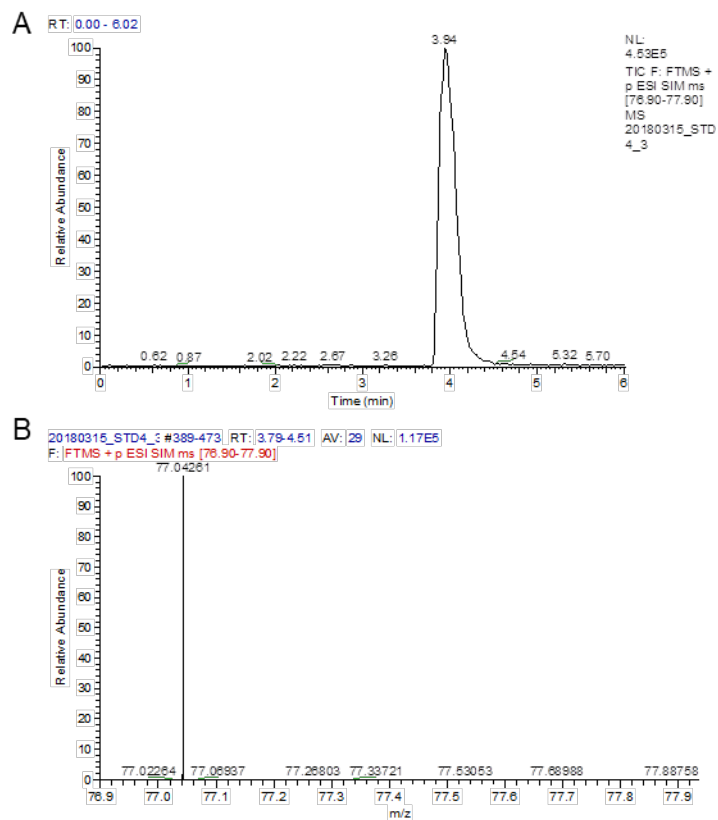


Figure A.2-2. LC-MS profile of glycine-C13, used as the internal standard for glycine. (A) The area under the elution curve of glycine-C13 was used in relation to the elution area of glycine (Figure A.2-1) to form a standard curve and (B) MS peak used to detect glycine C-13, operated with conditions shown in table A.2-1.

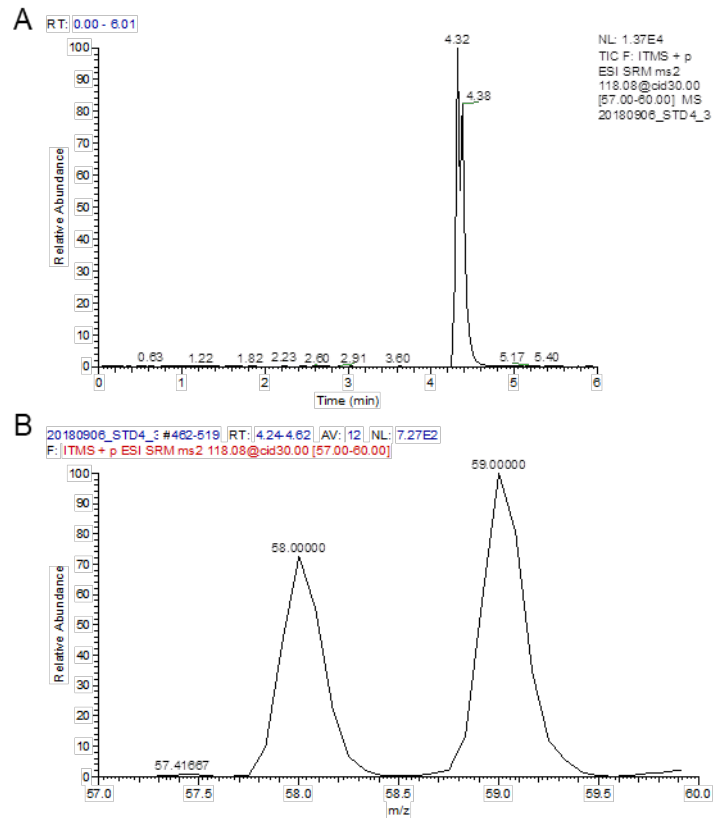


Figure A.2-3. LC-MS profile of betaine. (A) The area under the elution curve of betaine was used in relation to the elution area of betaine-D11 (Figure A.2-4) to form a standard curve and (B) MS peak used to detect betaine, operated with conditions shown in table A.2-1.

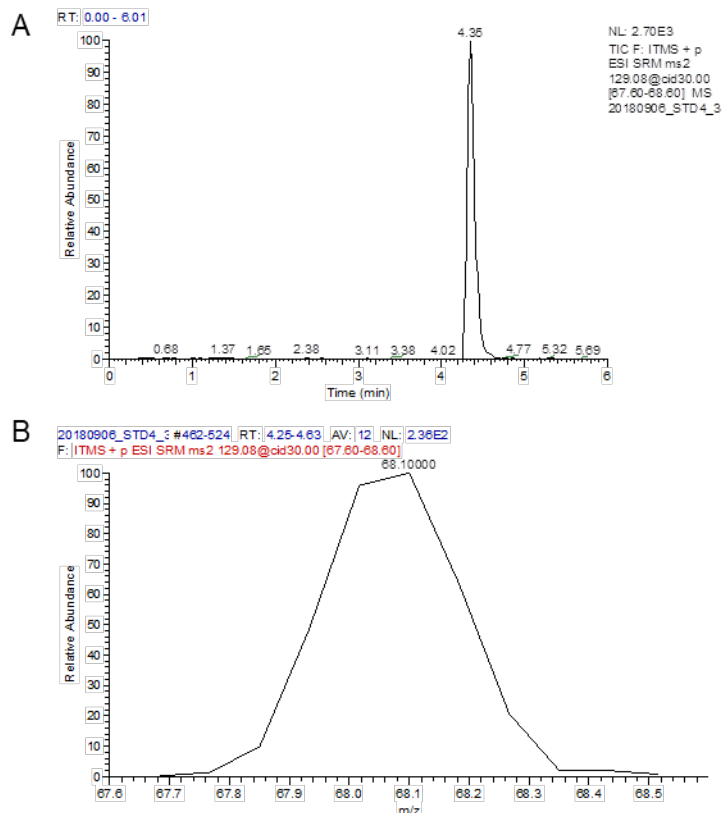


Figure A.2-4. LC-MS profile of betaine-D11 used as the internal standard for betaine. (A) The area under the elution curve of betaine-D11 was used in relation to the elution area of betaine (Figure A.2-3) to form a standard curve and (B) MS peak used to detect betaine-D11, operated with conditions shown in table A.2-1.

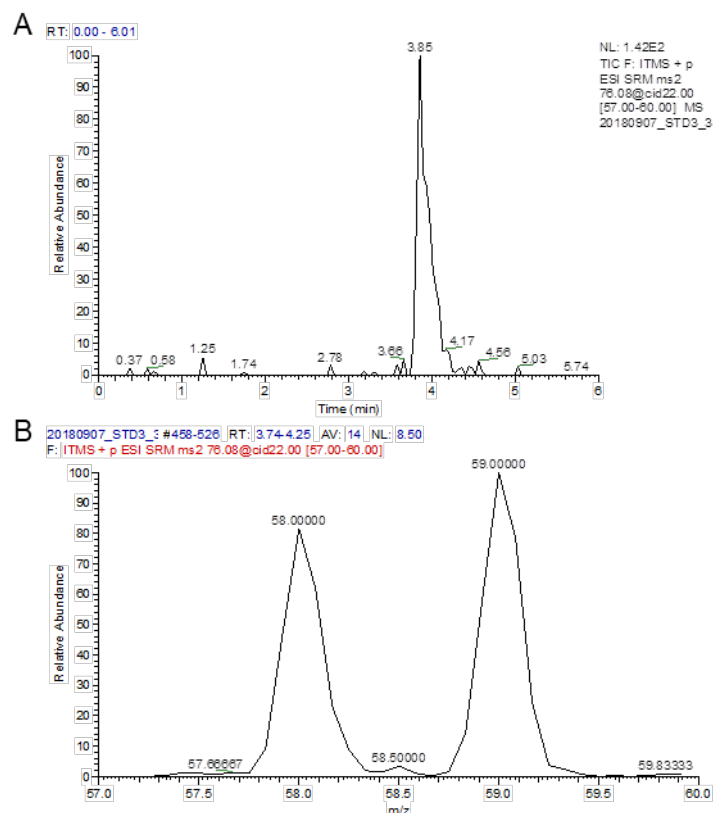


Figure A.2-5. LC-MS profile of TMAO. (A) Area under the elution curve of TMAO was used in relation to the elution area of TMAO-D9 (Figure A.2-6) to form a standard curve and (B) MS peak used to detect TMAO, operated with conditions shown in table A.2-1.

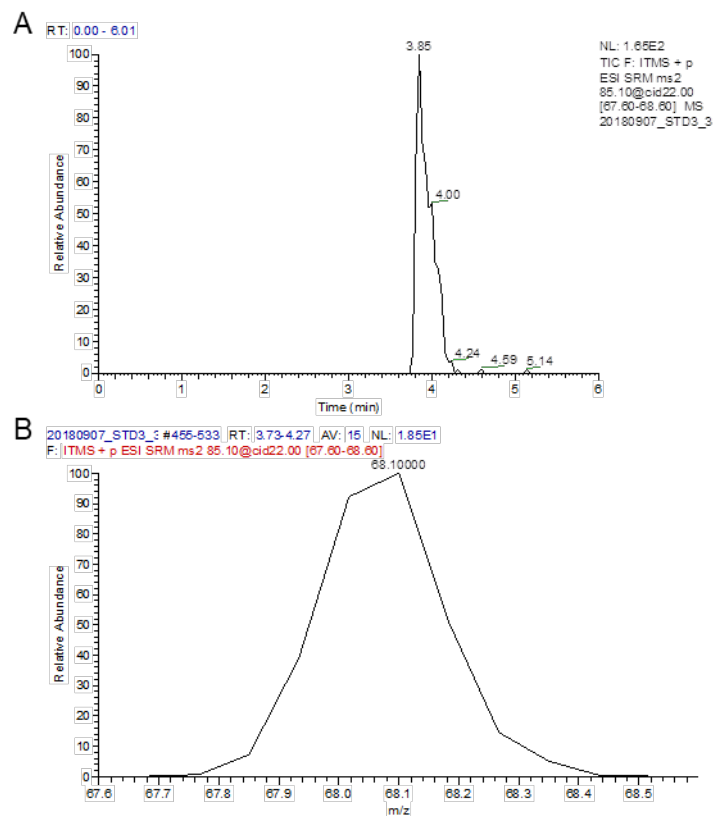


Figure A.2-6. LC-MS profile of TMAO-D9 used as internal standard for TMAO. (A) Area under the elution curve of TMAO -D9 was used in relation to the elution area of TMAO (Figure A.2-5) to form a standard curve and (B) MS peak used to detect TMAO-D9, operated with conditions shown in table A.2-1.

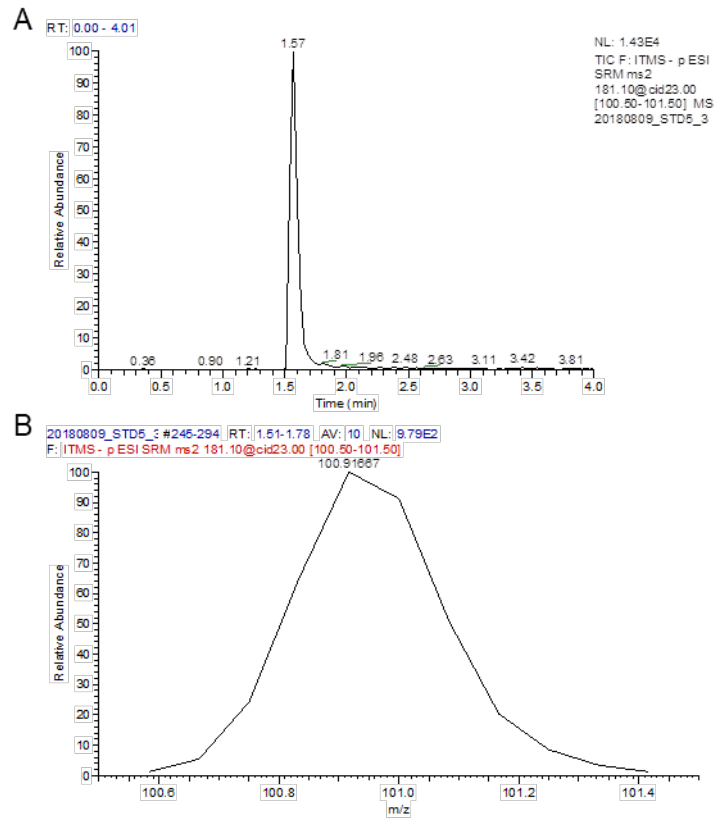


Figure A.2-7. LC-MS profile of mannitol. (A) Area under the elution curve of mannitol was used in relation to the elution area of mannitol-U-13C6 (Figure A.2-8) to form a standard curve and (B) MS peak used to detect mannitol, operated with conditions shown in table A.2-1.

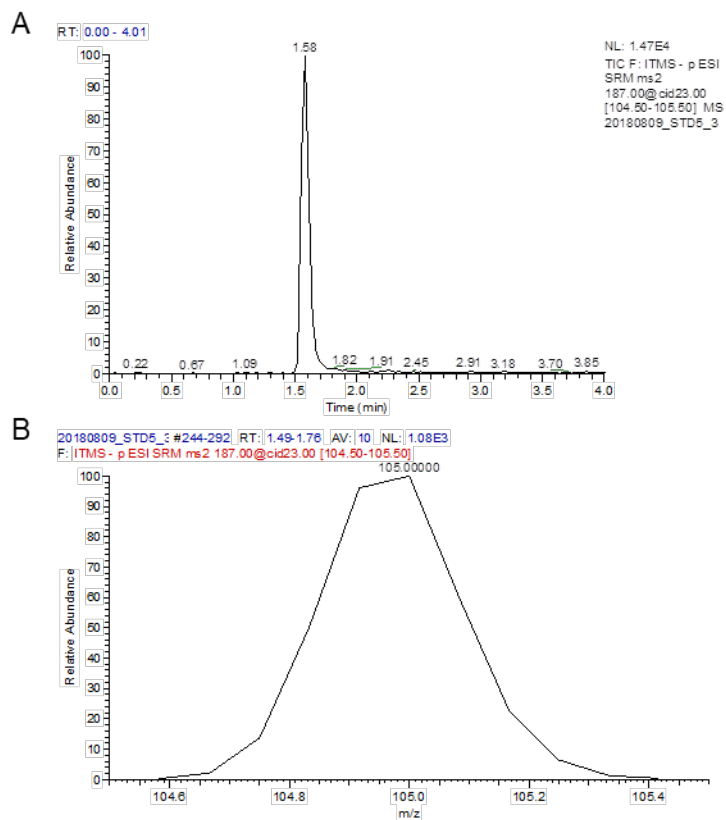


Figure A.2-8. LC-MS profile of mannitol-U-13C6, used as the internal standard for mannitol. (A) Area under the elution curve of mannitol-U-13C6 was used in relation to the elution area of mannitol (Figure A.2-7) to form a standard curve and (B) MS peak used to detect mannitol-U-13C6, operated with conditions shown in table A.2-1.

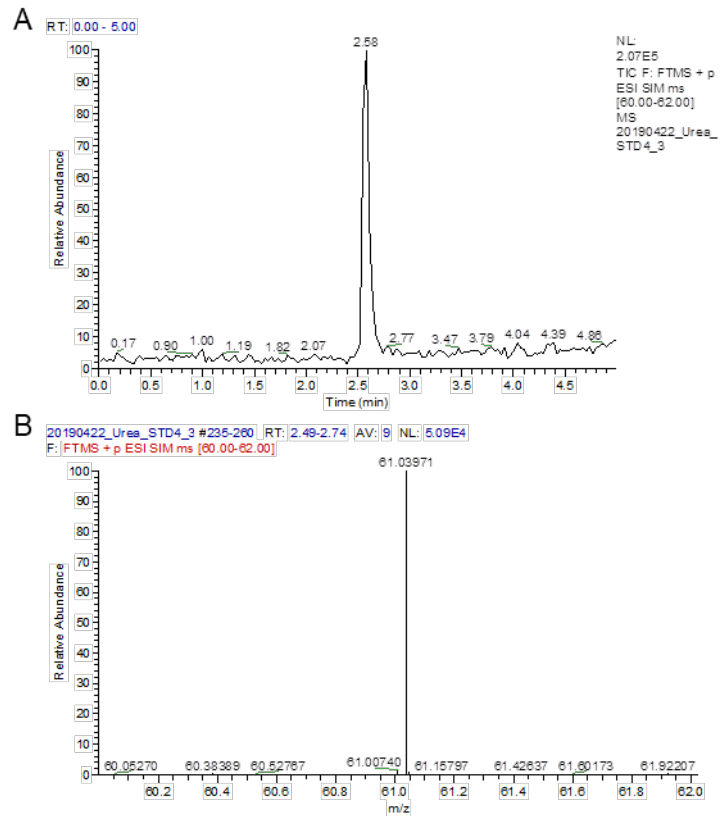


Figure A.2-9. LC-MS profile of urea. (A) Area under the elution curve of urea was used in relation to the elution area of Urea-C13-2N15 (Figure A.2-9) to form a standard curve and (B) MS peak used to detect urea, operated with conditions shown in table A.2-1.

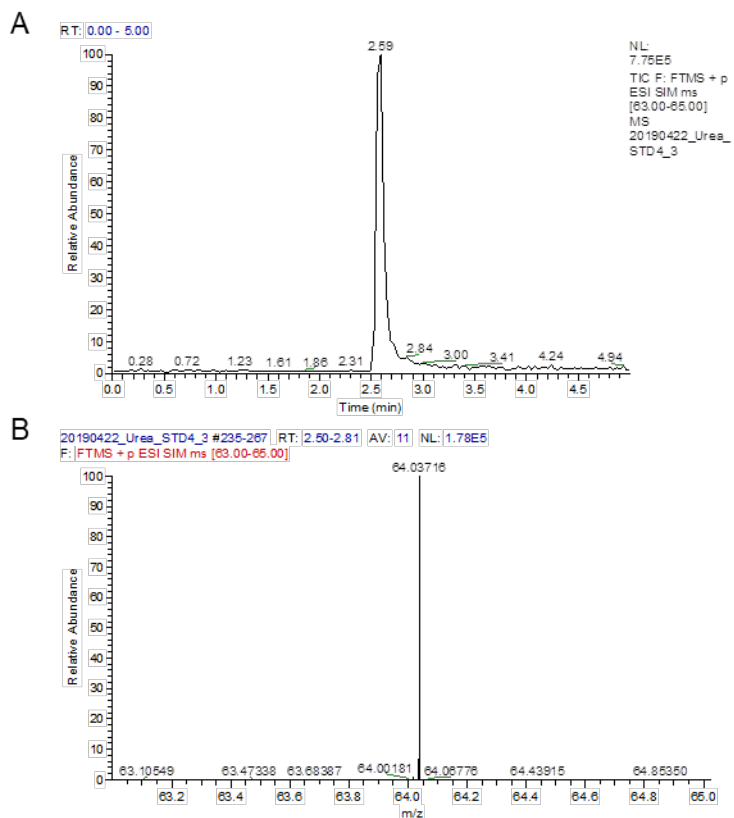


Figure A.2-10. LC-MS profile of urea-C13-2N15, used as the internal standard for urea. (A) Area under the elution curve of urea-C13-2N15 was used in relation to the elution area of urea (Figure A.2-9) to form a standard curve and (B) MS peak used to detect urea-C13-2N15, operated with conditions shown in table A.2-1.

Table A.2-2. Average of PPV titers across TL ratio and TLL in osmolyte-containing ATPS.

Glycine			
TLL	Avg. Top Titer	Avg. Bottom Titer	Avg. Top Titer
Low	7.7 ± 0.5	6.7 ± 0.4	
Mid	8.0 ± 0.3	5.8 ± 0.6	7.9 ± 0.4
High	8.1 ± 0.2	4.3 ± 0.9	
Betaine			
TLL	Avg. Top Titer	Avg. Bottom Titer	Avg. Top Titer
Low	7.1 ± 0.5	7.8 ± 0.4	
Mid	7.7 ± 0.3	5.7 ± 0.5	7.5 ± 0.4
High	7.6 ± 0.2	4.8 ± 0.3	
TMAO			
TLL	Avg. Top Titer	Avg. Bottom Titer	Avg. Top Titer
Low	5.0 ± 0.4	7.4 ± 0.2	
Mid	6.8 ± 0.4	5.6 ± 0.5	6.3 ± 0.9
High	6.9 ± 0.3	4.9 ± 0.3	
Urea			
TLL	Avg. Top Titer	Avg. Bottom Titer	Avg. Top Titer
Low	5.4 ± 0.9	7.3 ± 0.5	
Mid	6.3 ± 0.7	5.1 ± 0.5	6.1 ± 0.9
High	6.6 ± 0.4	3.5 ± 0.9	

All titer values are represented as \log_{10} (MTT₅₀/mL) measured using MTT assay.

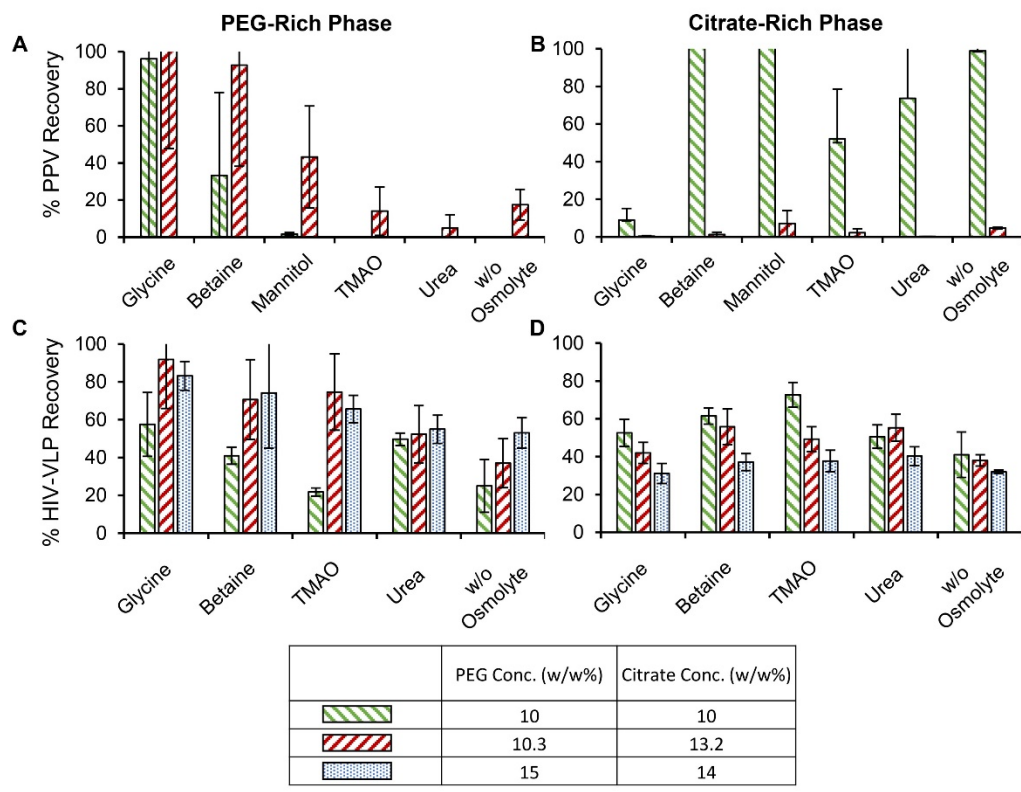


Figure A.2-11. PPV and HIV-gag VLP recoveries in (A & C) PEG-rich and (B & D) citrate-rich phases, at three common global compositions in presence of different osmolytes. The open columns indicate 100% recovery in the represented phase. The error bars represent standard deviation of experiments done in triplicates. The high error bars are because of the sensitivity of the MTT assay measured in log and converted to percentages.

Table A.2-3. Viscosities of the PEG-rich phase with and without addition of osmolytes of systems at different TLL

Osmolyte	TLL	Viscosity (mPa-s)
None	Low	31 ± 6
	Mid	122 ± 41
	High	221 ± 7.8
Glycine	Low	97 ± 21
	Mid	265 ± 87
Betaine	Low	73 ± 17
	Mid	239 ± 76
TMAO	Low	71 ± 17
	Mid	221 ± 79
Mannitol	Low	94 ± 25
	Mid	279 ± 85
Urea	Low	27.2 ± 5
	Mid	110 ± 34

Low: system composition of 10 w/w% PEG and 10 w/w% citrate

Mid: system composition of 10.3 w/w% PEG and 13.2 w/w% citrate

High: system composition of 15 w/w% PEG and 14 w/w% citrate

A.3 Multimodal affinity ligand based aqueous two-phase system for virus purification

Table A.3-1. Correlation of tie-line ratio and volume ratios of the selected systems on different tie-line lengths

Tie-line length (w/w%)	Tie-line ratio	Volume ratio
15	1	0.6
	2.3	0.3
25	1	0.5
	2.3	0.3
36	1	0.8
	2.3	0.5

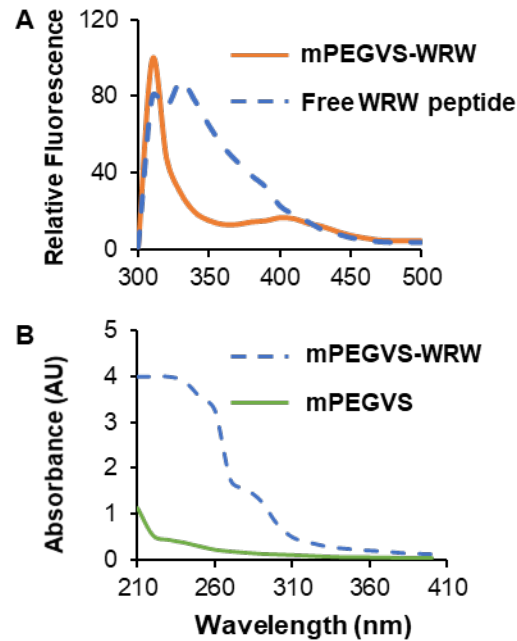


Figure A.3-1. Conjugation confirmation of mPEG-VS and GRCD-WRW by (A) relative fluorescence spectra comparison of free WRW peptide and PEGVS-WRW and (B) absorbance spectra comparison of free mPEGVS and mPEGVS-WRW in 1x PBS, pH 7.4. The presence of fluorescence at 310 nm and a high relatively absorbance between 210-280 nm confirms the successful attachment of PEGVS to the peptide with the target sequence of WRW

B Enveloped virus partitioning in ATPS

Aqueous two-phase system (ATPS) has been identified as a potential candidate for virus purification in the downstream processing of viral products. However, the lack of partitioning mechanisms and experience with the viral behavior in ATPS leads to a large experimental space to optimize the recovery process. The viral partitioning studies must be expanded to familiarize the influence of viral structural characteristics on the partitioning. A systematic study that involves the viral partition behavior in a pre-defined standard system needs to be conducted to develop empirical prediction models. The standard system can be defined with a set polyethylene glycol (PEG) molecular weight and salt type operated under similar process conditions such as pH and temperature. A database of the relationship between the viral partitioning deviations from a model virus behavior and differences in the structural and physicochemical characteristics could yield a better design for the high-throughput screening of the optimal system.

The standard system determined from the tie-line framework proposed in *Chapter 3* can be used to understand viral partitioning behavior of other viruses. Our previous work developed a tie-line framework to study the partitioning behavior of porcine parvovirus (PPV) in a PEG 12 kDa-citrate system at pH 7 (refer to *Chapter 3* for details). PPV was a non-enveloped virus model sized 18-26 nm in diameter with a pI ~5. In the framework, most of PPV was recovered in the citrate-rich phase at the lowest tie-line length (TLL). PPV salted-out from the citrate-rich phase with an increasing TLL. However, the viral particles accumulated at the interface due to the lack of driving force to cross the interface. It was at the highest TLL studied where the salted-out PPV partitioned to the PEG-rich phase. This partitioning behavior of PPV can be compared to more virus models with varied structural features to get a better understanding of the partitioning mechanism.

The previously developed tie-line framework was extended to an enveloped virus model, herpes simplex virus -1 (HSV) to add to the partitioning behavioral database.

HSV is a dsDNA virus, 200-250 nm in diameter, with a pI ~5. The envelope presence makes a virus more fragile and susceptible to structural disintegration under environmental stress as compared to a non-enveloped virus. The partitioning behavior of infectious HSV was studied in the pre-defined PEG-citrate system.

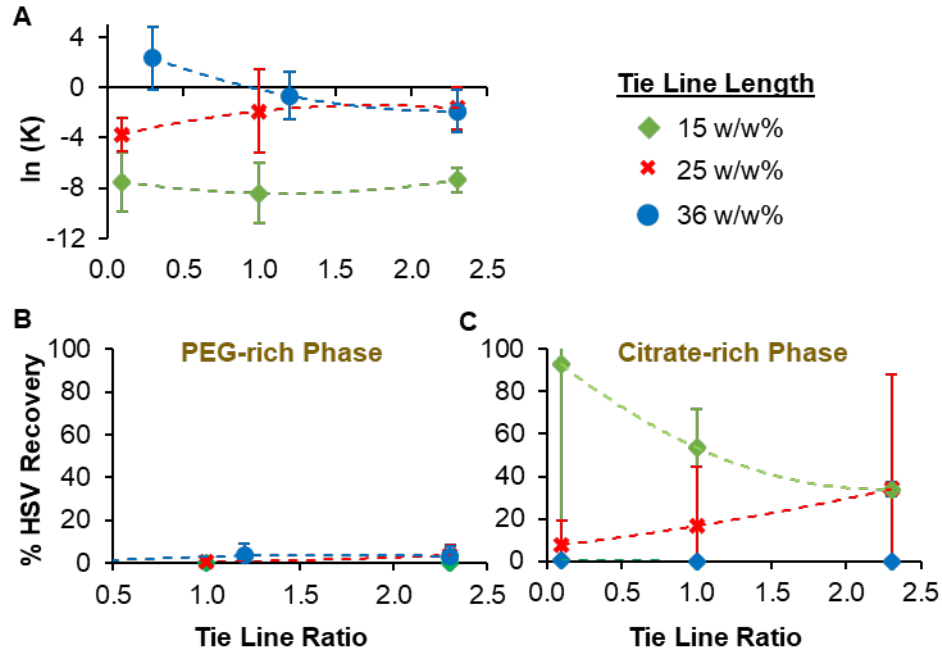


Figure B-1. HSV-1 partitioning behavior studied with the tie-line framework. (A) Partitioning coefficient of HSV at increasing TLL and TLR. Recovery of HSV-1 in (B) PEG-rich phase and (C) citrate-rich phase. The experiments were performed in triplicates, and the error bars represent standard deviation.

An overall increase in the HSV partition coefficient trend was observed with an increasing TLL (**Figure B-1A**). However, the partitioning coefficients were < 1 , indicating lower partitioning to the PEG-rich phase. HSV was salted-out of the citrate-rich phase with the increasing TLL, as demonstrated by the lower recoveries in the citrate-rich phase, but not recovered in the PEG-rich phase (**Figure B-1B and C**). The lower recoveries of salted-out HSV in the PEG-rich phase likely signifies two possibilities. First, HSV partitioned to the PEG-rich phase but was rendered non-

infectious. Second, HSV partitioned to the interface due to ineffective driving forces. Additional non-infectivity assays, such as ELISA, or DLS, are required to evaluate the possibilities of the presence of the inactivated virus or aggregated viral particles.

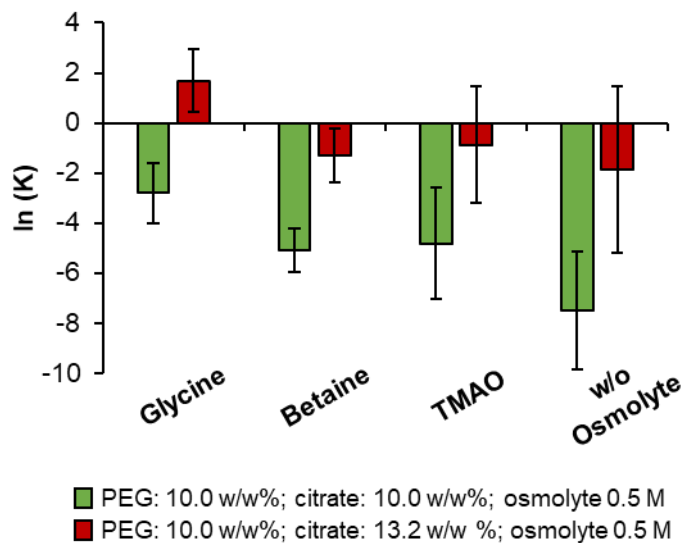


Figure B-2. Effect of osmolytes on the partitioning coefficient of HSV in PEG 12kDa-citrate pH 7 systems. The experiments were performed in triplicates. The error bars represent the standard deviation.

To evaluate the possibility of ineffective driving forces, previously used protecting osmolytes, glycine, betaine, and TMAO were added to the system (see *Chapter 4* for details on PPV). The osmolyte addition increased the overall HSV partition coefficients in the order of glycine > betaine > TMAO as compared to the osmolyte-free systems (**Figure B-2**). The most substantial increase in the partition coefficient by glycine did not yield a higher HSV recovery in the PEG-rich phase (**Figure B-3A**). Addition of glycine increased the salting-out ability of the glycine-containing citrate-rich phase (**Figure B-3B**). The other osmolytes showed a similar enhanced salting-out ability in the order mentioned above without increasing the HSV recovery in the PEG-rich phase. On the other hand, the same osmolytes used in this study increased the recovery of the enveloped HIV-VLPs (see *Chapter 5* for details). All three virus models, PPV, HSV,

and HIV-VLP were negatively charged, which enabled a better salting-out ability of the citrate-rich phase. However, the interface and PEG-rich phase interaction with the viruses differed. Thus, additional work needs to be performed to understand the enveloped virus-PEG interaction and virus-interface interaction.

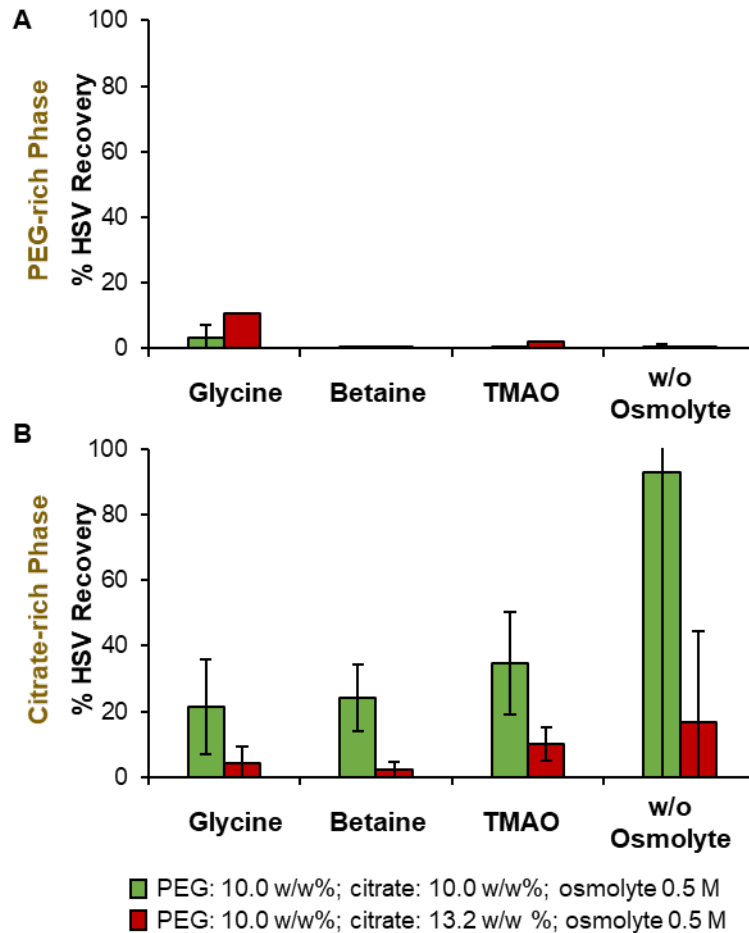


Figure B-3. Effect of osmolytes on HSV recovery in (A) PEG-rich phase and (B) citrate-rich phase. The experiments were performed in triplicates. The error bars represent the standard deviation.

C Copyright documentation

C.1 Reuse license for Figure 2-5

JOHN WILEY AND SONS LICENSE

TERMS AND CONDITIONS

Jul 09, 2020

This Agreement between Pratik Umesh Joshi ("You") and John Wiley and Sons ("John Wiley and Sons") consists of your license details and the terms and conditions provided by

John Wiley and Sons and Copyright Clearance Center.

License Number 4864770679619

License date Jul 09, 2020

Licensed Content Publisher John Wiley and Sons

Licensed Content

Publication Journal of Applied Microbiology

Licensed Content Title Isoelectric points of viruses

Licensed Content Author T. Graule, B. Michen

Licensed Content Date Jul 9, 2010

Licensed Content Volume 109

Licensed Content Issue 2

Licensed Content Pages 10

Type of use Dissertation/Thesis

Requestor type University/Academic

Format Print and electronic

Portion Figure/table

Number of figures/tables 1

Will you be translating? No

Title Virus Purification and Enhancement in Aqueous Two-Phase Systems

Institution name Michigan Technological University

Expected presentation date Jul 2020

Portions Figure 3

Requestor Location Pratik Umesh Joshi

411 Holland Street, Apt. 4

HANCOCK, MI 49930

United States




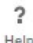


Attn: Pratik Umesh Joshi


Publisher Tax ID EU826007151

Total 0.00 USD

C.2 Reuse license for Figure 2-7

7/9/2020 Rightslink® by Copyright Clearance Center

   Home  Help  Email Support  Pratik Umesh Joshi



Downstream processing of cell culture-derived virus particles
Author: Michael W Wolf, Udo Reichl
Publication: Expert Review of Vaccines
Publisher: Taylor & Francis
Date: Oct 1, 2011
Rights managed by Taylor & Francis

Thesis/Dissertation Reuse Request

Taylor & Francis is pleased to offer reuses of its content for a thesis or dissertation free of charge contingent on resubmission of permission request if work is published.

[BACK](#) [CLOSE](#)

© 2020 Copyright - All Rights Reserved | Copyright Clearance Center, Inc. | [Privacy statement](#) | [Terms and Conditions](#)
Comments? We would like to hear from you. E-mail us at customer@copyright.com

C.3 Reuse license for Figure 2-9

ELSEVIER LICENSE
TERMS AND CONDITIONS
Jul 09, 2020

This Agreement between Pratik Umesh Joshi ("You") and Elsevier ("Elsevier") consists of your license details and the terms and conditions provided by Elsevier and Copyright Clearance Center.

License Number	4864850764164
License date	Jul 09, 2020
Licensed Content Publisher	Elsevier
Licensed Content Publication	Fluid Phase Equilibria
Licensed Content Title	Influence of the molecular weight of polymer, temperature and pH on phase diagrams of poly (ethylene glycol) + di-potassium tartrate aqueous two-phase systems
Licensed Content Author	Alireza Barani, Mohsen Pirdashti, Zahra Heidari, Elena-Niculina Dragoi

Licensed Content Date	Mar 15, 2018
Licensed Content Volume	459
Licensed Content Issue	n/a
Licensed Content Pages	9
Start Page	1
End Page	9
Type of Use	reuse in a thesis/dissertation
Portion	figures/tables/illustrations
Number of figures/tables/illustrations	1
Format	both print and electronic
Are you the author of this Elsevier article?	No
Will you be translating?	No
Title	Virus Purification and Enhancement in Aqueous Two-Phase Systems
Institution name	Michigan Technological University
Expected presentation date	Jul 2020
Portions	Figure 2, The experimental binodal curves of PEG 4000 DPT water [32] compared to PEG 1500 DPT water, and PEG 6000 DPT water at pH 7.74 at 298.15 K. The solid line calculated from equations (3), (4). Pratik Umesh Joshi 411 Holland Street, Apt. 4
Requestor Location	HANCOCK, MI 49930 United States Attn: Pratik Umesh Joshi
Publisher Tax ID	98-0397604
Total	0.00 USD

C.4 Reuse license for Figure 2-10

ELSEVIER LICENSE
TERMS AND CONDITIONS

Jul 09, 2020

This Agreement between Pratik Umesh Joshi ("You") and Elsevier ("Elsevier") consists of your license details and the terms and conditions provided by Elsevier and Copyright Clearance Center.

License Number	4864911238270
License date	Jul 09, 2020
Licensed Content Publisher	Elsevier
Licensed Content Publication	Journal of Chromatography B
Licensed Content Title	The step-wise framework to design a chromatography-based hydrophobicity assay for viral particles
Licensed Content Author	Sarah A. Johnson, Alison Walsh, Matthew R. Brown, Scott C. Lute, David J. Roush, Michael S. Burnham, Kurt A. Brorson
Licensed Content Date	Sep 1, 2017
Licensed Content Volume	1061
Licensed Content Issue	n/a
Licensed Content Pages	8
Start Page	430
End Page	437
Type of Use	reuse in a thesis/dissertation
Portion	figures/tables/illustrations
Number of figures/tables/illustrations	1
Format	both print and electronic
Are you the author of this Elsevier article?	No
Will you be translating?	No
Title	Virus Purification and Enhancement in Aqueous Two-Phase Systems
Institution name	Michigan Technological University
Expected presentation date	Jul 2020

Portions	Figure 4.(b) Elution salt concentration and relative hydrophobicity to the Phenyl as compared to RNase, calculated using the fraction containing the highest titer. Pratik Umesh Joshi 411 Holland Street, Apt. 4
Requestor Location	HANCOCK, MI 49930 United States Attn: Pratik Umesh Joshi
Publisher Tax ID	98-0397604
Total	0.00 USD